ADDIS ABABA UNIVERSITY
COLLEGE OF NATURAL AND COMPUTATIONAL SCIENCES
SCHOOL OF EARTH SCIENCES

STRATIGRAPHIC, PETROGRAPHIC AND GEOCHEMICAL CHARACTERISTICS OF THE GOHATSION FORMATION IN THE BLUE NILE BASIN, CENTRAL ETHIOPIA: IMPLICATIONS FOR PALEOENVIROMENT RECONSTRUCTION

By:
SAMUEL GETACHEW

A thesis submitted to the School of Graduate Studies of Addis Ababa University in partial fulfillment of the requirements for the degree of Master of Science in Earth Sciences (Petrology)

June, 2018

ADDIS ABABA UNIVERSITY

SCHOOL OF GRADUATE STUDIES

SCHOOL OF EARTH SCIENCES

STRATIGRAPHIC, PETROGRAPHIC AND GEOCHEMICAL CHARACTERISTICS OF THE GOHATSION FORMATION IN THE BLUE NILE BASIN, CENTRAL ETHIOPIA: IMPLICATIONS FOR PALEOENVIROMENT RECONSTRUCTION

BY

SAMUEL GETACHEW CHERNET

ADVISOR: BALEMWAL ATNAFU (Dr.)

Co-ADVASOR: ASFAWOSSEN ASRAT (Prof.)

A thesis submitted to the School of Graduate Studies of Addis Ababa University in partial fulfillment of the requirements for the degree of Master of Science in Earth Sciences (Petrology)

July 2018 Addis Ababa, Ethiopia

ADDIS ABABA UNIVERSITY

SCHOOL OF GRADUATE STUDIES

SCHOOL OF EARTH SCIENCES

STRATIGRAPHIC, PETROGRAPHIC AND GEOCHEMICAL CHARACTERISTICS OF THE GOHATSION FORMATION IN THE BLUE NILE BASIN, CENTRAL ETHIOPIA: IMPLICATIONS FOR PALEOENVIROMENT RECONSTRUCTION

BY

SAMUEL GETACHEW CHERNET

Approved by the Examining Committee

Dr. Balemwal Atnafu	_____	_____
Head, School of Earth Sciences	Signature	Date
Advisor		
Prof. Asfawossen Asrat	Asfawossen Asrat	_____
Co-Advisor	Signature	Date
Dr. Mulugeta Fisseha	_____	_____
Examiner	Signature	Date
Prof. Dereje Ayalew	_____	_____
Examiner	Signature	Date

ABSTRACT

This thesis investigates the stratigraphic, petrographic and geochemical characteristics of the Gohatsion Formation in the Blue Nile Basin, central Ethiopia. In addition to detailed geological mapping and stratigraphic logging in the field, petrographic, mineralogical and major/trace element chemical analysis was performed on 27 samples by means of XRD, ICP-MS/AES analysis. The Formation consists cyclic intercalation of fine siliciclastic and evaporite beds and has been classified into 3 informal members namely, the Upper Mudrock Member, Gypsum Member and the Lower Mudrock Member. Four lithostratigraphic sections were constructed at the Gohatsion-Dejen, Mugher and Jemma localities. Lithofacies at an outcrop and petrographic scale indicates the presence of complex geological history. The Lower and Upper Mudrock Members were formed under tidal influenced environments such as intertidal, supratidal, lagoonal, back-barrier mudflats and tide dominated estuary. The Gypsum Member shows both subaqueous and subaerial facies formed under holomictic brine flux with both continental and marine influences. Geochemistry of mudrock samples showed lower compositional maturity and low weathering index (CIA and PIA values) which is indicative of first cycle deposition. Trace element analysis showed that the provenance composition for such rocks are felsic to intermediate metamorphic to plutonic rocks formed under an active continental arc setting. Diagenetic evolution of sandstone and dolomitic packstone rocks seem to be influenced by meteoric and late stage diagenetic processes whereas the gypsum recorded much of telogenetic processes.

Key words: *Blue Nile Basin, Gohatsion Formation, Lithofacies, Provenance, Diagenesis*

ACKNOWLEDGMENT

This thesis work could not be successfully accomplished without the contributions of several institutions and individuals.

First off, I would like to thank Addis Ababa University, School of Earth Sciences for offering me the opportunity to pursue my Masters program as well as the provision of funding for this thesis research along with logistical resources needed to conduct the field work.

Secondly, my deepest gratitude goes to my advisor Dr. Balemwal Atnafu and my co-advisor Prof. Asfaowssen Asrat for their constructive comments, follow-ups and encouragement throughout the life time of this thesis work. ALS services plc are duly acknowledged for facilitating and conducting geochemical analysis with discount. I also thank the central laboratory of Geological Survey of Ethiopia for thin section preparation. I would also like to thank Dr. Worash Getaneh for his support in providing me with the data needed for geochemical analysis.

I would also like to thank my friends and colleagues at Addis Ababa University, especially Mr. Million Alemayew, Mr. Bahru Zinaye and Mr. Takele Mengiste, for their much needed assistance during field work and throughout the research. Finally I also thank my family, mom, dad and brother for their support and encouragement during my study.

TABLE OF CONTENTS

LIST OF TABLES

LIST OF FIGURES

LIST OF ACRONYMS

1. BNB: Blue Nile Basin
2. MB: Mekele Basin
3. CIA: Chemical Index of Alteration
4. ICV: Index of Compositional Variability
5. PIA: Parson's Index of Alteration
6. REE: Rare Earth Elements
7. LOI: Loss on Ignition
8. HREE: Heavy Rare Earth Elements
9. LREE: Light Rare Earth Elemetns
10. PAAS: Post Archean Australian Shale
11. UCC: Upper Continental Crust
12. NASC: North American Shale Composite
13. G k-G: Guttin K-feldspar Granite
14. UGD: Ujjukke Granite and Granodiorite
15. MIR: Mafic-Intermediate Rocks
16. XRD: X-Ray Diffractometer
17. ICP-MS: Inductively Coupled Plasma- Mass Spectrometry
18. ICP-AES: Inductively Coupled Plasma-Atomic Emission Spectrometry
19. AAU- Addis Ababa University

CHAPTER 1:

INTRODUCTION

1.1. Background

Stratigraphic and sedimentological approach to study the origin and nature of sedimentary rocks has been the fundamental source of information about surface history of our planet. Studies have showed that the application of petrographic and geochemical methods could also be as useful in determining the provenance and diagenetic studies in macro and micro scale (eg. Bhatia, 1983; Andre et al., 1986; Condie, 1993; McLennan et al., 1993; Paikaray et al., 2007; Descourvieres et al., 2011; Khan and Khan 2015; Ejeh, 2016). When applied properly, geochemical and petrological methods often prove to be very helpful and precise in addressing several questions that are difficult to be answered via sedimentological and lithostratigraphic analysis.

Fine siliciclastic and evaporite sequences formed under transitional depositional environments mostly form under highly localized and restricted depositional settings. Hence, it is often challenging to correlate and construct their depositional history with respect to the evolution of the basin itself. Furthermore, primary lithofacies, especially in evaporites, tend to be highly affected by diagenetic processes. Luckily, carful study of macro and micro textures of such rocks both in the field and in the laboratory, coupled with mineral and element chemistry analysis often prove useful even when such rocks underwent chaotic geological history (eg. Gandin and Wright, 2007; Rahimpour-bonab et al., 2007)

Though there have been several works concerning the evolutionary history of the sedimentary basins in Ethiopia, characterization of the siliciclastic and evaporite sequences has not been systematically addressed.

The Blue Nile Basin in central Ethiopia is one of the five major sedimentary basins in the country and is believed to be a NW-SE trending branch of the Ogaden Basin which is currently exposed in the southeastern part of the country. According to Geological Survey of Ethiopia (2016), the Blue Nile Basin covers an area of 63,000 km^2 in the NW Ethiopian Plateau. Most of the previous studies of the Paleozoic-Mesozoic sedimentary successions in northern and central parts of Ethiopia focuse on the stratigraphic and sedimentological characteristics; while the few geochemical and petrological studies were only on clastic (sandstones) and biochemical (limestone) formations. Such works include those of Conforto et al. (1993),

Worash Getaneh and Valera (2002) on the Antalo limestone Formation, Worash Getaneh (2002) and Barsisa Bekele (2011) on the Adigrat Sandstone.

The Gohatsion Formation in the Blue Nile basin represents a major marine transgression initiated by thermal subsidence and a global climate change record due to eustatic sea level rise nearly 170Ma ago (Russo et al., 1994; Wolela Ahmed, 2008; Abbate et al., 2015). This Formation is formed by diverse and cyclic intercalations of sediments ranging from fine sandstones to silt and mudstones, carbonates and gypsum. This Formation provides rich geological record which could be exploited for reconstructing the paleoenvironmental history of the basin.

1.2. The study area

1.2.1. Accessibility

The specific regions of interest for the current study are located at the south eastern and south western parts of the basin where the Gohatsion Formation is well exposed. These sites are: the Mugher, the Gohatsion – Dejen (type area according to Getaneh Assefa (1981)) and the Lower Jemma (figure 1.1).

The Mugher area can be accessed along a 55km asphalt road from Holeta, located 42km west of Addis Ababa along the Addis Ababa-Nekemte highway. The Gohatsion-Dejen Study area can be accessed along the Addis Ababa-Debre Markos highway between 198 and 205 Km markers within the Abay River Gorge. The Lower Jemma area is located 175 km northwest of Addis Ababa, near the confluence of Jemma and Abbay rivers, and accessed along the dry weather gravel road by taking the Addis Ababa-Bahirdar Highway then taking a dry weather gravel road branching at the 135km mark from the Addis Ababa-Debre Markos highway. These sites have been selected based on the following criteria: (i) distribution of the unit with respect to the basin; (ii) availability of data from previous studies, especially geological maps; (iii) ease of accesses and (iv) good exposure.

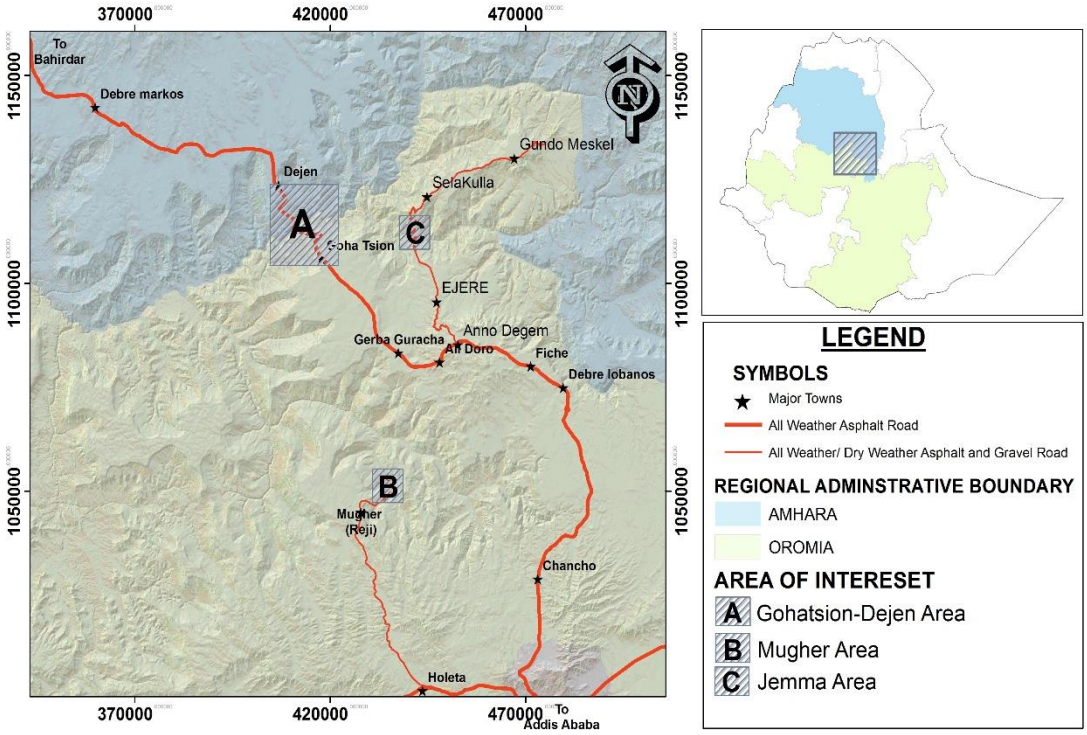

Figure 1.1. Location and accessibility map of the study areas

1.2.2. Physiography

The physiography of the Blue Nile basin in central Ethiopia is ragged and mountains terrain dissected by major and minor river canyons in the central and eastern parts, where as in western parts, lowlands dominate the basin. The altitude within the basin ranges from 498m to 4261m m.s.l. (Aster Denekew and Seleshi Bekele, 2009).

In the low lands of the basin, the annual rainfall is less than 1500mm whereas in the highlands, it ranges from 1500-2200mm per year (Aster Denekew and Seleshi Bekele, 2009). The major tributaries that flow into the Blue Nile (Abay) River such as Jemma, Mugher, Guder, Beles and Welaka Rivers dissect and form huge canyons that expose the bed-rocks. The eastern highlands of the basin are dominantly cultivated while grasslands and forests become dominant towards the western part of the basin. (Ministry of Water resources, (1999, as cited in Aster Denekew and Seleshi Bekele, 2009)).

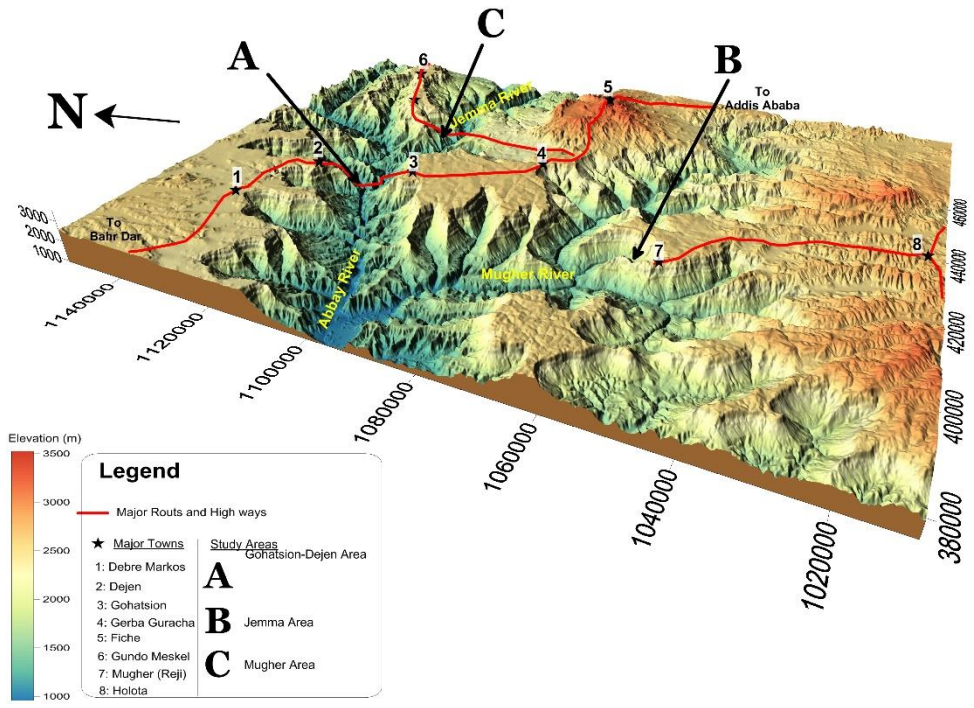

Figure 1.2. Physiographic makeup of the study area

1.3. Literature review

1.3.1. Overview of basic terminologies and concepts

1.3.1.1. Sedimentary facies

Over the years, various aspects of sedimentary rocks have been studied by different works. The depth and richness of information gained form such rocks about depositional environments rose the need to systematically categorize the information into 'facies'. Headberg (1976,p.15) defines facies as '*aspect, nature or manifestation of character (usually reflecting conditions of origin) of rock strata or specific constituents of rock strata*'. According to Krumbein and Sloos (1951), the term facies may or may not be constrained to a specific rock unit or bed. Several aspects of a given rock succession can be described as facies and to avoid confusion, it is advisable to have a reference for which we are attributing the facies to. Hence terms such as, marine facies, clastic facies, biofacies and lithofacies can be used (Headberg, 1976; Krumbein and Sloos, 1951). 'Facies association' refers to an approach designed to integrate different facies types with genetic relationships that might indicate a certain depositional system (Dawit Lebenie, 2010 and references there in).In this study, facies analysis was done both in outcrop and thin section level by giving emphasis on the petrographic and sedimentological aspects of the observed rocks.

1.3.1.2. Evaporite and fine siliciclastic sedimentary textures and their implications

The main problem that is faced when dealing with evaporite texture, especially gypsum, is differentiating primary depositional (syn-depositional) textures from diagenetic and telogenetic textures. According to Warren (2006) and Schreiber et al. (2007), the major challenge in studying evaporite genesis is the lack of realistic assessment and uniform working models for ancient evaporite basins in a modern environment.

Basin wide studies show the presence of textural signatures attributed to sedimentary processes associated with active and passive rift margin settings (Xiasong, 1987; Warren, 2006; Schreiber et al., 2007; Hovorka et al., 2007). Evaporite deposits formed under tectonically quiescent basins such as sags and failed arms of rifts show different facies assemblage than tectonically active basins such as foredeep and foreland basins. Tectonically passive basins tend to favor thick successions of laminated gypsum and carbonate succession along with pseudomorphic relics of selenite that are indicative of bottom growth under shallow water conditions (Warren, 2006; Hovorka et al., 2007; Schreiber et al., 2007). Pseudomorphic relics was also noted as 'gypsum ghost' by several works such as Warren and Kendall (1985), Rouchy et al. (1987) who used impure lamina as traces for the delineation of such structures . Evaporite rocks from tectonically passive margins tend to preserve their primary fabric because in such settings, the rocks would have less chance of reworking. However, primary textures may be subjected to mechanical reworking during stormy seasons or halokinetic conditions (Rouchy, et al., 1987; Schreiber et al., 2007; Warren, 2016).

Variation in evaporite textures as indicators of depositional settings has also been noted by several works (eg. Warren and Kendall, 1985; Muir, 1987; Handford, 1991; Warren, 1991; 2006; Pueyo et al., 2001; Babel, 2007; Matano, 2007; Playa et al., 2007; Al-Juboury et al., 2007). According to Warren (1991), evaporites may form in marginal platform settings with both continental and marine influences. Modern platform settings can be classified into subaerial or subaqueous settings. Marine evaporites formed under subaerial or subaqueous settings show different textural and lithological facies assemblages (Warren, 2006; Babel, 2007). Subaqueous settings such as salina are evaporite dominated lithology that dominantly show shoaling upwards facies along with primary or pseudomorphic, bottom nucleated crystals deposited as massive, laminated or wavy beds accompanied by subordinate carbonate and continental sediments (Warren and Kendall, 1985; Babel, 2007). Subaerial settings such as

sabkha are mostly matrix supported lithology that also shows shoaling upwards facies with peritidal sequence.

According to Babel (2007), marine salina can be described as a salt lake supplied by a nearby sea not as over wash (as in the case with salt pan) but rather in underground seepage. Common characteristic of salina type basin is the formation of shoaling, deepening or brining upwards sequence caused by fluctuating water level. Shoaling upwards sequence in ancient evaporite beds may be identified by a succession of poorly bedded to non-bedded massive mosaic anhydrite at the bottom followed by bedded nodular anhydrite nodules with preferential elongation topped by laminated nodular anhydrite (Warren and Kendall, 1985). Babel (2007) also noted a strong interaction between hydrography and hydrochemistry and evaporitic textures justified by the existence of mixing cycles of a brine column. Hence, evaporitic facies are linked to a particular stratified water zones separated by a pycnocline. Pycnocline separates two zones having distinct textures of evaporite sequences as a result of systemic variation as a function of relative stability, depth and the permanence of the precipitating brine (Warren, 2006; Hovorka et al., 2007). On the biases brine stratification, salina basins can also be classified as meromictic and holomictic pans; the former formed stratified facies whereas the latter undergo seasonal mixing cycle (Babel, 2007).

Evaporite textures have also been used as indicators of different stages of diagenetic processes (eg. Warren, 2006; Gindre-Chanu et al., 2015). According to Warren (2006), genesis of evaporite rocks is not only by primary means, but also by diagenetic processes; hence the name secondary and tertiary evaporites. For instance, dehydration and rehydration of gypsum can form burial salts in nearby non-evaporitic layers (collectively implied as part of ‘hetrolitic gypsum’ in this study) or it can also precipitate in subaerial environments such as sabkha in the form of nodular gypsum which is collectively known as secondary gypsum (Warren, 2006). On the other hand, exhumation (uplift) can also form rehydration textures such as alabastrine or satin spar gypsum especially when such processes are happening in active to stagnant phreatic or vadose zones of groundwater seepage system.

In evaporite carbonate rocks, similar textural variations can also be key in identifying depositional setting and diagenetic texture. Similar to shoaling and stratified facies in gypsum, seasonal fluctuations of brine in carbonate precipitation can also show different textures. For instance, systemic textural variation can be seen when going from subaerial setting to perennial subaqueous setting (Alderman and Skinner, 1957; Curtis et al., 1963; Matter, 1967; Warren,

2006). In such settings, association of stromatolites, pisolites, intraclsts and associated teepes typify conditions of fluctuating shorelines at the edge of more permanent brine lake (Warren, 2016).

Tidal flats are one of the most complicated sedimentary depositional environments accommodating several types of sediments including siliciclastic and evaporite sediments. They present an ideal site for different mechanisms of sedimentation (Matter, 1967; Potter et al., 2005; Tucker, 2011; Flemming, 2012).

In fine grained siliciclastic sediments such as mudstones and siltstones, sedimentary differentiation plays an important role in transforming parent rocks into fine grained sediments (Potter et al., 2005). Because of the difficulty in handling such rocks for detailed microscopic analysis, they are often neglected (Schieber, 1999; Potter et al., 2005). Mudstone show diagnostic sedimentary textures when they are found inter laminated with siltstones. Common sedimentary structures and textures observed from such rocks include lamination (when it is not disturbed by bioturbation), cross laminations, scours, wavy laminations, graded bedding and basin scale to local scale slumps. A combination of such structures can provide insight to transportation and depositional processes such as distal turbidity currents, storm depositions and deposition under weak tidal currents (Potter et al., 2005). It should also be noted that some textures such as local slumps and micro faults could be induced during burial diagenesis process.

1.3.1.3. Depositional environments of evaporite sequences and associated transitional environments

Intermingling of clastic transitional sediments along with evaporite sediments usually show a very dynamic geological history where continental influence is as important as marine influence (Warren, 2006; Schreiber, et al., 2007). Furthermore, Hovorka et al. 2007 also noted the intermingling of clastic and evaporite sediments as an indicator of depth of the basin.

1.3.2. Application of petrography and geochemistry in evaporite and fine siliciclastic rocks

Several factors affect the composition and property of sedimentary rocks. Among them, composition of the source rock, intensity of weathering, climatic conditions (temperature, atmospheric and water chemistry, relief and rainfall), transportation mechanism and diagenetic processes are the main ones (Krumbein and Sloos, 1951; Potter et al., 2005; Tao et al., 2014).

Hence, textural and chemical framework of most sedimentary rocks are attributes of their genetic history that can be deciphered via geochemical and petrological approaches.

Petrographic study, i.e, identification of minerals, their modal proportion and textural association of mudrock (eg. Schieber, 1999), evaporites (eg. Sherman et al., 1972; Warren, 2006; Tunic et al., 2009; Rhimpour-Bonab et al., 2010; Aleali et al., 2013; Gindre-Chanu et al., 2015), and sandstones (eg. Pettijohn et al., 1987; Garzanti, 2016; Xiong et al., 2016; Yuan et al., 2017) give insight about the source material and the processes involved in the formation of the rock. Studies such as Golden et al. (1985), Odin (1990), Velde (2003), Driessche et al. (2012), Xie et al. (2013) showed the association of certain minerals in evaporites and fine siliciclastic rocks with a specific depositional, diagenetic and environmental conditions.

Although fine grained siliciclastic rocks such as mudrocks dominate much of the sedimentary record, little has been done in terms of utilizing the information they hold (Totten and Hanan, 2007). Recent works, however, advocate the use of fine siliciclasts in geochemical characteristics and provenance study due to higher homogenization and wider range of provenance compared to coarser siliciclastic rocks such as sandstones (Khan and Khan, 2015). Furthermore, closely related sandstone and mudstone rocks may come from different provenance, hence separate geochemical analysis of these rocks is warranted (Khan and Khan, 2015; Tao et al., 2014).

Geochemical analysis in evaporite rocks focuses on the determination of the properties of the precipitating liquid (parent brine). The chemical composition and mineralogy of evaporite minerals is closely related with the composition of salts dissolved in the evaporating water (Kushnir, 1981; Warren, 2006; Playa et al., 2007; Babel and Schreiber, 2014). The main components of evaporite minerals present in modern oceans are Na^+, K^+, Mg^+, Ca^+ along with three major anions Cl^-, SO_4^{2-} and HCO_3^-. However, differences in physiography and chemistry of ancient and modern oceans has been noted by works such as Babel and Schreiber (2014) and references there in. Ancient ocean chemistry interpreted form evaporite deposits shows a stratified ocean chemistry. Hence, geochemical analysis of evaporite rocks will yield in determining the type of precipitating water (Marine, continental or mixed).

Major element chemistry

Simple major element bivariate plot is not as helpful as those of sandstones due to the potential effect of post depositional alteration (Potter et al., 2005). However, discriminant functions that

help eliminate overlaps, may show genetic relationship between mudstones and sandstones (Roser and Korsh, 1988). Another major clue that can be extracted from major element chemical analysis is determination of weathering intensity of provenance by Chemical Index of Alteration (CIA) (Nesbitt and Young, 1982), using the following relationship:

$$CIA = 100 * \left(\frac{Al_2O_3}{(Al_2O_3 + CaO^* + Na_2O + K_2O)} \right)$$

Where CaO is the value for silicate bound calcium free from carbonates.*

The Index of Compositional Variability (ICV) ratio (Cox et al., 1995; LaMaskin et al., 2008) also proved to be helpful in discriminating first cycle deposits from highly recycled sediments, and is calculated in the following manner;

$$\text{ICV} = \left(\frac{Fe_2O_3 + K_2O + Na_2O + CaO + MgO}{(Al_2O_3)} \right)$$

Compositionally mature mudstones (in terms of the dominance of clay silicate minerals) have lower ICV values whereas, compositionally immature mudstones have higher ICV values. The later are often results of first cycle deposits under tectonically active settings (Lee, 2002 and references there in). Furthermore, a cross plot of CIA and ICV values could also help discriminate mudstones with different composition of the source area (Lee, 2002; Potter et al., 2005; LaMaskin et al., 2008).

Trace element chemistry

Trace element analysis plays an important role in provenance studies. According to Potter et al. (2005), trace elements such as Th, Sc and Cr can be good indicators of provenance due to their insoluble nature that enables them to faithfully reflect the characteristics of provenience material. Furthermore, cross plots of trace element ratios (Th/Sc against Sc or Cr/Th against Sc/Th, Cr/V against Y/Ni) could also indicate felsic or mafic source (Jehlicka, 2002; Lee, 2002; Potter et al., 2005; Critelli et al., 2008; Tao et al., 2014; Khan and Khan, 2015). ‘

As mentioned above, chemical composition of sediments can also be influenced by physical sorting during transportation and sedimentary recycling. This will result in progressive enrichment of heavy minerals (Jehlicka, 2002; Potter et al., 2005). In this case, cross plots of Th/Sc against Zr/Sc will indicate sediment recycling. The latter will increase during sediment recycling independently of changes in the former ratio.

Among the geochemical signatures of trace elements, rare earth elements give the most valuable information about provenience (Nance and Taylor, 1976; Cullers, 1995; McLennan, 2000; Nyakairu and Koeberl, 2001; Worash Getaneh, 2002; Potter et al., 2005; Khan and Khan, 2015). They are not fractionated by most surface and sedimentary processes. Once freed from parent material via weathering, REE elements tend to concentrate in caly minerals and represent chemistry of the protolith; once this happens, REE concentrations are unaffected by diagenetic processes.

REE patterns are normalized either with condrite (eg. Cullers et al., 1979; McLennan et al., 1993; Nyakairu and Koeberl, 2001; Ejeh, 2016) or Post Archean Shale (PAAS) (eg. Worash Getaneh, 2002; Shadan and Hosseini-Barzi, 2013) to avoid differences resulting from cosmic abundance of even vs. odd atomic numbers.

1.3.3. Mineralogical and textural analysis and its implication for diagenetic evolution

The term ‘diagenesis’ was introduced in the late 18th century (Larsen and Chilingar, 1967); it implies the process that acts on deposited sediments that enables them to transform into a rock. According to Fairbridge (1967), three phases of diagenesis exist: syndiagenesis (lasting 1000-100,000 years in 1-100 meters depth) marked by syngenetic autogenesis, anadiagenesis (lasting form 103-108 years at 1-10,000 meters) marked by hepogene autogenesis resulting from non-magmatic water (pore fluid); and epidiagenesis (lasting 103-109 years at 1-3,000 meters) marked by meteoric water influence.

Diagenesis is not uniform for all sediemtary rocks. Sometimes, diagenesis may start contemporaneously with deposition or very close to the depositional realm (Tucker, 2001). The most ideal rocks to observe such transformation are evaporites (sulfate and carbonate rocks). Precipitation and dehydration of gypsum to form secondary anhydrite in a sabkha environment or the formation of entrolitic or nodular anhydrite in a very shallow depth (as shallow as 2 meters) can be a perfect example for such process (Warren, 2006). In carbonate rocks, early cementation, micritization and early dolomitization (in hypersaline conditions) are very common syndepositional processes (Rahimpour-Bonab et al., 2010). In Sandstones and fine siliciclastics, early diagenesis may revolve around compaction and closure of primary porosity by secondary or autogenetic cements such as calcite, quartz and clays minerals (Lonoy et al., 1985; Tucker, 2001; Yuan et al., 2017). Such shallower diagenetic processes leave their own textural and mineralogical imprint on the rock. For instance, in carbonates, the presence of

bioclasts with micritized outlines, porosity filled by micritic or drusy calcite, and isopacheous calcite cement can be indicators of such process (Rahimpour-Bonab et al. 2010). In sandstones, cementation of calcite, quartz overgrowth, kaolin autogenesis or compaction and suturing of grain boundaries may be observed.

Deeper diagenetic processes may either destroy primary textures (often happening in gypsum rocks) or even destroy shallow diagenetic textures. In carbonate rocks, neomorphic transformations of calcite to idiotopic (fabric destructive) dolomite is one example (Tunik, et al., 2009). In fine siliciclastic rocks rich in clay minerals, the transformation of primary and early autogenetic minerals such as kaolinite and smectite to illite and other mica type minerals (eg. palygorskite and sepiolite) marks deeper diagenetic realm (Golden et al., 1985; Odin, 1990; Velde, 2003; Xie et al., 2013)

Telogenesis (uplift) also plays its part in imprinting its own textural and mineralogical markers. In gypsum, the formation of satin spar and roseate gypsum is associated with rehydration resulted when the rock comes in contact with phreatic water zone (Warren, 2006; Cheanu, et al., 2015). In carbonate and siliciclastic rocks, telogenesis may result in dissolution that leads to the formation of successive generations of secondary porosity which may or may not be filled by autogenetic minerals such as gypsum, calcite or quartz (Golden, et al., 1985; Lonoy et al. 1985; Warren, 2006; Rahimpour-Bonab et al. 2010; Xie et al., 2013; Yuan, et al., 2017).

1.3.4. Overview of previous works on the Gohatsion Formation

Gohatsion Formation, as formally named by Getaneh Assefa (1981), was known as either the '*strata of Abbay'* (Krenkel 1926 as cited in Getaneh 1981) or '*Shale and Gypsum'* Unit (Jespen and Athearn 1961). It represents a complex transitional depositional system comprising intertidal, lagoonal and sabkah depositional settings (Getaneh Assefa, 1981; Russo et al., 1994, Dawit Lebenie, 2010). It is overlain by a Callovian-Lower Kimmeridgian Calcareous unit (Antalo Limestone Formation) and conformably underlain by Premo-Triassic Adigrat Sandstone (Getaneh Assefa, 1981; Russo et al., 1994).

As mentioned above, prior to Getaneh Assefa (1981), the Gohatsion Formation was known by different names or was treated as part of a lager series within the Mesozoic sequence of the basin itself. The pioneering work of Krenkel (1926 as cited in Getaneh Assefa, 1981) assigned the name "*Strata of Abbay*" to this transitional unit and gave Liassic Age for it, whereas Mohr (1962, as cited in Getaneh Assefa, 1981), named it as "*Abbay Beds*" which also included the

lower part of the overlaying limestone formation. Furthermore, Mohr (1962) gave Bathonian age with insufficient data to formally name the Formation. Jaspen and Athearn (1961), on the other hand, gave an informal name "*Shale and Gypsum Unit*" and described it as a succession of Shale-Gypsum-Shale-Siltstone from top to bottom. Kazmin (1975), categorized the Gohatsion Formation as part of "*Antalo Group*" which comprises Abbay Beds (Gohatsion Formation), Antalo Limestone and Agula Shale which represent Mesozoic Marine Sequence in Central and Northwestern Plateau. Mengesha Tefera et al. (1996), in their description and revision of the geology of Ethiopia, described Gohatsion Formation as "*Abay Formation*" and gave Middle Jurassic age.

The first formal lithostratigraphic and biostratigraphic description was done by Getaneh Assefa (1981); wherein a formal type section was assigned to the Gohatsion locality. It is also worth mentioning that modifications in the stratigraphy have been proposed by more recent works such as Wolela Ahmed (2008), who added a 50 meter 'transitional unit' between the contacts of Adigrat Sandstone and Gohatsion Formation, and Gani et al. (2008), who reclassified Antalo limestone and Gohatsion Formation as Upper Limestone, Lower Limestone and Glauconitic Sandy Mudstone units.

Lithofacies of this unit includes cyclic inter-bedding of bioturbated mudstone, siltstone, shale, marlstone, gypsum and dolostone (Getaneh Assefa, 1981, Russo et al., 1994, Wolela Ahmed, 2008, Dawit Lebenie, 2010). Accordingly, Gohatsion Formation, at least in its type section, can be informally sub-divided into four sub members which are the Mudstone member (31.4m), lower claystone member (43.2m), Gypsum Member (252.2m) and the upper claystone member (112.6m) (Getaneh Assefa, 1981). However, the application of such subdivision for the entire basin was not applied by other works and was not confirmed by the work of Getaneh Assefa (1981). Serawit Amene and Tamrat Mojo (1996; 1999), Tamrat Mojo and Tibebe G/Selassie (1997) and Zelalem Shiferaw (2005) described Gohatsion Formation as having upper, middle and lower sub-units in Gindeberet Jeldu area, Jemma River and Mugher River sections, respectively. Gypsum Member of the Gohatsion Formation could be related to major sea level low stand at 179Ma ago (Russo et al., 1994, Wolela Ahmed, 2008).

Thickness of this Formation, as noted by several works, varies within the basin. According to Getaneh Assefa (1981), the thickness of this unit in its type section reaches up to 450m and can be found exposed in a road cut along Addis Ababa-Dejen-Debre Markos highway. Russo et al. (1994) also noted the difference in thickness of this unit increasing towards southeast. Wolela

(2008) noted the maximum thickens of 350m within the basin. According to Serawit Amene and Tamrat Mojo (1996), Tamrat Mojo and Tibebe G/Selassie (1997) and Zelalem Shiferaw (2005), a 290m thick succession can be found along Jemma river section, 300m in the Mugher area, and 150m in Gendeberet Jeldu area. Thickness of the Formation reported in Kazmin (1975), Merla et al. (1979) and Mengesha Tefera et al. (1996) seem to be variable and sometimes exaggerated due to the fact that they have regarded the formation in conjunction with the overlaying limestone unit.

Regarding age of the Gohatsion Formation, earlier works put a broad age range of Triassic to Late Bathonian (eg. Aubry, 1886 and Ficcarelli, 1968 as cited in Getaneh Assefa, 1981) on the basis of stratigraphic position and fossil evidence. Getaneh Assefa (1981), assigned Liassic to late Bathonian age on the basis of diagnostic foraminifera (eg. *Naulileculina circularis),* stromatoporodia (eg. *Cladocoropsis mirabilis* Felix). The presence of mega fossils such as bivalvs and gastropods (eg. *Corbiculinae, Lucinids* and *Protocerithium*) is interpreted as peritidal and associated lagoonal and pond water enviroments (Russo et al., 1994; Dawit Lebenie, 2010). Lithostratigraphic and chronostratigraphic correlation have been proposed with the Upper Hammanlei Formation (Tenneco, 1974 as cited in Russo et al., 1994; Tamrat Worku and Astin, 1992; Wolela Ahmed, 2008). Shigut Geleta (1998) also noted carbonate evaporite facies of sabkha type facies, correlable with the Gohatsion Formation in BNB, rimmed by a shallow carbonate platform to the east in Ogaden basin.

1.4. Objective of the study

1.4.1. General objective

This thesis is intended to determine the stratigraphic, petrographic and geochemical conditions for the formation of clastic and evaporite sequence formally known as the Gohatsion Formation in the Blue Nile Basin of central Ethiopia. Investigation of lateral facies variation of this Formation within the basin is also another major objective.

1.4.2. Specific Objectives

..Specific objectives of the research are to:

- Analyze macro and micro textures and structures both in the field and laboratory in order to elucidate depositional facies and diagenetic attributes of the Formation;
- Construct additional lithostratigraphic sections besides the type section in order to characterize facies distribution and variation of the Formation in the basin;

- Determine the petrological and geochemical signatures that can indicate the depositional and diagenetic conditions of the Formation;
- Determine the genetic relationship between the underlying unit (Adigrat Sandstone) and the lower siliciclastic rocks of the Gohatsion Formation.

1.5. Methodology

1.5.1. Field mapping and section logging

The distribution of lithological and textural facies within a basin indicates the origin of sedimentary rocks and their formation condition. This is especially true for evaporite sequences formed under highly restricted environments such as lagoons, ponds and tidal flats. Hence, field investigations and detailed logging of 4 lithostratigraphic sections as well as refining pre-exsisting regional geological maps have been conducted with the objective of outlining lateral facies variations.

1.5.2. Mineralogy, petrography and element chemistry analysis

Mineralogical and chemical composition of clastic and evaporite rocks are controlled by several factors such as the composition of source rock, atmospheric chemistry, climate and environmental conditions, weathering intensity, transportation and diagenetic mechanisms (Lentz, 2003; Potter et al., 2005; Warren, 2006). Hence, geochemical and petrographic data will give invaluable clues to decipher the geological history of this Formation. A total of 31 samples were collected, out of which, 27 were submitted for laboratory analysis as summarized in table 1.1.

Table 1.1. Summary of petrographic and geochemical methods utilized for the study.

No	Type of analysis	No. of samples submitted	Analysis
1	Petrographic (thin section analysis)	14	observation and characterization of micro textures and mineral association in order to desipher diagenetic hostory
2	XRD analysis	3	Determination of mineral chemistry, especially clay mineralogy
3	Element chemistry (ICP-AES/MS)	10	Determination chemical proxies that trace source, evolution and diagenetic conditions of different rock types

Petrographic analysis: thin sections of 14 representative samples from all, except claystone and shale, were prepared at the central Geological Laboratory of the Geological Survey of Ethiopia. Petrographic analysis for determination of modal composition and micro-textures of rocks was conducted using Lecia Petrographic Microscope at AAU.

XRD analysis: a total of 3 samples (2 mudrock and 1 gypsum) were analyzed at ALS Metallurgy and Mineralogy laboratory in Australia. Each sample was pressed into a back packed sample holder to minimize preferred orientation of particles. Powder X-ray diffraction was used to analyses each sample and a combination of matrix flushing and reference intensity ratio (RIR), as described in Davis et al. (1990). The derived constants were used in the quantification of minerals identified in each sample.

The XRD traces were collected under the following instrument conditions: Radiation Co Kα 1.789. Generation at 40kV40mA with an angular range of 5^0 to 77^0 2θ, time/step 120s with step size 0.0131^0 2θ, Divergence and Anti-scatter silt 0.5^0 and 7.5mm respectively, PIXcel in linear mode detector with rotation speed of 60rpm.

Elemental Analysis: a total of 13 samples were analyzed at ALS laboratory in Ireland. Lithium Borate Fusion Inductively Coupled Plasma Emission Spectrometry (ICP-AES) analysis was performed in order to determine 13 major elements whereas, Inductively Coupled Plasma Mass Spectrometry (ICP-MS) was used to determine 30 trace elements including REE and transitional metals. Samples were first crushed to 70% less than 2mm, ruffle split off 250g and then pulverized split to 85% <75μm before analysis.

The precision of analytical instruments has been calibrated with 6 standards from Mineral sciences laboratory in Canada, African mineral standards, Ore research and exploration Pty. Ltd in Australia. The precision of all measured samples fall under the confidence level with major elements like SiO_2, Fe_2O_3, CaO having 0.1-0.3% precision whereas, Al_2O_3 and alkali earth metal., oxides having 0.01% precision. The precision of most trace elements including REE, other than transitional metals, is better than 0.6%. In the case of transitional metals such as Co, Cu, Zn, Sc,Ni, the precision is better than 2.7%.

1.6. Limitations of the Research

The major limitation of this thesis work was the limited exposures for lithostratigraphic logging at the Jemma and Dejen localities primarily due to the fact that the localities are highly affected by tectonics and in many places covered by thick recent alluvium and colluvium. For this reason, the resolution of sections logged is different from Gohatsion and Mugher localities. Additionally, sample selection for laboratory analysis has been constrained to Gohatsion and partly Dejen and Mugher localities hence, the analyzed geochemical attributes may not represent the entire study area.

1.7. Research Outline

This thesis work has five main chapters. The first chapter introduces general information about the intentions of this study and the study area. The second chapter briefly discusses the regional geological setup of the region while chapter 3 introduces the geology of the areas of interest along with the observed lithofacies descriptions. Chapter 4 deals with petrographic and geochemical attributes of analyzed samples along with their description whereas in chapter 5, provenance and depositional setting along with diagenetic processes are discussed.

CHAPTER 2:

REGINAL GEOLOGICAL SETTING

2.1. Introduction

Sedimentary history of Ethiopia is recorded in five major sedimentary basins. According to Geological Survey of Ethiopia (2016), these are the Ogaden, Abbay (Blue Nile), Mekele, Gambela and Southern Rift basins, of which, the former three are results of a complex extensional stress following the inception of the Gondwana Rifts and formation of Neotethyan passive margin along the present day margin of eastern Africa (Schandelmeier et al., 1997; Dawit Lebenie and Bussert, 2009; Geological Survey of Ethiopia, 2016).

Regional plate tectonic reconstruction and sedimentary basin studies revealed that state of extension dominated the African continent since Late Paleozoic to early Mesozoic (Binks and Fairhead, 1991; Janssen et al., 1993). According to these studies, the three major episodes representing the evolutionary phases of intracontinental rift basins in the African continent are: (i) the formation of the Karoo rift (prior to 180 Ma); (ii) separation of South America from Africa and the formation of Central African Rift system (130-80 Ma); and (iii) formation of the East African Rift system (20 Ma to present). Janssen et al. (1993) sub divided the 3rd phase into two by incorporating the extension phase formed due to the rapid movement of Indian Plate towards Asian Plate.

Significant Permo-Triassic intracontinental rifting in the present day Southern and Eastern parts of African margin, commonly known as the Karoo rift, was followed by the development of the Indian Ocean (Binks and Fairhead, 1991; Bosellini, 1992; Wolela Ahmed, 2008; Geological Survey of Ethiopia, 2016). Post ~180 Ma, active rifting ceased due to the development of oceanic crustal material along the southern parts of Africa. Nonetheless, sedimentation, accommodated by subsidence of the basin, continued (Binks and Fairhead, 1991; Russo et al., 1994; Solomon Tadesse et al., 2003).

According to Kazmin (1972, as cited in Mengesha Teferea et al., 1979) and Mogesse et al. (2002), three major transgression and regression cycles occurred during the Mesozoic era. The first cycle was responsible for the formation of the majority of Mesozoic sediments in Ethiopia including the Gohatsion Formation. The second and third cycles are recorded only in the Ogaden Basin by the Mustahil and Ferfer Fromations and the Jessoma Formation and Taleh Evaporites, respectively (Abbate et al., 2015).

The Blue Nile basin in central Ethiopia is also one of the northern most failed arms of the Mesozoic rifts in eastern Africa (Russo et al., 1994). The ~1200m thick Paleozoic-Mesozoic sedimentary succession within the Blue Nile basin represents full transgression and regression accommodated by rifting and subsidence of the present day passive margin of eastern Africa (Binks and Fairhead, 1991; Russo et al., 1994).

According to Russo et al. (1994), Mogesse et al. (2002), Gani et al. (2008) and Dawit Lebenie (2010), the geodynamic history of Blue Nile basin can be summarized as follows:

1. Period of collision and terrain accretion and formation of East African Orogen followed by tectonic quiescence and intense weathering and erosion of basement rocks (Neoproterozoic-mid Ordovician)
2. Regional glaciations followed by intracontinental rifting due to the breakup of Gondwana which began in the Late Carboniferous and subsequently filled by various sediments as NeoTethys sea transgressed and regressed in early to late Jurassic.
3. Tertiary Flood Basalt volcanism from deep seated mantle plume related to the separation of Arabia from Northeast Africa.

The present structural framework of the Blue Nile Basin in Ethiopia is attributed to several extensional regimes that occurred at different geodynamic stages of the rift evolution described above. According to Gani et al. (2008), extensional structures observed in the basin can be categorized in the following manner:

- Neoproterozoic basement rocks within the basin show *NNE-ESE* trending normal faults and fractures that are oblique to the major extension regime that formed the basin. Such structures are interpreted as manifestations of regional Neoproterozoic deformation structures;
- Mesozoic sedimentary rocks are dominated by *NW* and *NE* trending normal faults where the older sequences are mostly affected by *NW* trending faults while the younger units are mostly affected by *NE* trending faults. This indicates that the Mesozoic sediments were accumulated under the influence of Jurassic-Cretaceous *NE-SW* trending extensional fault system that later was overprinted by Late Miocene *NW-SE* trending fracture system associated with the inception of the Main Ethiopian Rift;
- Early to late Oligocene volcanic rocks show dominant *NE* trending faults and fractures related to Miocene extension of the Main Ethiopian Rift (Bekele Abebe et al., 2007)

and subordinate NNE-SSW trending fractures that could be related to the effect of the E-W trending Ambo Lineament.

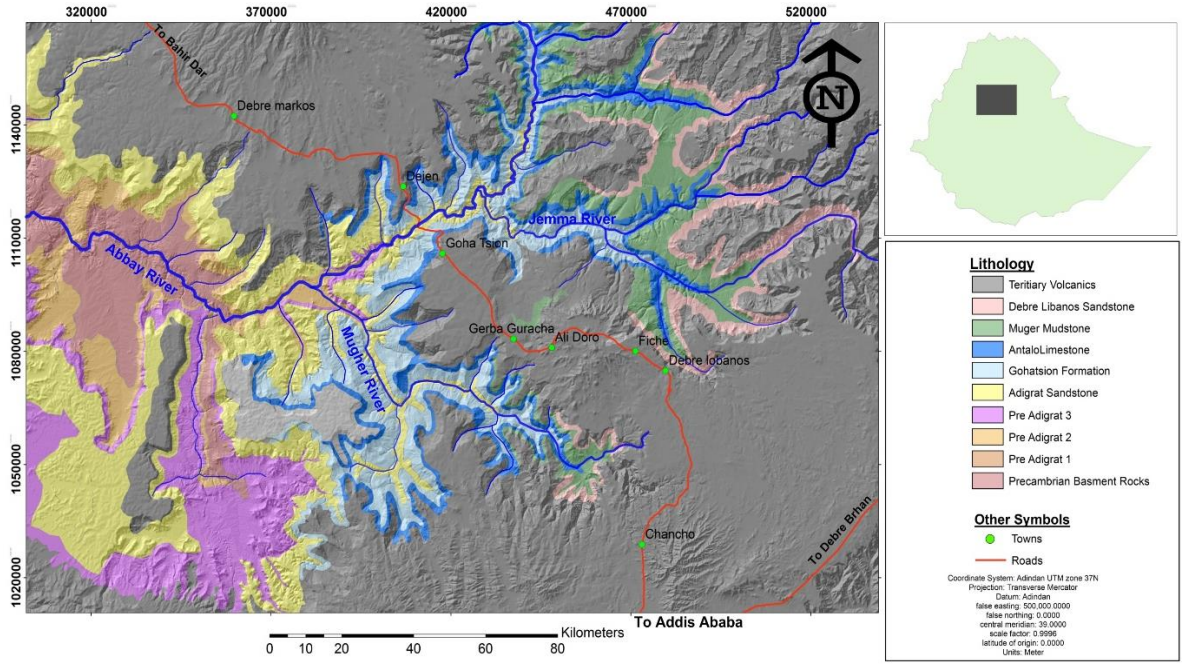

Figure 2.1. Geological map of Blue Nile Basin (after Jepsen and Athearn, 1961; Dawit Lebenie, 2010)

2.2. Regional Stratigraphy

The Blue Nile basin in central Ethiopia is composed of crystalline basement rocks (32%), Paleozoic-Mesozoic sediments (11%) and Cenozoic volcanic rocks (52%) (Ministry of Water Resources, 1996 as cited in Gebrehiwot et al., 2010; Wolela Ahmed, 2008).

Brief description of the dominant rock units exposed in the basin is given below.

2.2.1. Precambrian basement rocks

The Precambrian basement rocks of Ethiopia represents a transition zone between low grade mafic, ultramafic and volcano sedimentary complex with abundant ophiolites regionally known as the Arabian Nubian Shield and poly-deformed high-grade gneisses, migmatites and granulitic rocks along with ophiolitic fragments regionally known as the Mozambique Belt (Asfawossen Asrat et al., 2001; Solomon Tadesse et al., 2003; Dawit Lebenie, 2010). In the Blue Nile basin, the high grade metamorphic rock assemblages are known as Alghe group and the low grade rocks are named as Tulu Dimtu Group (Asfaowssen Asrat et al., 2001). The Alghe group is composed of biotite and hornblende gneiss, migmatite with minor metasedimentary gneiss whereas the Tulu Dimtu Group is represented by undifferentiated metasediments and metavolcanics along with minor marble, quartzite and ultramafics. Various

granitoid bodies intruded the metamorphic rocks (Tesfaye Kebede et al., 1999). The metamorphic basement rocks are unconformably overlain by either Paleozoic-Mesozoic sediments or Tertiary volcanics, except in the western part of the basin where the basement rocks are extensively exposed on the surface (Dawit Lebenie, 2010).

2.2.2. Paleozoic Mesozoic Sedimentary Succession

Getaneh Assefa (1979, 1991 as cited in Russo et al., 1994) informally established five major lithostratigraphic units of the Mesozoic sedimentary successions in the Blue Nile basin. These are the Lower Sandstone (Adigrat Sandstone), Gohatsion Formation, Antalo Limestone, Mugher Mudstone and Debrelibanos Sandstone (Upper Sandstone) units. However, this classification has been modified by recent works such as by Gani et al. (2008), Wolela Ahmed (2008) and Dawit Lebenie (2010). According to Gani et al. (2008) the Gohatsion Formation and Antalo Limestone units have been revised as Glauconitic Sandy mudstone (lower part of Gohatsion), lower limestone (Upper Gohatsion and Lower Antalo limestone) and upper limestone (the remaining part of Antalo limestone). Whereas Wolela Ahmed (2008) included the 'Pre Adigrat' unit along with unnamed 'transitional units' with 50m thickness between the upper Sandstone and Antalo Limestone as well as the lower Sandstone and Gohatsion Formation.

More recently Dawit Lebenie (2010) assigned 8 informal stratigraphic units in the Blue Nile basin by adding pre-Adigrat I, pre-Adigrat II, pre-Adigrat III on to Getaneh Assefa's (1979, 1991 as cited in Russo et al., 1994) classification (figure 2.2).

A brief description of these units, as described in Russo et al. (1994) and Dawit Lebenie (2010), is given below.

Pre-Adigrat I: represents the oldest sedimentary succession in the Blue Nile basin. It is found in isolated outcrops in the northwestern parts of the basin with thickness of up to 50 m. It is composed of poorly sorted, massive and cross bedded medium to coarse grained sandstones and conglomerates. Lithofacies such as soft sediment deformation, large scale trough cross bedding and channel type cut and fill structures makes it similar to the Enticho Sandstone of northern Ethiopia.

Pre-Adigrat II: relatively widespread sediments of floodplain, crevasse spalys and aeolian dune depositional conditions reaching up to 400m thickness in the Fincha valley. They either

unconformably overlay Precambrian rocks or Pre-Adigrat I. Pre to late Carboniferous age is assigned to this unit on the basis of lithostratigraphic position (Dawit Lebenie, 2010).

Pre-Adigrat III: composed of three successive cyclic sheet sandstones capped by overbank fines and crevasse splay deposits with thickens ranging from 350m to less than 100m eastward. Unlike the underlying units, fossils such as palynomorphs, leaf imprints and coaly streaks are abundant in this unit. Compositional immaturity combined with the above biofacies suggests close proximity to source and formation under alluvial plain or lacustrine deltaic environment. On the basis of palynological data, this unit is dated early to late Permian and is correlable with the Karoo sediments of the Ogaden basin. As a result of domal uplift that separated depositional areas of NE and central Africa from E Africa (Schandelmeier et al., 1997) there were an erosional truncation and fluvial incision of Pre-Adigrat sediments by NE and E trending rivers (Dawit Lebenie and Bussert, 2009).

Adigrat Sandstone Formation: represents a maximum of 300 meter Triassic to middle Jurassic sandstone succession. It is unconformably underlain by either the basement or the Pre-Adigrat units and conformably overlain by Gohatsion Formation. Although, the presence of conformable contact between the Adigrat Sandstone and Gohatsion Formation is challenged by Dawit Lebenie, (2010) who noted the presence of widespread pedogenesis and lateritisation in Mekele basin and proposed that the abrupt change in facies form coarse sandy upper shoreface facies to evaporite dominated Gohatsion formation in the Blue Nile basin should be given attention. Earlier works such as Russo et al., (1994) Wolela Ahmed (2008), Mogessie et al. (2002) interpreted this unit to be of continental origin with dominant sandstone beds intercalated with siltstones, mudstones, and conglomerates. Recently, however, Dawit Lebenie and Bussert (2009) and Dawit Lebenie (2010; 2016) outlined 3 unconformity bounded stratigraphic units within this succession. According to these works, the bottom of this formation, informally named as Unit I, represents estuarine storm dominated shoreface deposit whereas the second unit informally named Unit II represents a barrier/inlet spit origin. Unit III, although not observed in the Basin, represents a transgressive barrier lagoon system (Dawit Lebenie, 2010). The recent detailed description of three types of paleosoles (Dawit Lebenie, 2016) is also a testament to the unconformity gap within this unit.

Geochemical and Provenance studies (Worash Getaneh, 2002; Barsisa Bekele, 2011) reveal that the source rock for this formation is nearby silicic to intermediate basement rocks via intense weathering under hot and humid climate in a passive margin setting.

Gohatsion Formation: which is the main focus of this study, represents a period (Liassic-late Bathonian) of sedimentation under coastal, lagoonal and intertidal environment that marks the early flooding of the East African Craton (Getaneh Assefa, 1981; Russo et al., 1994; Dawit Lebenie, 2010; Abbate et al., 2015). It is conformably overlain by a Callovian-Lower Kimmeridgian calcareous unit (Antalo Limestone Formation) and underlain by Premo-Triassic Adigrat Sandstone. Lithofacies of this unit involves cyclic inter-bedding of Bioturbated Mudstone, Siltstone, Shale, Marlstone, Gypsum and Dolostone (Getaneh Assefa, 1981; Russo et al., 1994; Wolela Ahmed, 2008; Dawit Lebenie, 2010). The Gypsum Member of the Gohatsion Formation could be related to major sea level low stand 179 Ma ago (Russo et al., 1994; Wolela Ahmed, 2008).

Thickness of this Formation, as noted by several works, varies within the basin. According to Getaneh Assefa (1981), the thickness of this unit in its type section reaches up to 450m and can be found exposed in a road cut along the Addis Ababa-Dejen-Debre Markos highway. Russo et al. (1994) noted the increasing thickness of this unit towards southeast. Wolela Ahmed (2008) noted a maximum thickens of 350m within the basin, whereas Serawit Amene and Tamrat Mojo (1996) and Tamrat Mojo and Tibebe G/Selassie (1997), reported a 290m thick succession along Jemma River section, 300 m thickness in the Mugher area and 150 m in the Gendeberet Jeldu area.

Antalo Limestone: this 420m thick Callovian to Kimmeridgian carbonate succession represents the drowning of the carton in the Blue Nile Basin. This unit conformably overlays the Gohatsion Formation. This unit can be sub classified into three parts (Russo et al., 1994). At the base is a 180m thick succession of burrowed mudstone that grades into oolitic and coquinoid limestone along with intercalated marl and massive limestone along with scattered corals. In the middle, a 200m succession represented by fossiliferous inter bedding of marly limestone and marls occur. The top part is represented by a 50m thick planar laminated oolitic reefal limestone. Each sub-unit, classified based on fossil assemblages, represents different stages of sea transgression. The first group facies is interpreted as a shallow water environment and the middle group represents a shelf to open marine environment whereas the top most group represents the return of shallow water conditions. This unit is considered to be the result of the global sea level high stand 155 Ma ago (Russo et al., 1994).

Geochemical study of Worash Getaneh and Valera (2002) revealed Ce depletion and REE enrichment is not related with carbonate constituents but of mixed siliciclastic components.

This was interpreted to be the result of formation of this rock unit under a relatively shallow basin and reducing conditions where sea water can be contaminated by continteal input. Conforto et al. (1993) also noted the control of major elements such as Al, K and Fe by insoluble clastic residue. REE patterns also resemble associated clastic rocks within the basin, suggesting similar provenance for REE elements.

Mugher Mudstone: this formation represents a 15-320m thick sea ward prograding flood plain sequence during early Cretaceous (Schmidt and Warner, 1998). It conformably overlays the Antalo Limestone Formation and is overlain by the Debre Libanos Sandstone. According to Russo et al. (1994) and Getaneh Assefa (1991 as cited in Dawit Lebenie, 2010), this succession can be sub categorized into two based on lithofacies. The upper part (240m) comprised of inter bedded sand, silt and mudstone with localized occurrences of lignite and scattered plant fragments interpreted as meandering river system deposit. The lower part (15m) represents supratidal/lagoonal depositional environment with inter-bedding of nodular gypsum, shale and dolomite beds. In terms of fossil record, this formation is one of the most productive units in the entire basin with several species of both invertebrate and vertebrate fossils along with different plant species (Russo et al., 1994; Schmidt and Warner, 1998; Dawit Lebenie, 2010). This unit is also inferred as 'Ambaradem Sandstone Formation' in some works, in conjunction with the overlaying sandstone formation, with the intent of correlating it with a formation found in northern Ethiopia (Wolela Ahmed, 2008).

Debre Libanos Sandstone: also known as Upper Sandstone, is a few meters to 280m thick succession representing sandy braided river deposit on a broad alluvial plain (Russo et al., 1994). Lithofacies of this unit can be described as alternating sequence of mudstones and fine-grained sandstones at the base that changes into a cliff forming coarse grained sandstone beds towards the top. The contact between the underlying mudstone formation and this unit is gradational and conformable, while the upper boundary of the unit is unconformable and sharp against the Tertiary volcanics.

2.2.3. The Tertiary Volcanics

The Tertiary trap sequence of Ethiopia and Yemen were extruded within a short period of time (1 million years) around ~30 Ma ago (Hofmann et al., 1997, Kiffer et al., 2004). This volcanic activity is a result of the breakup of the Arabian Plate from eastern Africa and the formation of the Red Sea (Hofmann et al., 1997; Pik et al., 1998; Kiffer et al., 2004; Abbate et al., 2015). The Oligocene volcanics originally covered over 600,000 km^2 area with local thickness of over

2kms having dominantly basaltic and subordinate felsic (ignimbrite, rhyholite, and tuff) composition. They are overlain by several Oligo-Miocene shield volcanos, the most notable ones being the Simien shield, Choke Shield and Guguftu Shield (Keiffer et al., 2004, Dawit Lebenie, 2010). Geochemical analysis of these series indicates either theolitic (high or low Ti basalts) or alkaline magma sources (Hofmann et al., 1997; Pik et al., 1998; Keiffer et al., 2004). Their distribution throughout the plateau indicates spatial control rather than temporal evolution (Pik et al., 1998), where the low Ti basalts are exposed around the northern part of the plateau while high Ti basalts are dominantly exposed in the eastern and southern parts.

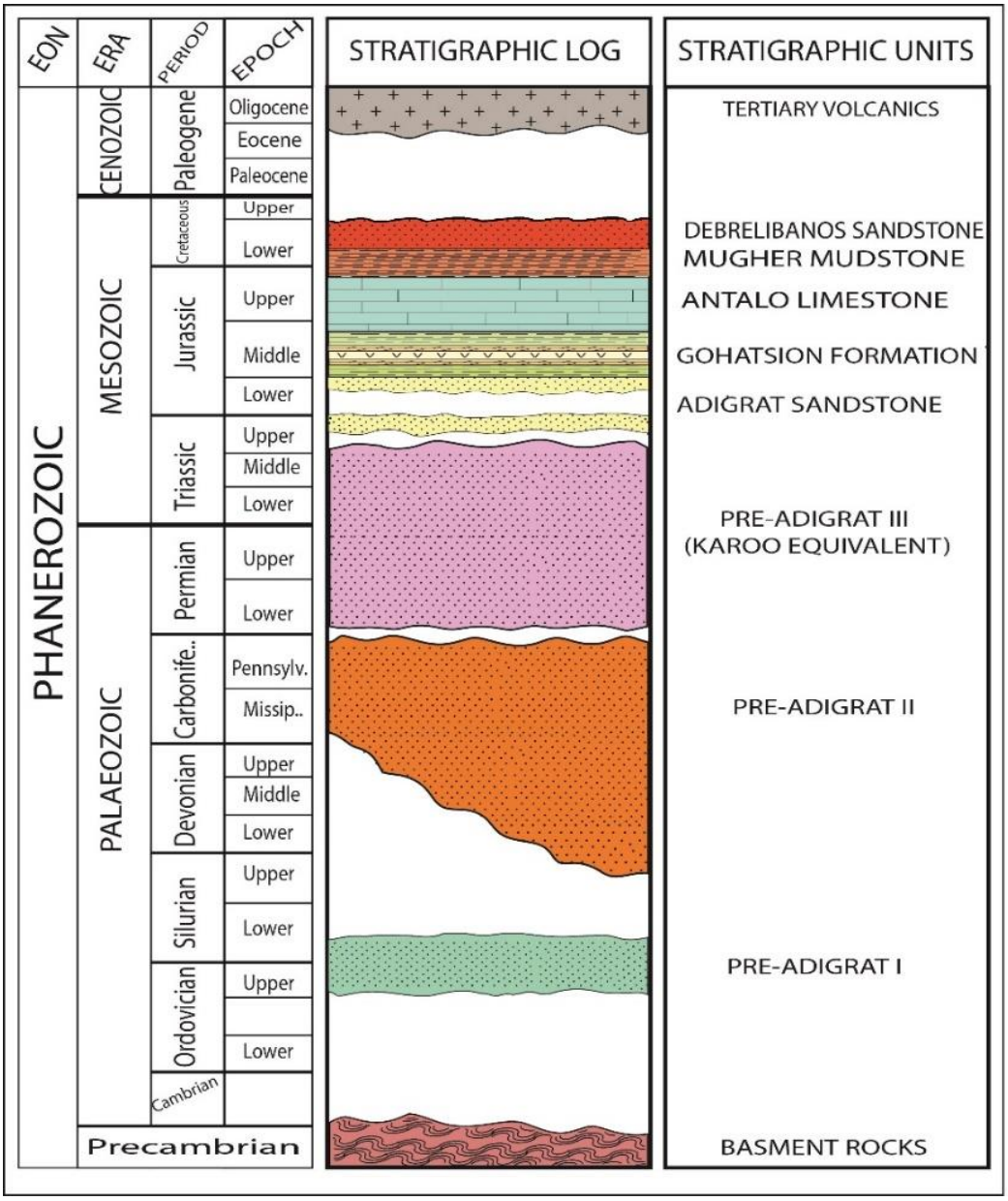

Figure 2.2. Chronolithostratigraphy of the Blue Nile Basin (after Dawit Lebenie, 2010)

CHAPTER 3:

GEOLOGY OF THE STUDY AREA

Lithostratigraphic succession of the Gohatsion Formation is described as being 'cyclic intercalation' of evaporite and siliciclastic rocks (Russo et al., 1994). Variation in terms of lithofacies and thickness was noted by previous works (eg. Getaneh Assefa, 1981). As described in chapter 1, three localities were chosen to investigate such variation. Description of these localities along with the observed facies variation and association is discussed below.

3.1. Section Localities

3.1.1. Mugher Area

The studied, 172m thick section is located in an active gypsum quarry for Mugher Cement Factory along Sodoble River bank (figure 3.1). In this section, in agreement with the regional stratigraphy, the Gohatsion Formation is conformably overlain by the Antalo Limestone formation with a gradational contact. However, the contact with the underlying sandstone unit is not exposed along the section.

Wider lithofacies observation shows cyclic interlayering of siltstone, dolostone, limestone, gypsum, claystone and shale. Shale along with carbonates (dolostone, limestone and marl) tend to dominate the upper and lower parts of the section whereas various types of gypsum interlaced with shale and siltstone dominate the middle part.

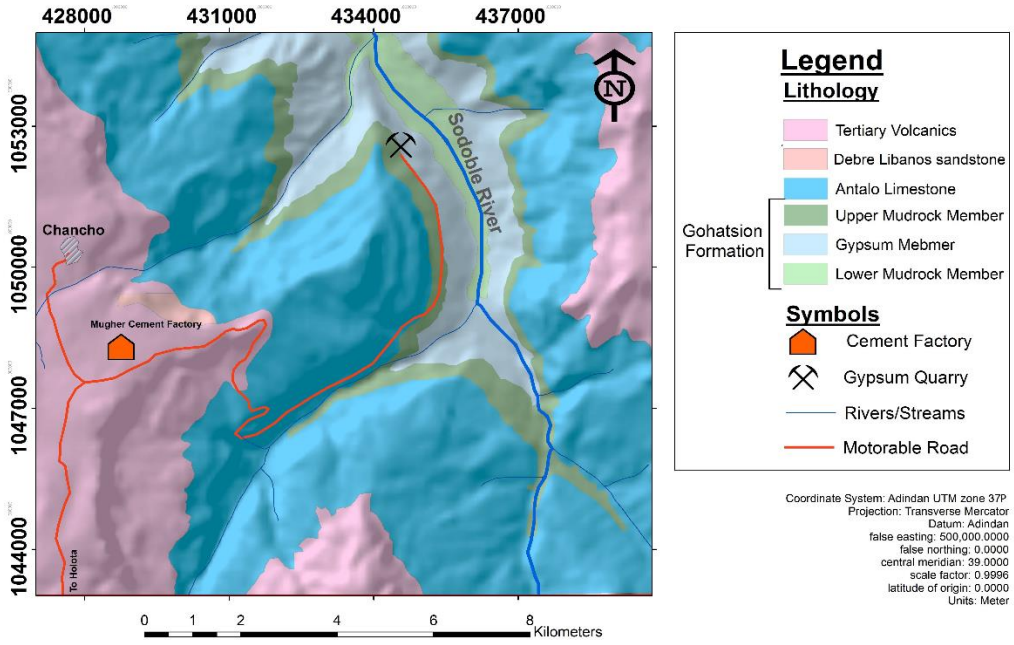

Figure 3.1. Geological Map of Mugher Area (after, Serawit Amene and Tamrat Mojo, 1999)

3.1.2. Gohatsion-Dejen Area

This area serves as a type section for the Formation (Getaneh Assefa, 1981). Two sections were logged, each on either side of Abbay River. The total thickness of the measured sections at Gohatsion and Dejen localities are 433m and 398m respectively (figure 3.2/ appendix A). In both sections, the Gohatsion Formation is conformably bounded by Adigrat Sandstone and Antalo Limestone from the bottom and the top, respectively. On the Gohatsion Side, abundant quarry and gully outcrops made it easy to log the section properly, whereas on the Dejen side, the thick recent alluvial and colluvial cover made it difficult to observe the bedrock. Hence, there exists a gap between the resolutions of sections logged between the Gohatsion side and the Dejen side. Regardless of this difference, variation in lithofacies can be observed between the two sections. The cyclic intercalation of evaporite and fine grained siliciclastic units show facies variation between the two logged sections (appendix A).

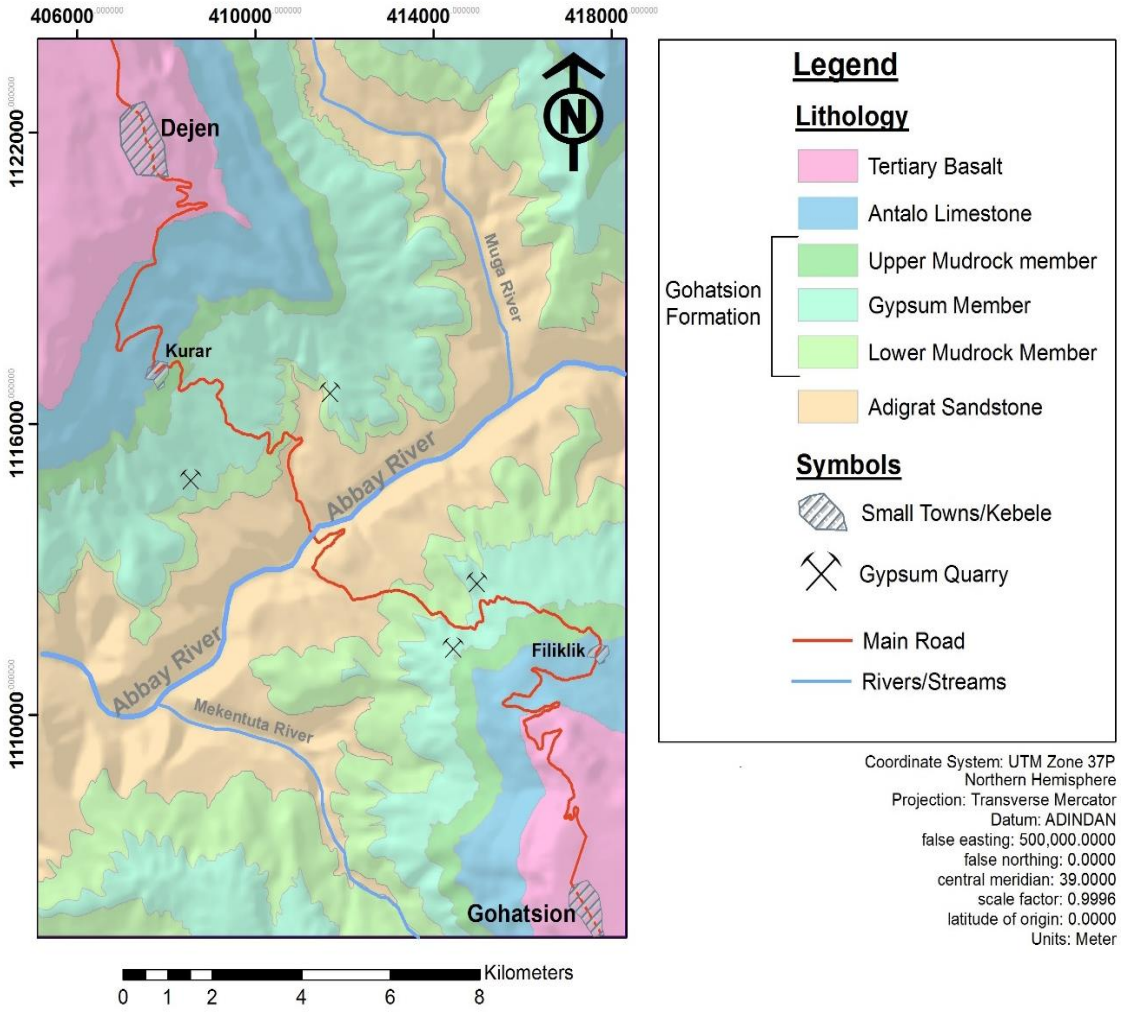

Figure 3.2. Geological Map of Gohatsion-Dejen Area (after, Getaneh Assefa, 1981)

3.1.3. Jemma Area

The studied section is located along a road cut connecting the Addis Ababa-Debre Markos highway to Gundomeskel town (figure 1.1). The area has experienced significant reworking (both tectonically and geomorphologically). Previous works (Serawit Amene and Tamrat Mojo, 1996; 1999) also observed the increasing structural influence and tilting of Mesozoic strata towards east, hindering an attempt to construct a high resolution lithostratigraphic section. Nonetheless, following careful consideration of such structures and tilting due to contortion of gypsum beds, a 400m section was constructed (appendix A). The Gohatsion Formation is conformably underlain by Adigrat Sandstone and overlain by Antalo Limestone. The section show cyclic inter bedding of evaporite and fine siliciclastic materials. Unlike the type section, siliciclastic sediments seem to dominate the succession.

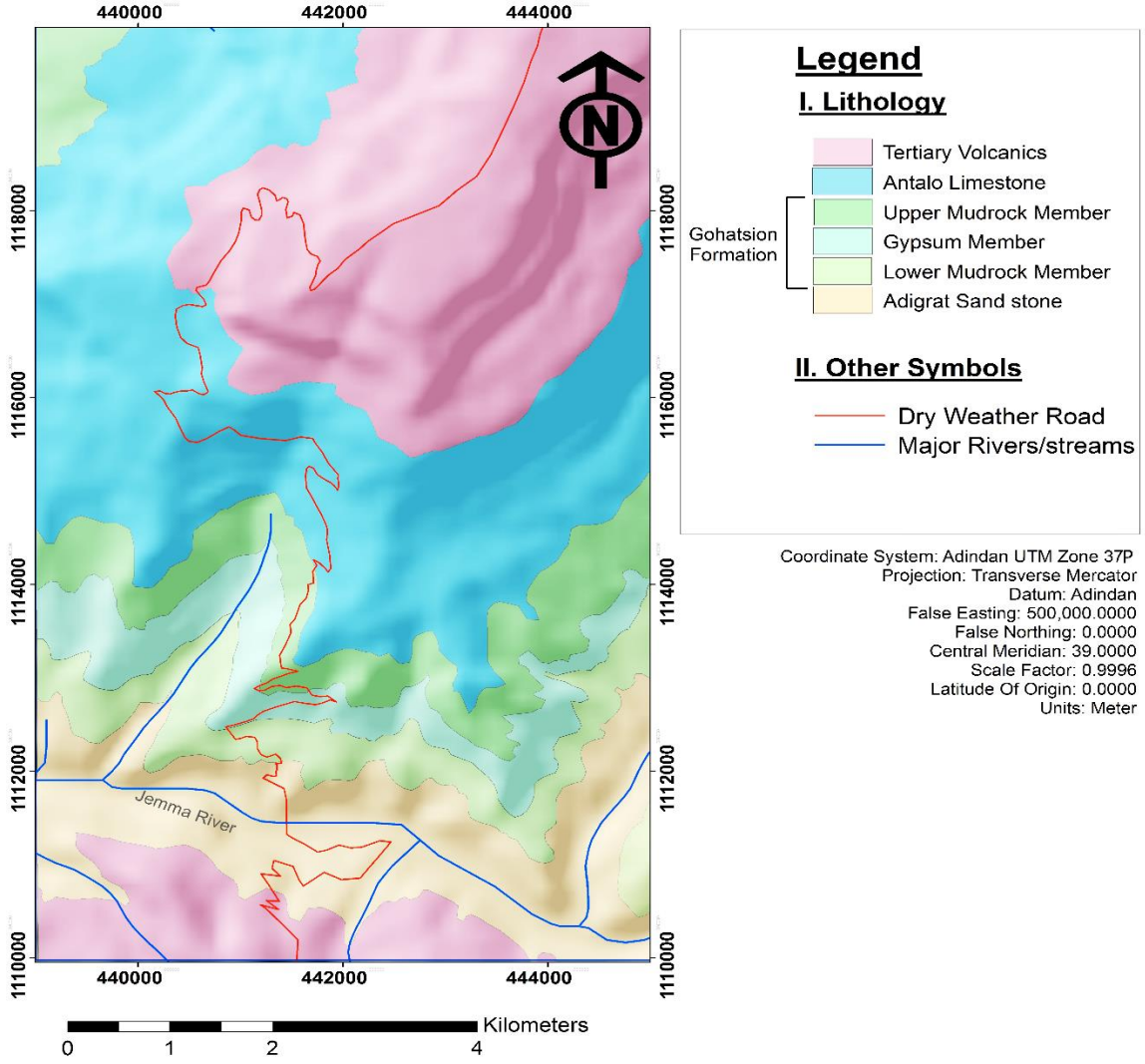

Figure 3.3. Geological Map of Jemma Area (after Serawit Amene and Tamrat Mojo, 1996)

3.2. Lithofacies analysis

On the baises of field observation, the Formation is sub devided into 3 informal members named the Lower Mudstone Member, Gypsum Member and Upper Mudrock Member. In this section, several lithological, textural and compositional variations observed in the three members and their associations in the studied locations are systematically discussed.

3.2.1. The Lower Mudrock Member

This Member is dominantly represented by fine grained siliciclastic rocks and subordinate evaporite beds. Within this member, three major lithofacies have been recognized at an outcrop and hand specimen scale.

Siltstone-mudstone Facies (Facies 1): in this facies, intercalations are dominated by siltstone, shale and mudstone (e.g., Bed 17 in Jemma section, beds 95 and 96 in Gohatsion Section, beds 14, 16-20 of Dejen Section in appendix A). Within this facies, several sedimentary structures have been observed such as siltstone channel scour fills, flute cast structures, planar cross bedded sandy silt with wave current ripples, migrating ripples and lenticular siltstone beds within shale. Heavy bioturbation has also been observed in mudstone and siltstone beds in the Dejen and Gohatsion sections. Hetrolithic bedding is also common in this facies. In the Gohatsion section, siltstone beds found near the contact to the Gypsum Member are micacious (figure 3.4, A).

The dominant lithology being finer siliciclastic sediments such as silt, sandy silt and muds, this sedimentary facies are typical characteristics of a back-barrier tidal flat setting (Flamming, 2012).

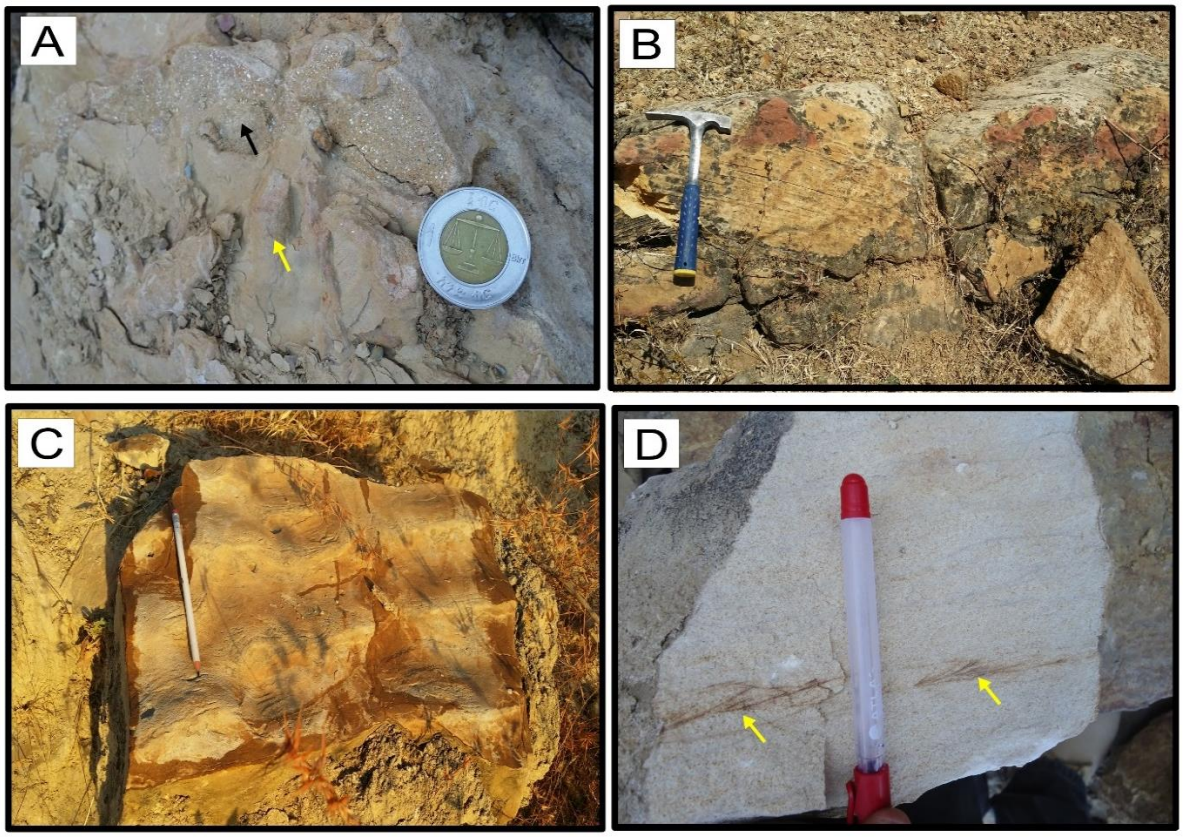

Figure 3.4. Lithofacies of siltstone in Lower Mudrock Member: (**A**) heavily bioturbated (indicated by the yellow arrow)and micacious siltstone bed (indicated by the black arrow) in the Gohatsion section; (**B**) Cross bedded siltstone in the Dejen Section; (**C**) Wave dominated (longuinal) ripple mark in the Gohatsion Section; (**D**) Planar cross lamination (shown by the yellow arrows) in sandy siltstone from the Jemma Section

Silt-sand-mudstone Facies (Facies 2): this facies is represented by intercalation of fine sand with silt and silty mudstone beds along with subordinate shale beds (e.g., Bed 13 in the Dejen section, beds 90, 92 and 94 in the Gohatsion Section, bottom parts of bed 17 and 18 in the Jemma section in appendix A). Within this succession, typical lithofacies observed are homogeneous mudstone beds, micacious siltstone, planar cross bedded to massive partly calcareous fine sandstone. Sedimentary structures such as lamination and wavy/lenticular bedding of claystone in mudstone, flute casts, planar crossbedding and associated migrating ripples (figure 3.13, D) in sandstones, bioturbated siltstone, wave ripple marks are also common within this succession.

This facies is very similar to facies 1, except the dominance of sandstone. The presence of micacious silts, bioturbation and wave current ripples imply tide dominated estuary mudflat and mixed flat system in which these facies were formed (Getaneh Assefa, 1981; Potter et al., 2005; Flemming, 2012). Furthermore, planar crossbedded sandstone also showing migrating

ripples interlayered with bioturbated mudstone can be attributed as a typical sand bar facies in an intertidal flat setting (Tucker, 2011).

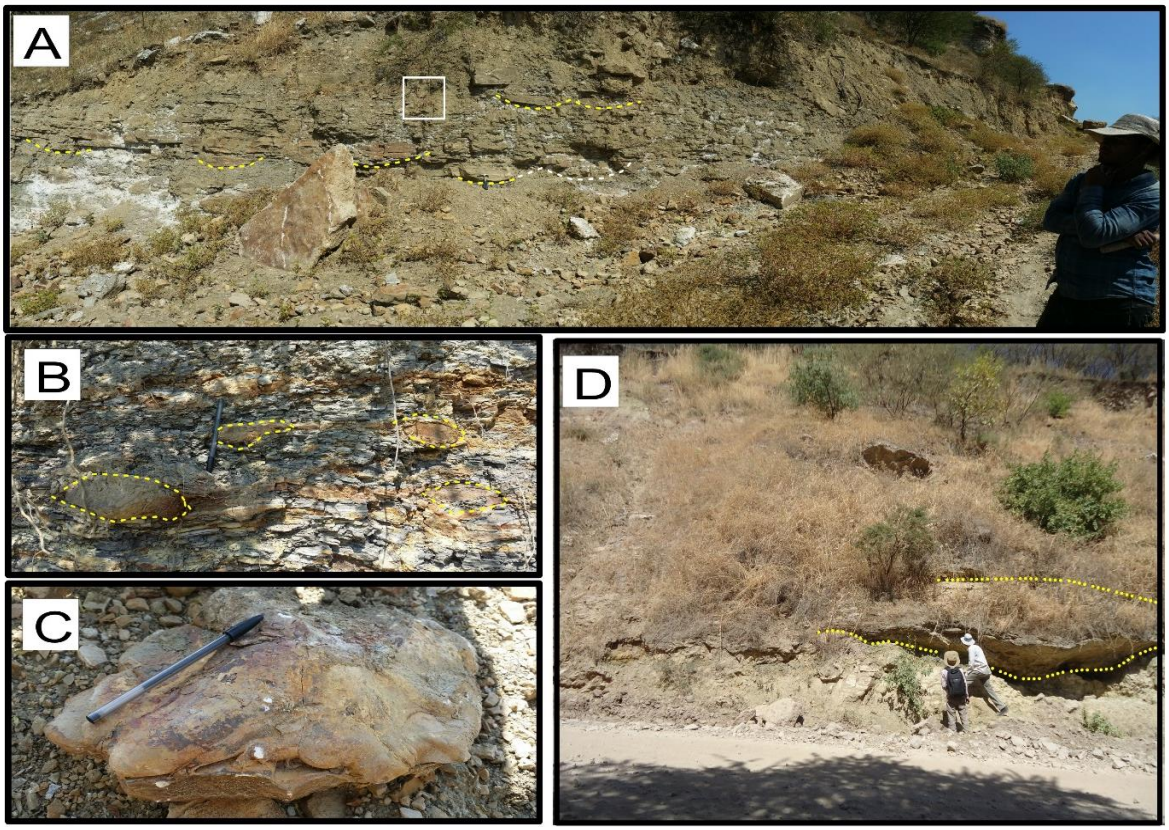

Figure 3.5. Channel scour in the Lower Mudrock Member: (**A**) Panoramic view of abandoned channel fill structures marked by yellow dashed lines in the Dejen section; (**B**) close up (white box in figure A) showing lenticular beds of sandy siltstone beds marked by yellow dashed lines; (**C**) Flute casts from the same bed in figures A&B; (**D**) large channel scour filled by siltstone with a gypsiferous shale base in the Jemma section.

Gypsiferous Silt and Shale (Facies 3): This Facies is only observed in the Jemma and Dejen sections (Bed 15 in Dejen section and Bed 18 in Jemma section in the appendix A). In the Jemma section, the gypsiferous siltstone is intercalated with 0.2 mm thick beds of gypsum and dolostone whereas in the Dejen section, gypsiferous shale (gypcrete) individual gypsum crystals are microcrystalline to coarse and lenticular along with gypsum crests.

Pediogenic gypsum or gypcrete occur in arid environments where annual mean monthly evaporation exceeds mean monthly precipitation in a soil profile (Aref, 2003). The presence of this facies in the Dejen and Jemma sections indicate localized arid environment where seasonal evaporative conditions prevailed; enabling evaporation and subsequent crystallization of gypsum crusts.

3.2.2. The Gypsum Member

The Gypsum Member represents evaporite dominated facies forming cyclic intercalations of gypsum, dolostone, limestone, shale and subordinate silt and mudstones. Since the dominant lithology within this member is gypsum, the main facies analysis focuses on this lithology. Accordingly, 6 different facies have been recognized from the studied sections at an outcrop scale.

Laminated Gypsum Facies (Facies 4): this facies is dominant in the Gohatsion section in contrast to the other sections. Several minor facies can be observed in this facies. Individual laminations can be traced laterally for a significant distance. In the Gohatsion section, this facies is represented by laminated beds which thin upwards (shoal upwards) within one massive bed (figure 3.6, B). Within one bed, several textures can be seen such as '*gypsum ghosts*' (Warren and Kandell, 1985) pseudomorphing bottom grown selenitic gypsum crystals with truncated top, gypsum nodules developed in thick beds found at the bottom of one massive bed. Entrolitic gypsum layers and gypsified microbial laminations forming tepee structure can also be seen (figure 3.7, B); in addition, laminated gypsum beds found at the top of the section also show contorted beds having curved gypsum ghosts flattened and capped by microbial laminated gypsum (figure 3.6, A). Some gypsum beds outcropping in the Gohatsion and Dejen Sections show nodules with preferred alignment and lenticular crystal (probably a result of displacive growth) structure matrixed by wavy laminations of stromatolitic gypsum.

Laminated gypsum facies is common in subaqueous shallow to deep salina ponds (Warren, 2006; Babel, 2007; Schreiber et al., 2007). In such settings, variations in water fluctuations can cause shallowing or deepening upwards sequence. In addition, shoaling upwards facies is also indicative of increasing salinity and brine mixing favorable for the formation of bottom nucleation justified by pseudomorphs of gypsum crystals forming thin layers (figure 3.7,A) (Warren and Kendall, 1985; Babel, 2007; Hovorka et al., 2007). Truncated and sharp contacts between laminations (layers) can be interpreted as either effects of seasonal subaerial exposure and evaporite drawdown (Babel, 2007) or seasonal flooding by under-saturated marine or fresh water under shallow conditions (Havorka et al., 2007). Regarding teepe structures, also termed as pressure ridges by some works (Warren, 2006 and references therein), Warren and Kendall (1985) noted the presence of such structures in sabkhas and salina settings. In salina settings, such structures are also associated with carbonate sheets composed of fenestral fabrics. The presence of microbial/stromatilitic laminated gypsum and interlayered fine siliciclastic rocks

can also be regarded as evidence for prolonged periods of lowered brine salinity and water level fluctuation (Matano, 2007).

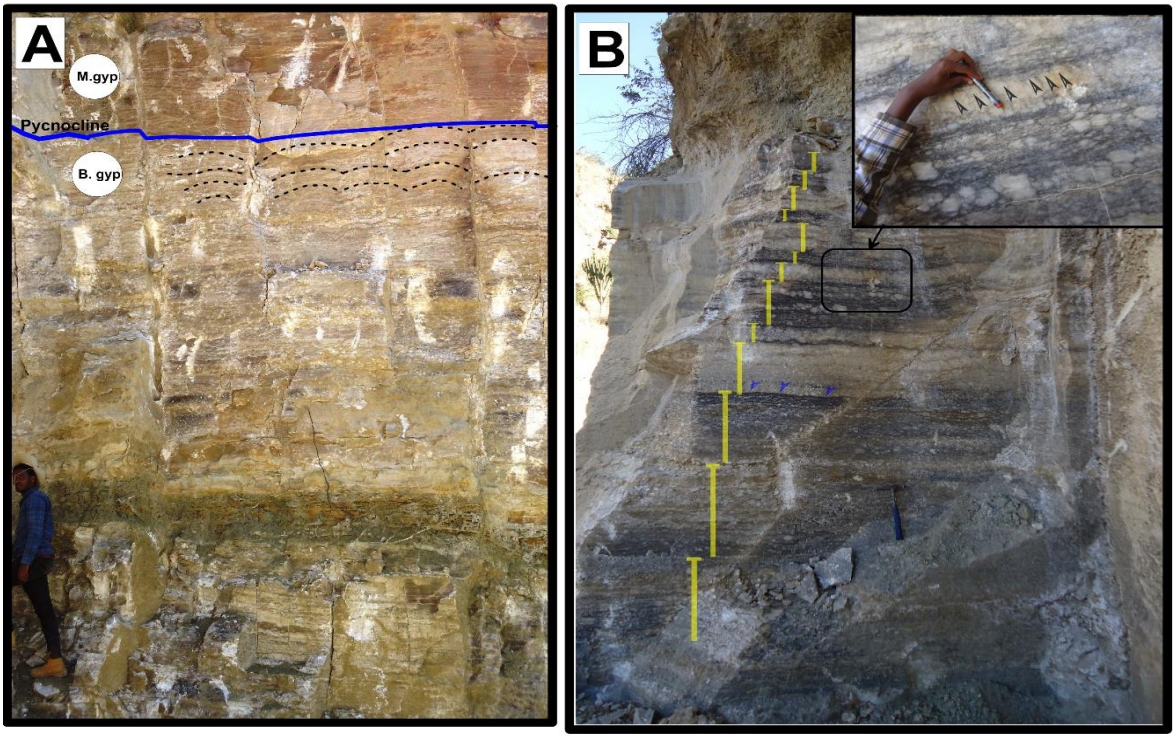

Figure 3.6.Aspects of laminated gypsum (**A**) Pycnocline (blue line) in laminated gypsum layer separating bent beds of bottom grown gypsum ghosts (traced by dashed lines) below and laminated microbial gypsum at the top; (**B**) Shoaling upwards facies in laminated gypsum along with a close up view showing gypsum ghosts forming pseudomorph after bottom grown crystals. The yellow bars indicate decreasing thickness of beds as a function of decreasing brine depth and increasing salinity. Magnified view of the outcrop (top left corner) showing gypsum ghosts (pseudomorphs) of bottom grown selenitic crystals indicated by the black arrow heads). The blue arrows indicate truncated and partly eroded surface between gypsum beds (indicative of subaerial exposure).

Nodular Gypsum Facies (Facies 5): this is the most dominant gypsum facies observed in all the measured sections. It exists both as thin and thick beds. The size of individual nodules vary from very coarse alabastrine gypsum forming chicken wire texture to sparsely distributed pebble sized nodules within a massive gypsum texture. This facies also shows both sharp and gradational contact with the laminated gypsum facies (figure 3.8). Alabastrine gypsum nodules are also found filling fractures and voids in other rocks such as siltstones and carbonates (figure 3.9, I). This facies especially dominates in the Jemma and Mugher sections. In some beds logged in the Gohatsion and Dejen sections, nodular gypsum is within carbonate mud rather than algal matrix.

The presence of coarse alabastrine gypsum nodules within thin algal lamella matrix along with lenticular gypsum nodules suggest primary sabkah origin (Warren and Kendall, 1985). However, Gindre-Chanu et al. (2015) suggested the formation of such textures as a result of diagenetic processes and may resemble 'primary' nodular anhydrite. Such processes include dehydration and transformation of primary gypsum due to burial or shallow telogenetic processes influenced by pervasive fluid flow or as an end product of sulfate rich water precipitation resulting from dissolution of halite beds in a deep burial environment. The absence of diagnostic features such as pseudomorphs of halite or any halite bed makes the last hypothesis unlikely in the case of the observed facies.

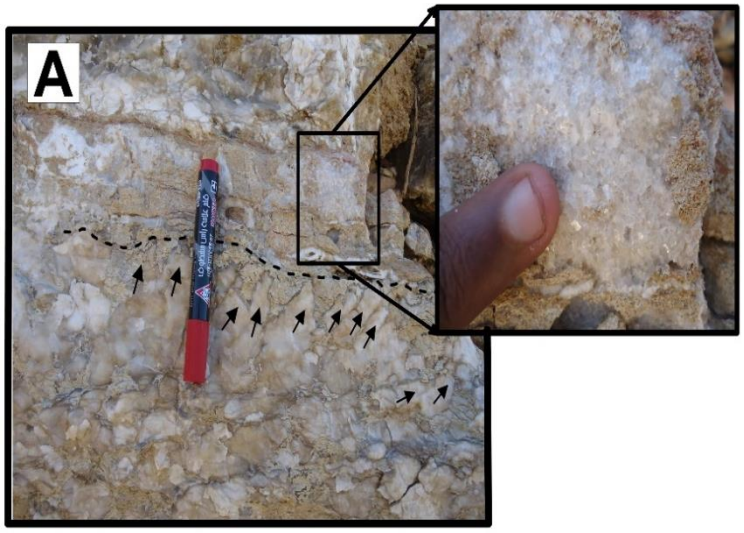

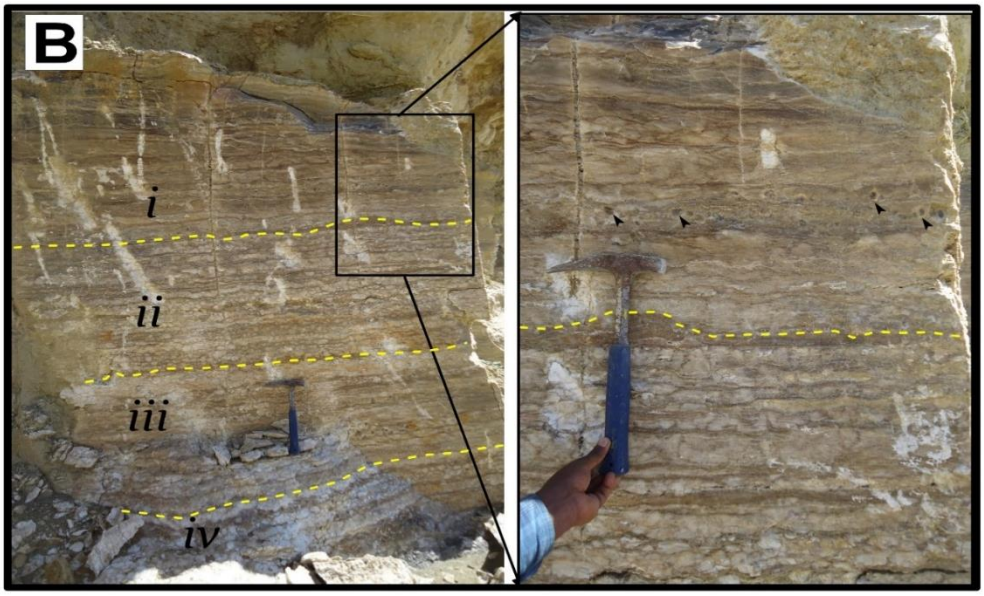

Figure 3.7. Laminated gypsum facies **(A)** 'Gypsum Ghosts', pseudomorphs after bottom grown gypsum crystals, crystal growth direction shown by black arrows; a close-up view of void filling selenite crystals (top left corner) hosted by calcareous siltstone in the Gohatsion Section; **(B)** typical laminated gypsum facies, microbial laminated gypsum marked by I, gypsum ghosts along with entrolitic gypsum beds marked by ii, secondary nodular gypsum with preferred horizontal growth (displacive growth) marked by iii and iv. Note that in the last two beds nodular gypsum shows increasing dominance. The black arrow heads indicate displacive daisy gypsum crystals.

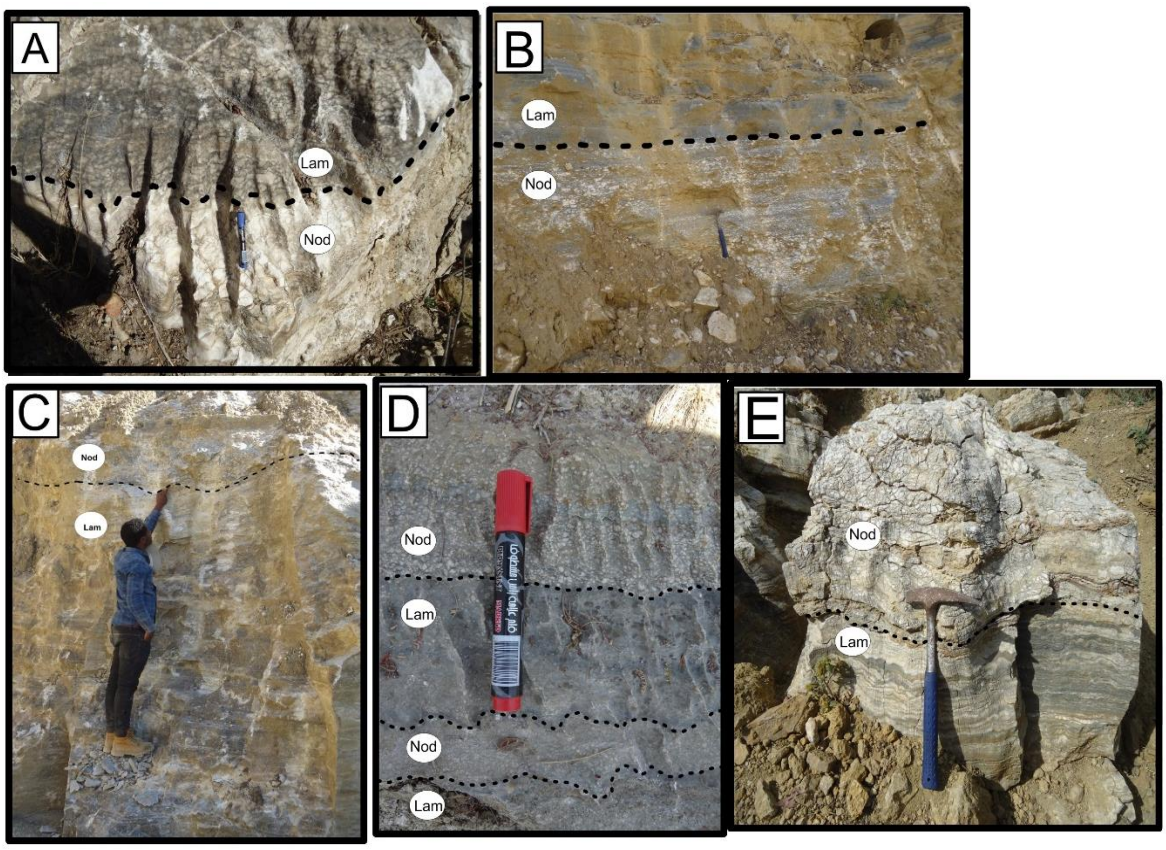

Figure 3.8. Relationship between nodular and laminated gypsum textures. (**A, B)** (Gohatsion section) and (**D)** (Dejen section) show gradational change from dominantly nodular to laminated whereas **C** (Gohatsion section) and (**E)** (Mugher section) show sharp contact between the two (probably erosive contact).

Clastic Gypsum Facies (Facies 6): this facies is rarely observed in the Mugher, Dejen and Gohatsion sections. Clastic gypsum consists of pebble to cobble sized gypsum (gypsrudites and pebbly gypsarenites as described in Matano, 2007) and siltstone clasts within gypsum cement matrix (figure 3.9, C & H; 3.11, A). In the Dejen section, clastic gypsum is observed inter-mingled with displacive nodular gypsum within carbonate cement matrix.

Clastic gypsum facies may form under high energy and shallow water gypsum brine conditions where the wave base can affect the brine column in which case very fine sand sized gypsum crystals can precipitate (Havorka et al., 2007). In addition, clastic (detrital) gypsum and other evaporite rocks can form under in situ dissolution and karstification (Alberto et al., 2007). The latter two conditions seem the likely processes in the study area, since the size of gypsum and associated silt clasts are dominantly coarser and are associated with siliciclastic sediments. In addition, the presence of post depositional slumps near clastic beds (figure 3.10, D & E) along with secondary displacive anhydrite nodules associated with clastic gypsum beds in the Gohatsion and Dejen sections can serve as proof for the karstification and ground water influence (possibly during telogenesis).

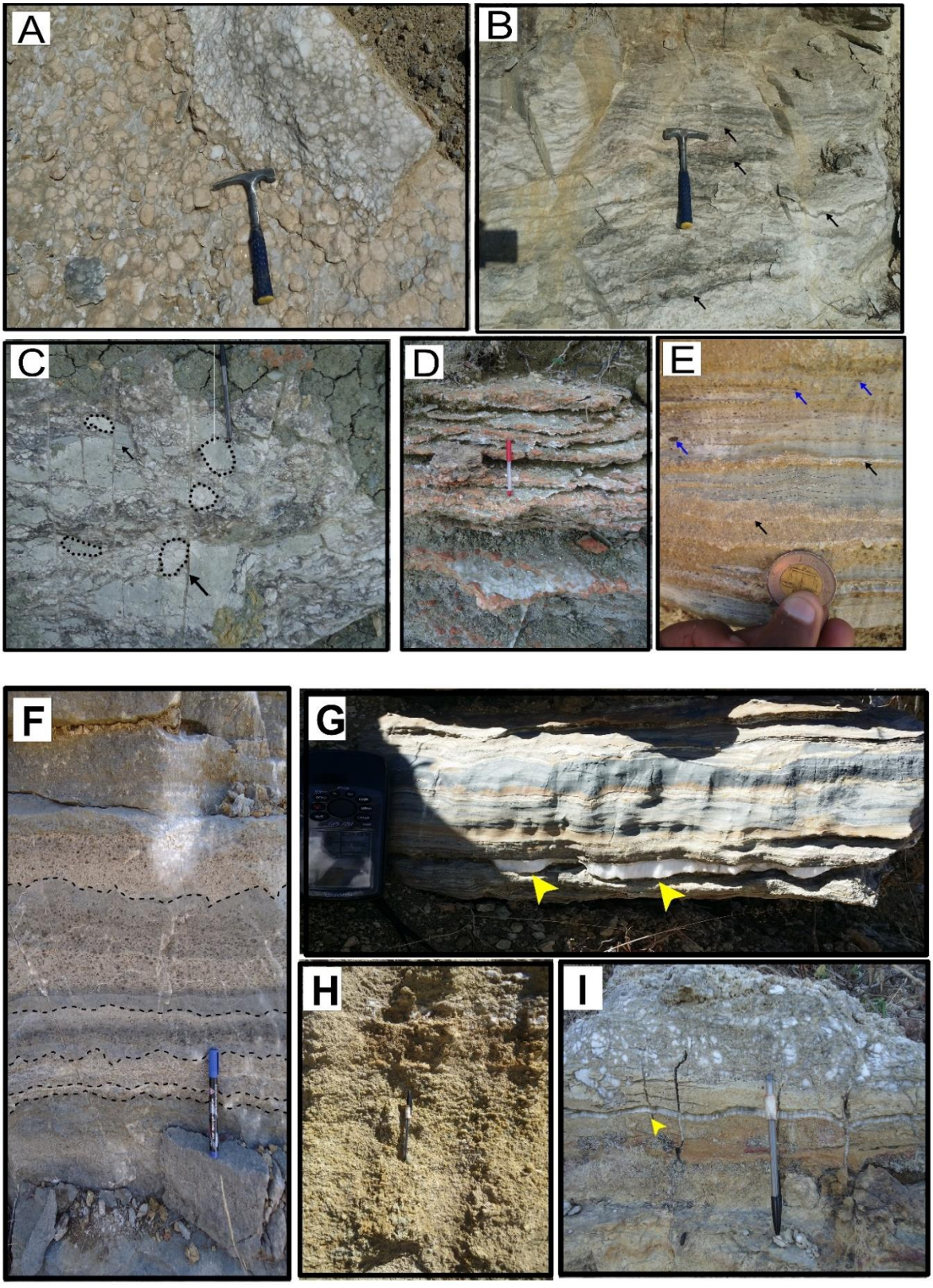

Figure 3.9. Lithofacies of the Gypsum Member: (**A**) Nodualr gypsum with coarse slightly pink alabastrine nodules partly within algal lamina matrix (Dejen section); (**B**) Microbial gypsum lamination shown by the black arrows (Gohatsion section); (**C**) Clastic gypsum with reworked gypsum and rare siltstone breccia (indicated by the black circles) and black arrows showing fracture filling secondary satin spar gypsum (Mugher section); (**D**) intercaltion of 'desert rose' gypsum with mudstone in the upper mudstone member near the contact with Gypsum Member (Gohatsion section); (**E**) Hetrolithic gypsum with laminated carbonaceous silt; the black

arrows show gyparenate laminations whereas the blue arrows showing secondary dispalcive lenticular gypsum crystals with a preferred orientation (Gohatsion section); (**F**) syndepositional soft sediment deformation forming flame structure in laminated gypsum (traced by the black dashed line), creating wavy bedding impression; most of the beds are affected by secondary lenticular dispacive gypsum crystals with preferred allingment (Gohatsion Section); (**G**) Hetrolithic gypsum affected by secondary fracture filling satin spar gypsum, shown by yellow arrow heads (Gohatsion section); (**H**) gypsiferous shale (gypcrete) in the Jemma section; (I) Siltstone affected by secondary alabastrine and satin spar fracture and void filling gypsum; possibly intra sediment gypsum precipitation by hyper saline pore fluids in phreatic zone (Gohatsion section).

Hetrolitic (intra-sediment) Gypsum Facies (Facies 7): as its name implies, this gypsum facies consists several types of lithologies including silt, sand, clay and carbonate laminations incrusted by gypsum. The term 'hetrolithic bedding' is used in describing inter-bedding between sand and mud laminations (Potter et al., 2005) but in this context, it is used to imply inter-lamination between siliciclastic and evaporite rocks. This facies manifests itself in the Gohatsion, Dejen and Mugher sections, where thin to thick beds of laminations of the above mentioned rocks are exposed. In the Gohatsion section beds of this type also showed intense soft sediment deformation (figure 3.9, E & G; 3.10, C).

Siliciclastics inter-bedded with evaporite rocks are indirect indicators of fluctuating water depth in a brine pool (Hovorka et al., 2007). It also signifies subaerial exposure. Siliciclastic input may also be aeolian since majority of the clastic particles are very fine sand to silty clay. Interlamination of siliciclastic sediments with evaporites also indicate seasonal flooding of a 'starved basin' (Hovorka et al., 2007), where flooding of a basin suppresses and 'starves' a basin of siliciclastic sediment input. Another possibility is that sediments may also accumulate as a result of sedimentation of insoluble material from a dissolving fluid via cavity networks in actively dissolving gypsum host within a vadose zone (Gindre-Chanu et al., 2015). Such process usually leaves thin irregular laminations at the base of re-precipitated gypsum layers, which seem to be the case in most of the beds that show this facies.

Massive Gypsum (Facies 8): this facies is rare in the logged sections. It shows no significant texture or internal bedding with the exception of the presence of alabastrine nodules noted in the Gohatsion and Mugher sections.

Although the origin of such facies is not well known (Boggs, 2009), massive gypsum or anhydrite presumably represents uniform conditions of depositions. It is also suggested that massive gypsum (rehydrated anhydrite) forms from a brine solution with salinity close to halite precipitation condition (Boggs, 2009 and references therein). The presence of alabastrine nodules and displacive gypsum crystals can be the effect of burial diagenesis and subsequent uplift and rehydration.

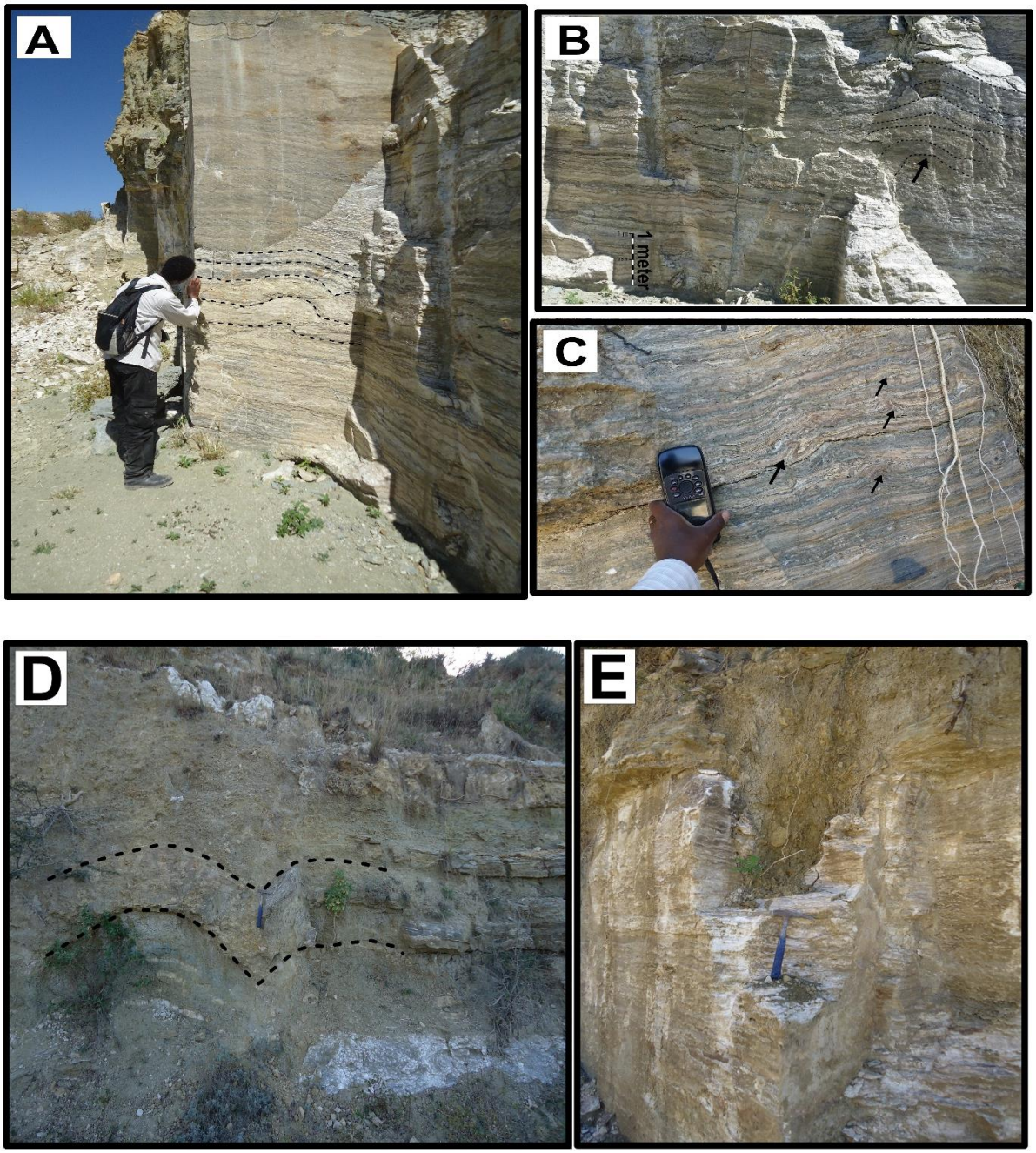

Figure 3.10. Soft sediment/ syn to post depositional structures. (**A&B**) Tepee (pressure ridge) structures in laminated gypsum [A] and microbial gypsum [B] indicated by black dashed lines and an arrow (Gohatstion section); (**C**) soft sediment deformation and folds (shown by the black arrows) in hetrolithic gypsum bed (Gohatsion section); (**D &E**) local slumps and dissolution cavities filled by the overlaying sediment results of post depositional dissolution and localized karstifiation (Gohatsion and Dejen sections respectively).

Other minor facies of Gypsum and associated rocks (Facies 9): minor gypsum facies observed in all measured sections include secondary gypsum growth structures such as veins dissecting all rock types filled with satin spar gypsum, displacive gypsum growth structures in laminated and nodular gypsum beds, secondary selenitic gypsum crystals filling veins and void spaces within silt (figure 3.9, G & I), carbonate and gypsum beds (in the form of intra sediment

evaporites). In the Dejen section, microbial laminated carbonate bed (figure 3.12, A) was observed along with voids filled by gypsum and carbonate mud forming geopetal botryoidal gypsum crystals were observed (figure 3.11, B).

Pediogenic gypsum and gypsified shale are also found interlayered with gypsum beds. Dolostone in the Gohatsion and Dejen sections also show fenestral and vuggy fabric whereas in the Mugher section, dolomites become more fossiliferous. Apart from this, paleokarst features and localized slumps were observed in the Gohatsion section (figure 3.10, D & E).

Syn-depositional intra sediment evaporites often form replacive and displacive nodular anhydrite and gypsum from hyper saline pore fluids in the capillary and upper phreatic zone (Warren, 2006). Secondary gypsum textures may also develop during post depositional stages (Warren, 2006; Gindre-Chanu et al., 2015). Voids and fractures filled with secondary satin spar gypsum are indicative of the end of burial diagenesis and the beginning of telogenesis (uplift) (Warren, 2006). Fibrous gypsum (satin spar) grow in brine filled veins induced by hydraulic fracture during various stages of exhumation (Tucker, 2011; Warren, 2006). In areas where voids and intragranular porosity formed by prior dissolution, displacive daisy gypsum crystals may also grow (Gindre-Chanu et al., 2015).

As described earlier, pediogenic gypsum forms within semi-arid soils in areas surrounding saline water bodies (Aref, 2003). According to Warren (2006), two of the mechanisms for the formation of pediogenic gypsum include an oceanic aerosol source creating sulfate rich precipitation and detrital wind reworking or in-situ oxidation of sulfide minerals. The former mechanism has typical associations with sabkha, playas and semi-arid and desert settings. Regarding the study area, the former mechanism seems likely since this facies is laterally extensive.

Dolomite and subordinate limestone beds show variety of facies (figure 3.12). The presence of fragmented partly marine fossils indicates subtidal origin (Matter, 1967); whereas the presence of microbial structures along with fenestral and ribbon structure indicate intertidal to supratidal setting (Matter, 1967; Warren, 2006). Microbialites are biogenic structures created by microphytic algae or cyanobacteria and are commonplace in evaporite strand zones (Warren, 2006).

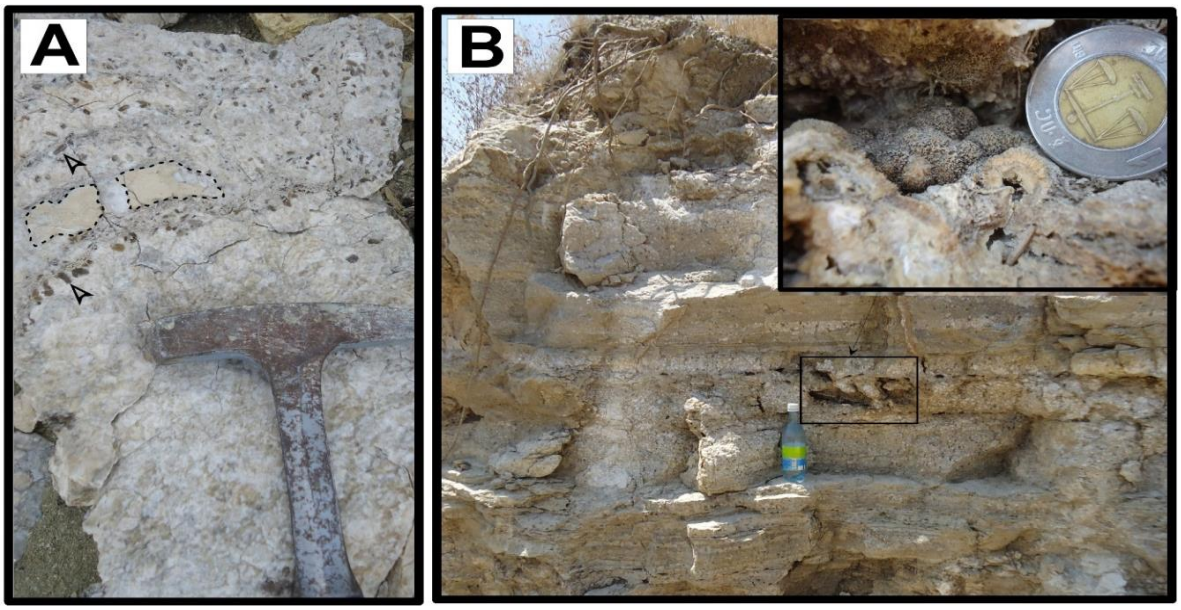

Figure 3.11. Telogenetic footprints on gypsum (**A**) alabastrine gypsum also hosting limestone intraclast breccia (marked by dashed lines) also affected by displacive daisy gypsum crystals indicated by arrowheads (Mugher section); (**B**) a quarry outcrop showing clastic gypsum affected by displacive nodular anhydrite and cavities filled by daisy gypsum crystals also forming botryoidal habit (close up photo on the corner represents the box in the large photo) (Dejen Section).

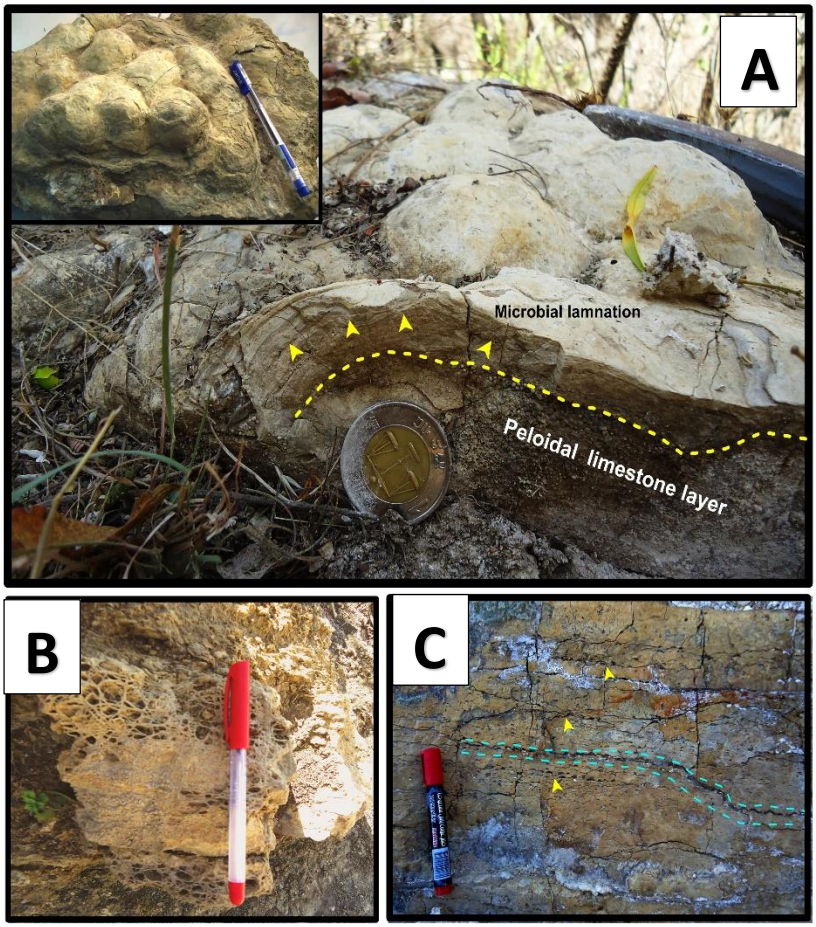

Figure 3.12.Various attributes of Dolomitic limestone: (**A**) cross section view of microbial laminated carbonate from Dejen Section; top view shown at the top left corner. The yellow arrow heads indicate traceable microbial lamina underlain by peloidal limestone layer (**B**) vuggy dolomite bed having interconnected and erratic voids results of diagenetic degassing and dissolution (Gohatsion Section); (**C**) fenestral dolomitic limestone (fenestre showen by yellow arrow heads) also showing ribboned (traced by cyan dashed lines) texture indicative of subaerial exposure (Gohatsion section);

3.2.3. Upper Mudrock Member

This group represents a repetitive intercalation of mudstone, shale, siltstone and claystone with subordinate beds of carbonate and gypsum. This unit is categorized into 3 major lithofacies groups at an outcrop and hand specimen scale.

Mudrock-carbonate facies (Facies 10): this facies is recognized near the contact with the overlaying carbonate unit. In the Gohatsion section, this facies is characterized by micritic and partly fenestral limestone inter-bedded with marl, variegated shale and calcareous mudstone (figure 3.13, A). Mudstones also show irregular thin beds and laminations of claystone and siltstone. Siltstones also show coarsening upward sequence.

In the Dejen section, this facies is characterized by an intercalation of chertified and micritic limestone with marl and undifferentiated shale and mudstone. Shale and mudstone beds also show localized slumping which was also observed in the Mugher section, where mudstone beds have irregular to parallel laminations of claystone within them. In the Jemma section, this facies is represented by alternation of fossiliferous limestone, marl and partly calcareous shale and silty mudstone. Within this intercalation, siltstone also shows wavy and lenticular bedding along with longitudinal wave dominated ripples and fining upward sequence.

Irregular alternations of marine carbonates along with continental sediments such as mudrocks can be interpreted as a periodic or seasonal fluctuation of continental sediment flux under a broad and topographically low coastal environment, hence the irregular and wavy carbonate and mudstone intercalation (Getaneh Assefa, 1981; Potter et al., 2005). The interbedding of carbonate and fine siliciclastic rocks can also happen in deeper water sub tidal environments (Tucker, 2011). The localized slumps also indicate mass transport in the form of debris flow or slides. Such facies prograde into a carbonate dominated sequence indicating increasing marine influence possibly happening on a prograding broad shallow marine setting.

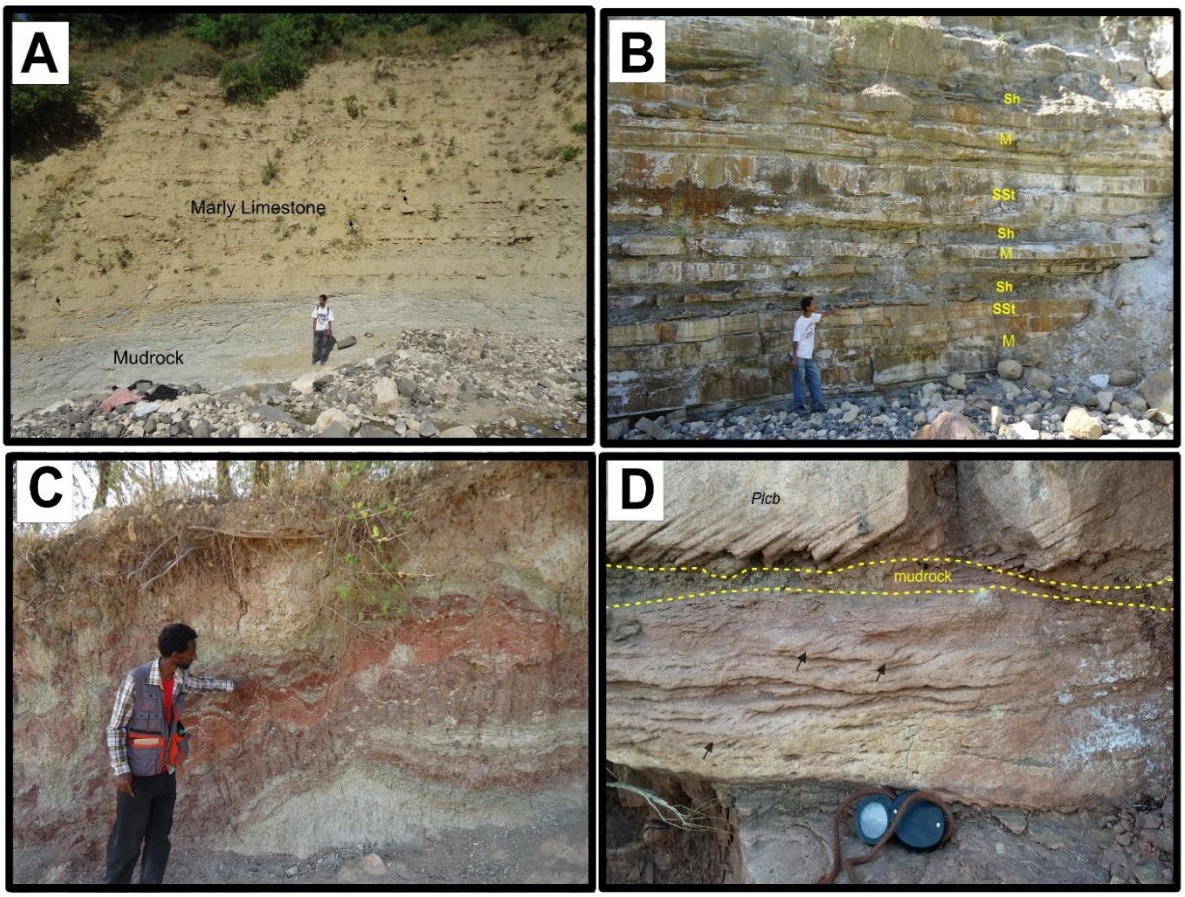

Figure 3.13. Nature of contact and aspects of Mudrock members: (**A**) Gradational contact between the Upper Mudrock Member and Antalo Limestone unit represented by marly limestone beds in the Gohatsion section; (**B**) River gully outcrop of Lower Mudrock Member near the contact to the Adigrat Sandstone, showing tidal bedding [Sh]-shale, [sst]-Sandstone, [M]-mudstone; (**C**) An outcrop of Upper Mudrock Member showing local slumps near the contact to Antalo limestone; (**D**) various bed forms shown in sandstone bed inter-bedded with thin mudrock near the contact with Adigrat Sandstone; the upper sandstone bed shows planar cross-bedding (Plcb) whereas in the lower horizon, migrating ripples can be observed as shown by the black arrows, indicating typical sand flat or sand bar deposit.

Shale-Mudrock facies (Facies 11): unlike the first facies, this facies is dominated by very fine siliciclastic sediments. In the Gohatsion section, this facies is represented by alternation of variegated shale, calcareous massive mudstone and subordinate siltstone. The siltstone shows fining upward sequence. At hand specimen scale, interlamination between siltstone, claystone and mudstone show irregular to parallel lamination with fining upward bedding. Claystone lamination within this bedding also show flame structure and rip up clay balls suspended within mudstones (figure 3.14, C).

In the Dejen section, this facies has similar attributes described in the Gohatsion section. On the other hand, in the Jemma section this facies is slightly different and additionally contains some highly calcareous mudstone beds and gypsiferous shale. Gypsiferous shale is also found interlayered with desert rose gypsum at the top which resembles to that of Facies 3. But the

difference is the dominance of very fine siliciclastic unit when compared to facies 3. In a hand specimen scale, small scale wave ripples can be observed within some mudstone beds.

In this facies, dominance of mudrocks containing irregular laminations of silt and claystone may indicate continental influence. Furthermore, the alternation between planar lamination, cross lamination, local scours, flame structures (suspension of mud by storms) and wavy lenticular laminations forming hetrolithic bedding suggest a broad mudflat setting influenced by seasonal river floods and weak tidal currents (Potter et al., 2005). In addition, the presence of silty mud associated with gypsum in the succession also suggests prolonged exposure and aridity that subsequently forms saline mud flats.

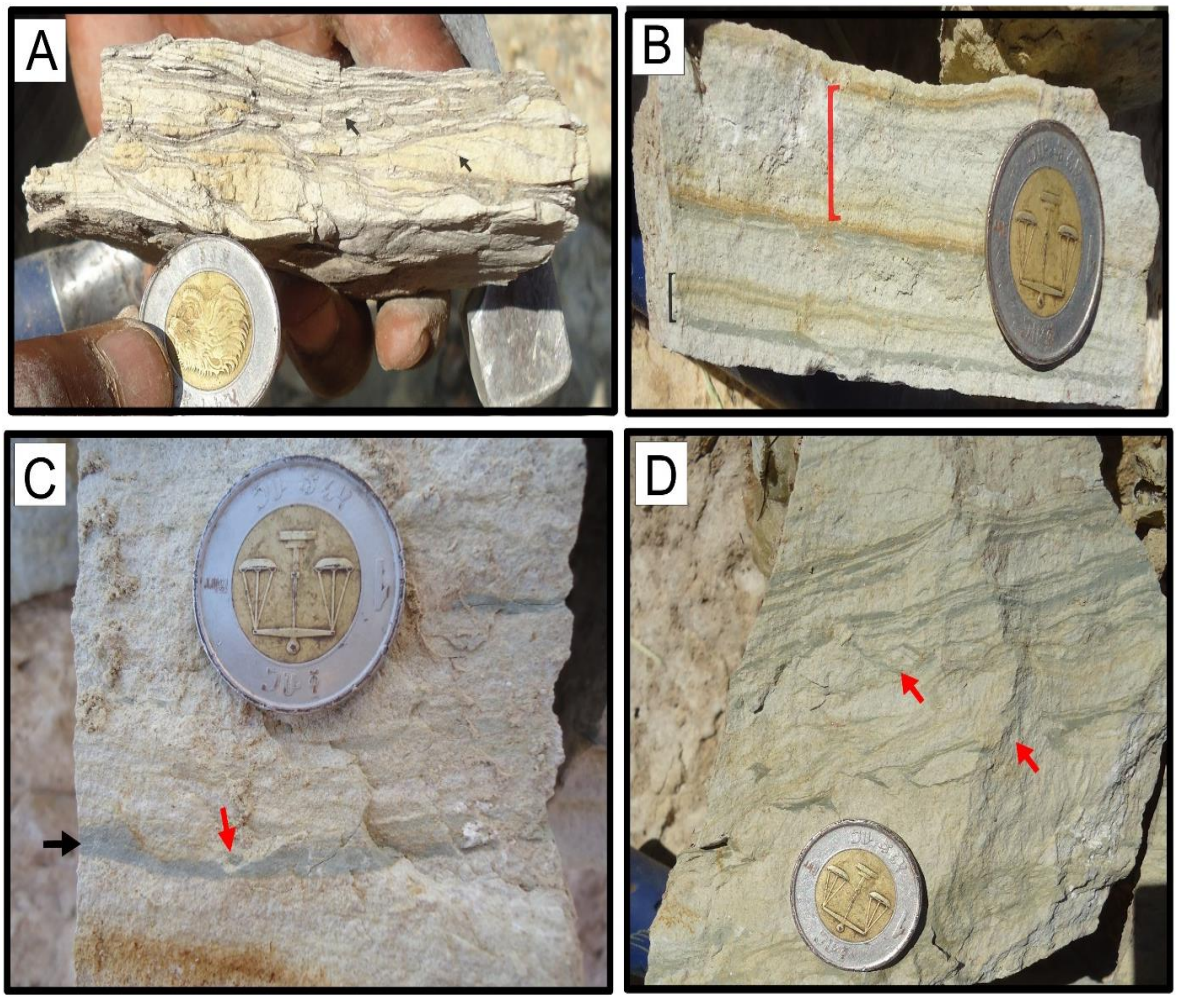

Figure 3.14. Lithofacies of the Upper Mudrock Member: (**A**) Hetrolithic mudrock form the Dejen section showing silt/mud copulates that show fading ripples, cross lamination and wavy/lenticular bedding; (**B**) Hand specimen from the Gohatsion section showing even silt/mud lamination (shown by red bar) along with sharp interlaminations with calcareous lamina and claystone at the bottom; (**C**) Claystone (shown by the black arrow) with a flame strucutre along with a clay ball (shown by the red arrow); (**D**) Disturbed claystone lamina in mudrock, indicative of bioturbation.

Shale-Gypsum Facies (Facies 12): this facies represents an alternation of shale and desert rose gypsum. In the Gohatsion section, dolostone beds are also intercalated along with shale and desert rose gypsum (figure 3.9, D). Subordinate intercalations of sandy siltstone and calcareous mudrock are also present within this facies. Similar facies assemblages persist in the Dejen, Mugher and Jemma sections, with very coarse desert rose gypsum becoming more dominant.

This facies represents a change in climate from restricted arid environment represented by the underlying gypsum facies to a productive coastal mud basin with humid climatic conditions.Warren (2006) noted the growth morphology of gypsum roseate crystals change under the influence of muddy and humic substrate and crystal habit modifying organisms. The absence of sand material within this unit, absence of fossil fragments or bioturbation, coupled with the presence of subaerial evaporite rocks may indicate supratidal condition.

CHAPTER 4:

PETROGRAPHIC, MINERALOGICAL AND GEOCHEMICAL ANALYSIS

4.1. Petrographic analysis

A total of fourteen representative samples from different horizons at the Gohatsion, Dejen and Mugher sections were selected for petrographic analysis. Two sandstone, one siltstone, four dolostone and calcitic dolostone (including one dyed), one limestone and five gypsum samples were analyzed. The thin sections are studied with the objective of deciphering petrogenetic and diagenetic history of the represented rocks.

4.1.1. Sandstone and siltstone

Sandstone: two sandstone samples from the Gohatsion and Dejen sections were analyzed. Both thin sections show poorly to moderately sorted texture with abundant autogenetic or detrital matrix (figure 4.1, A; 4.2, A & H). The main components of the sandstone include quartz, altered alkali feldspars (albite and microcline), plagioclase feldspar, biotite/muscovite, rock fragments, clay minerals, calcite cement and opaque minerals such as oxides and anhydrite crystals as accessory minerals (Table 4.1).

Table 4.1. Petrographic analysis of sandstone samples

Rock	Mineral	Modal proportion (%)	Texture
Sandstone	Quartz	58-62	Dominant mineral; found as monocrystaline or polycrystalline form; the polycrystalline quartz shows both sutured and concavo-convex contacts; Individual grains show sub angular to sub rounded morphology; in one sample, quartz grains along with other detritus are covered by poikilotopic autogenetic spari-calcite; micro cracks and undulose extinctions are common; in some quartz grains, the boundary between autogenetic quartz overgrowth and older detrital quartz grain boundary is marked by relic calcite precipitated prior to the formation of quartz overgrowth (figure 4.2, E & F)
	Alkali feldspar	3-7	Albite and microcline grains common but sparsely distributed; angular to sub angular with a few crystals having a well-rounded morphology; in one thin section, clay minerals dominate, and the feldspars are significantly altered; the alkalis

			are also zoned (figure 4.1, B) and display perthitic texture (figure 4.1, C)
	Plagioclase feldspar	4	grain shape and morphology similar to that of alkali feldspars
	Biotite/ Muscovite	0-9	Only observed in one thin section; show excellent birefringence with platy habit; generally aligned in a preferred orientation; Some of the crystals are deformed by protruding angular quartz grains (probably result of compaction)
	Rock fragments	1-8	Sparsely distributed in both thin sections, often formed form multiple quartz grains sutured together (in the form of Polycrystalline quartz) (figure 4.2, C); some rock fragments show prismatic crystals with random arrangements (figure 4.1, D) while other rock fragments in the calcite cemented sample show very fine components with partly oriented fabric (possibly shale or slate fragments) (figure 4.2, D)
	Clay minerals	1-15	Observed in one thin section only; found filling inter-grain boundary or as parts of rock fragments (figure 4.1)
	Calcite cement	>1-34	Observed as a dominant matrix in one thin section and as a subordinate filling in the other; in the former, it forms poikilotopic spari-calcite crystals that encompass other grains (figure 4.2, G & H); the grain contacts between calcite cement and quartz and feldspar grains are either sharp or protruded and leached (figure 4.2, B); in this thin section, well preserved feldspar grains can also be observed due to calcite cement hindering alteration
	Other trace minerals	>1	These include opaque minerals such as oxides that are found between grain boundaries and in the form of inclusions within quartz and feldspar grains. anhydrite crystal laths are also present in clacitic sandstone sample they are difficult to distinguish from biotite due to their higher interference color

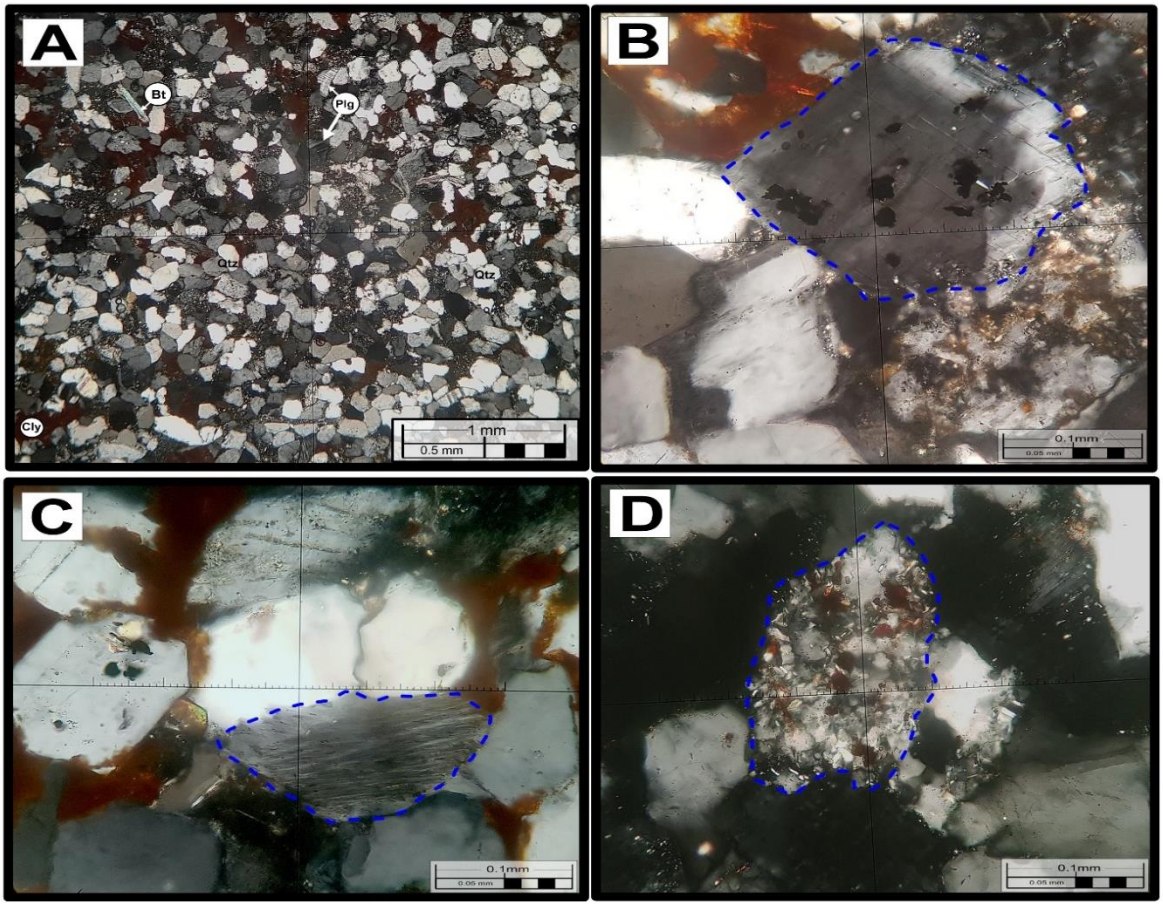

Figure 4.1. Photomicrographs of Sandstone from the Gohatsion section; (**A**) angular to sub rounded grains of quartz, feldspars and minor biotite surrounded by clay and subordinate calcite matrix. **(B**) 40x magnified plagioclase feldspar grain showing zoning; highly altered feldspar grain can also be seen at the lower left side of the zoned grain. (**C**) Perthitic texture in feldspar grain marked by the dashed blue line along with clay cement and quartz grains showing undulose extinction. (**D**) Rock fragment with polycrystalline quartz and feldspar laths showing random fabric; reddish lumps observed in the fragments are possibly results of feldspar alteration. The random arrangement of internal crystal fabric of feldspars suggest igneous origin.

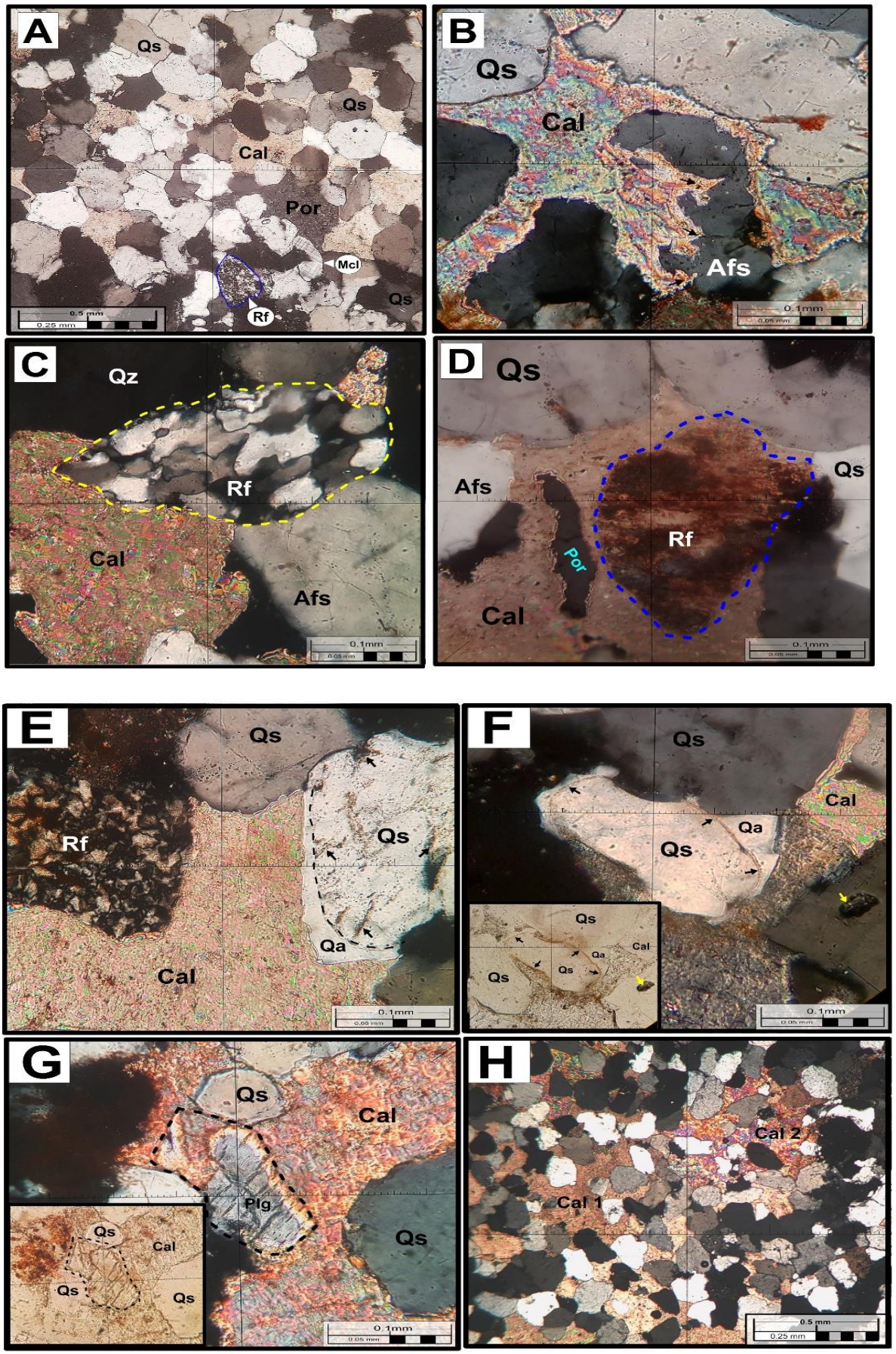
A
Qs
Qs
Cal
Por
Mcl
Rf
Qs
B
Qs
Cal
Afs
C
Qz
Rf
Cal
Afs
D
Qs
Afs
Qs
Rf
Por
Cal
E
Qs
Rf
Qs
Qa
Cal
F
Qs
Cal
Qa
Qs
Qs
Cal
Qa
Qs
Qs
G
Qs
Cal
Plg
Qs
Qs
Cal
Qs
Qs
H
Cal 2
Cal 1

Figure 4.2. Photomicrograph of calcareous sandstone from Dejen section. (**A**) A 10x magnified view of sandstone showing compacted and sutured sub angular to rounded quartz grains (Qs) along with calcite matrix (Cal), microcline (Mcl) and rock fragments (Rf). In the middle of the photograph, secondary porosity filled by the adhesive media (*Por*) can also be observed, **(B)** 40x magnified view of alkali feldspar grain shows an etched boundary relationship with calcite cement, the arrows show protrusion direction of calcite cement into the feldspar. **(C)** 4x magnified view of rock fragment with sutured and aligned quartz fabric indicative of metamorphic origin. **(D)** Rock fragment with an etched grain boundary and an unidentified minerals showing preferred orientation (possibly slate), notice the secondary porosity (*Por*). **(E)** Magnified view showing syntaxial quartz overgrowth (*Qa*); the older grain boundaries marked by the dashed line. Notice the presence of textural contrast between Qs and Qa; Qs is affected by early calcite leaching (indicated by the black arrows) whereas Qa shows no such texture. **(F)** Another example showing boundary relationship between syntaxial quartz overgrowth (*Qa*) and detrital quartz (*Qs*). The black arrows show contact line outlined by relic calcite. Bottom right corner shows plane polarized view while the yellow arrow shows dissolution pit in feldspar grain. **(G)** High magnification (40x) showing relic euhedral plagioclase crystal victim of autogenetic calcite replacement, bottom right corner: plane polarized view showing the euhedral shape of the crystal. **(H)** Photomicrograph showing two types of calcite cement that are different in texture (possibly due to different phases of autogenesis): '*Cal-1*' is the most dominant and has very fine and partly crystalline texture whereas '*Cal-2*' shows poikilotopic texture often leaching and replacing feldspar grains.

Although the four types of sandstone (quartz arenite, litharenite, greywacke and arkose) are typical to certain depositional environments, determining depositional setting is difficult primarily because of the effect of provenance on sandstone composition (Tucker, 2001). The analyzed thin sections fall under sub-arkose category (after Pettijohn et al., 1987). Grain morphology of both samples are angular to sub rounded which can be attributed to either lower reworking or proximal source. In both samples, the ratio of monocrystalline (Qm) to polycrystalline (Qp) quartz is high which is indicative of stable craton provenance (Tucker, 2001, Garzanti, 2016). The presence of microcline and plagioclase feldspar showing zonation and perthites along with sutured polycrystalline quartz grains is indicative of plutonic (intrusive) source (Tucker, 2001; Boggs, 2009). Sparse lithic fragments ranging from sutured polycrystalline quartz aggregates to fragments having undifferentiated but oriented grains along with grains having disoriented fibrous crystals are also indicative of mixed source between metamorphic and igneous terrains (Adams, et al., 1984), not surprising considering the fact that these sandstones were formed over the Precambrian basement which is dominated by metamorphic-plutonic associations.

Both samples seem to have passed through multiple stages of diagenesis. The presence of sutured contacts between quartz grains along with fractures indicate compaction, but such effect is often disturbed by poikilotopic calcite cement where the quartz grains seem to float on a calcite cement. Apart from detrital quartz grains, autogenetic quartz and quartz overgrowth textures also indicate early to late diagenesis, depending on their boundary relation with calcite cement. Overgrowth textures that predate calcite cementation tend to be corroded and affected by calcite cementation whereas quartz overgrowth post- or syn-calcite cementation tend to

show relict calcite inclusions aligned with the original grain boundary (e.g., Xiong et al., 2016; Yuan et al., 2017). In sandstone diagenesis, dissolution can also play an important role as it modifies primary porosity or creates secondary porosity. Dissolution of early calcite cement which forms acidic solution that etches grain boundaries of detrital materials will eventually re-precipitate to form secondary calcite cement; hence, difference in texture in calcite cements from different sites (figure 4.2, H) (Lonoy et al., 1986; Yuan et al., 2017). In sandstone diagenesis, replacement reactions often enable the transfer of material from grains to pore fluids or vice versa (Milliken, 2003). Pseudomorphic replacement of grain boundaries by calcite or other autogenetic minerals (eg ankerite) can also happen locally.

Siltstone: one siltstone sample was analyzed from the Gohatsion section. The thin section generally shows quartz dominated texture with major constituents such as quartz, alkali feldspar along with minor plagioclase feldspar, clay minerals, opaque minerals and muscovite.

Modal proportion of these minerals is difficult to estimate because of their very fine grain size. Typical sedimentary structure observed is graded lamination between coarse horizons dominated by quartz and feldspars and fine grained micaceous horizons dominated by micas and clay minerals (figure 4.3, A & B). Occasional lumps of clay are also observed along with void spaces (figure 4.3, C). Besides clay minerals, autogenetic calcite and quartz overgrowth serve as cementing materials. Alteration process makes sieved texture in most feldspar crystals.

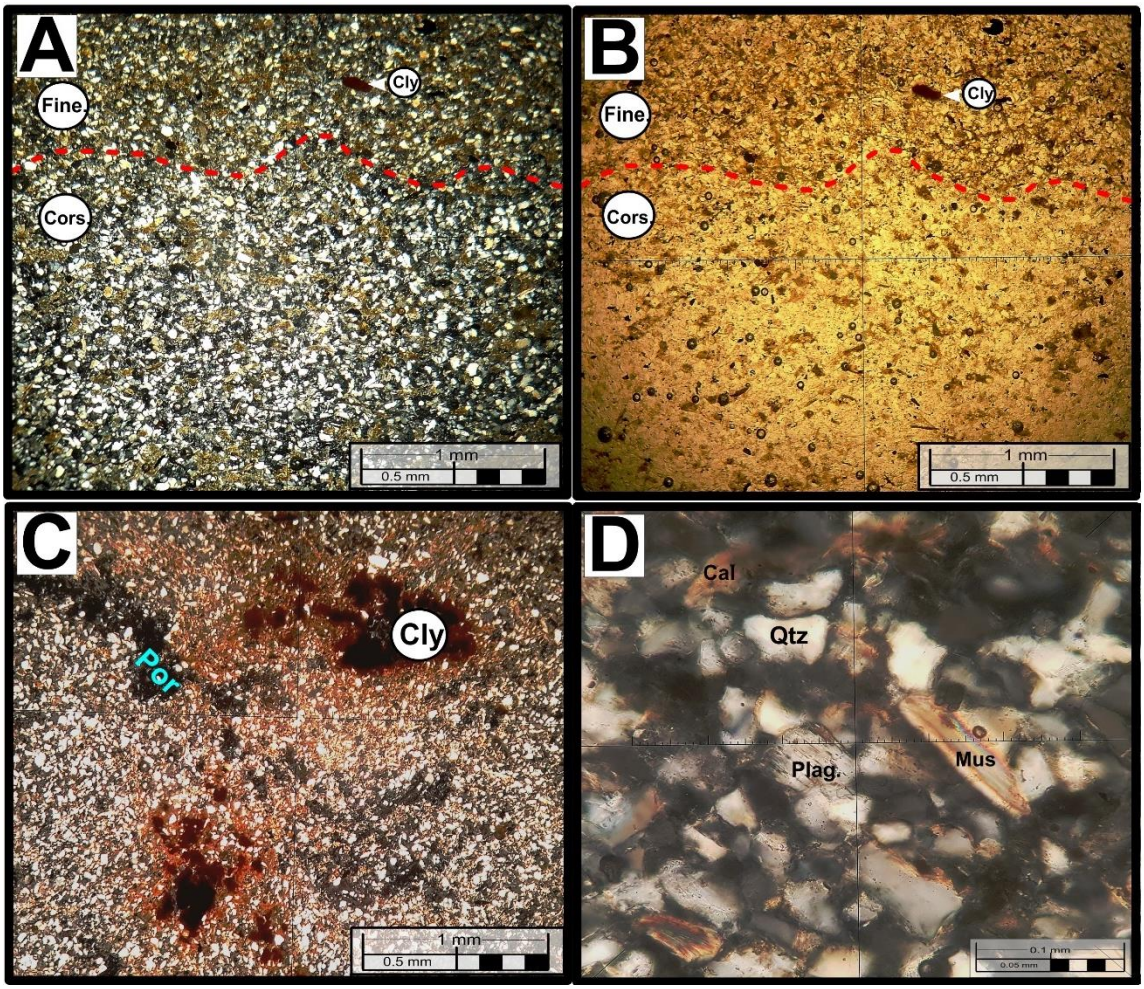

Figure 4.3. Photomicrograph of siltstone sample from the Gohatsion section. (**A&B**) 4x magnification showing graded lamination in XPL (A) and PPL (B); the two layers are marked by the red line, where the fine layer is dominated by clay and mica whereas the coarse layer is dominated by quartz and subordinate feldspars. (**C**) Lumps of clay distributed throughout the thin section along with intergranular porosity (*Por*). (**D**) 40x magnification showing different minerals such as quartz (*Qtz*), Micas (*Mus)*along with plagioclase (*Plag*) and subordinate calcite cement.

Similar interpretation can be attributed to siltstones as in sandstones regarding the presence of calcite cement, perthite texture in plagioclase feldspar, and overgrowth textures. Apart from this primary graded bedding is also observed and this could be related to fining upward sequence seen in macro facies of the rock.

4.1.2. Gypsum

Five thin sections were prepared from the Gohatsion, Dejen and Mugher sections. The main components observed are gypsum, anhydrite, calcite cement, microbial lamina, dolomite, clay balls and minor opaque minerals. The dominant gypsum texture is alabastrine but subordinate satin spar and selenitic gypsum crystals are also observed, in addition to some other textural variations.

Clacitic Gypsum: large (~1mm) porphyroblastic gypsum and microcrystalline, xenotopic alabastrine aggregates are observed within calcite matrix. Relicts of anhydrite crystals are also observed (figure 4.4, B). Some porphyroblastic gypsum crystals share leached grain contact with the surrounding calcite matrix (figure 4.4, B the yellow arrows). Network of satin spar veins interconnect different gypsum porphyroblasts and xenotopic alabastrine nodules. Displacive daisy gypsum crystals affecting the surrounding satin spar veins (figure 4.4, A), and clay balls floating in calcite matrix are also observed. The calcite matrix is partly crystalline (possibly rhombic dolomite crystals) and partly micritic.

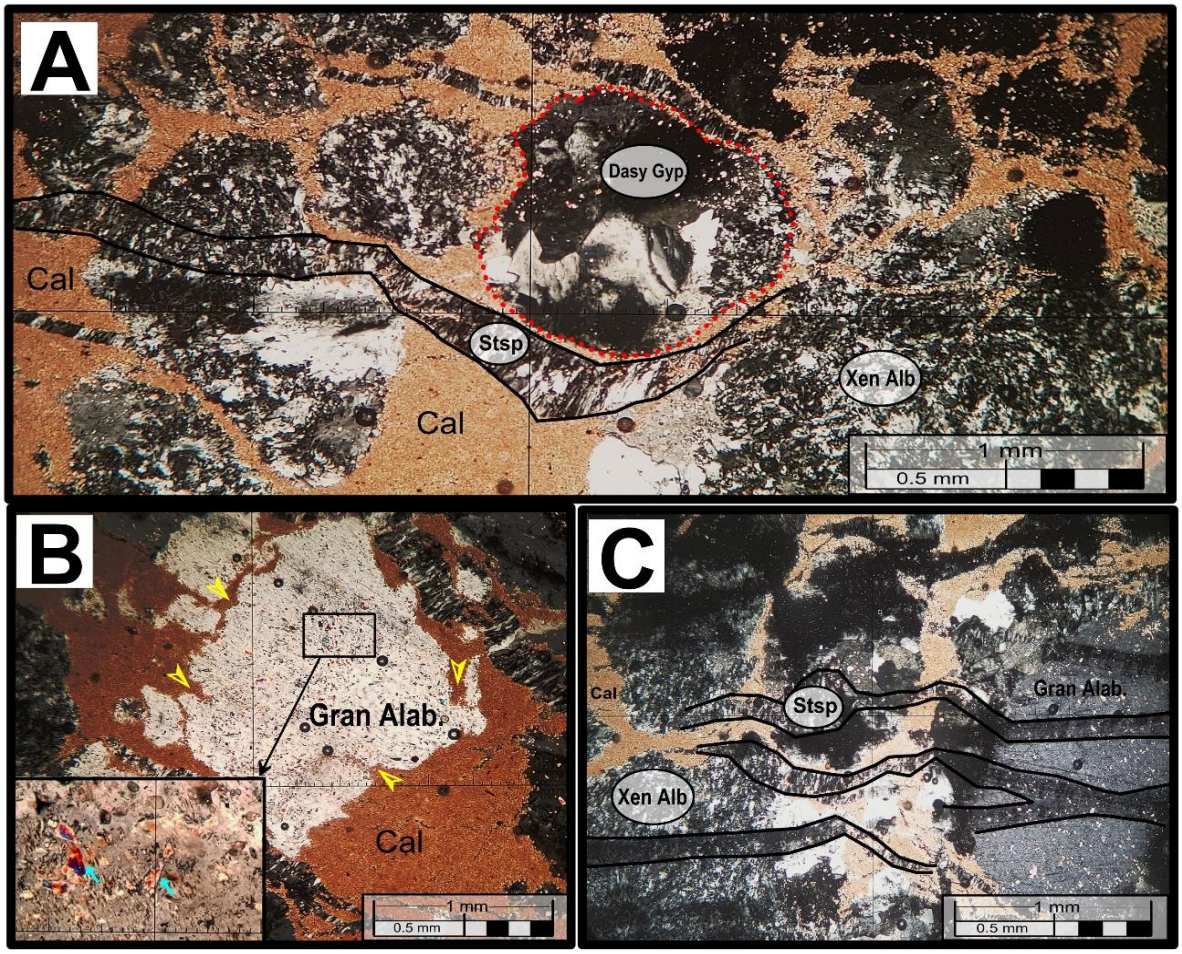

Figure 4.4.Photomicrograph showing attributes of calcitic gypsum. (**A**) Displacive daisy gypsum (*Dasy Gyp*) displacing a satin spar fracture filling vein (*Stsp*); alabastrine nodules (*Xen Alb*) show xenotopic texture within calcite cement matrix. (**B**) Granoblastic (porphyroblastic) gypsum with anhydrite relics (magnified view at the bottom left); boundary relationship with surrounding calcite matrix shows leaching indicated by the yellow arrows. (**C**) Network of satin spar veins cross cutting large porphyroblastic and xenotopic gypsum crystals.

Nodular Gypsum: in most of the analized thin sections, porphyroblastic replacive gypsum nodules covered by algal lamina can be observed (figure 4.5, A). The rest of the matrix is filled by fine xenotopic microcrystalline alabastrine gypsum fabric with random orientation. In some thin sections the two contrasting textures (porphyroblastic gypsum and xenotopic gypsum) are

zoned. Porphyroblasic gypsum crystals also show relic inclusions of anhydrite crystals with needle like habit, rare opaque mineral and calcite (or dolomite??) crystals. Network of anhydrite and gypsum laths with cross cutting microcrystalline xenotopic alabastrine fabric are also observed.

Nodular Anhydrite: is observed as a primary texture in one of the samples taken from the Dejen section. In this thin section, partly porphyroblastic and partly xenotopic anhydrite nodules within algal lamina matrix (figure 4.5, C) and a network of secondary alabastrine gypsum veins along with displacive porphyroblastic gypsum crystals are observed.

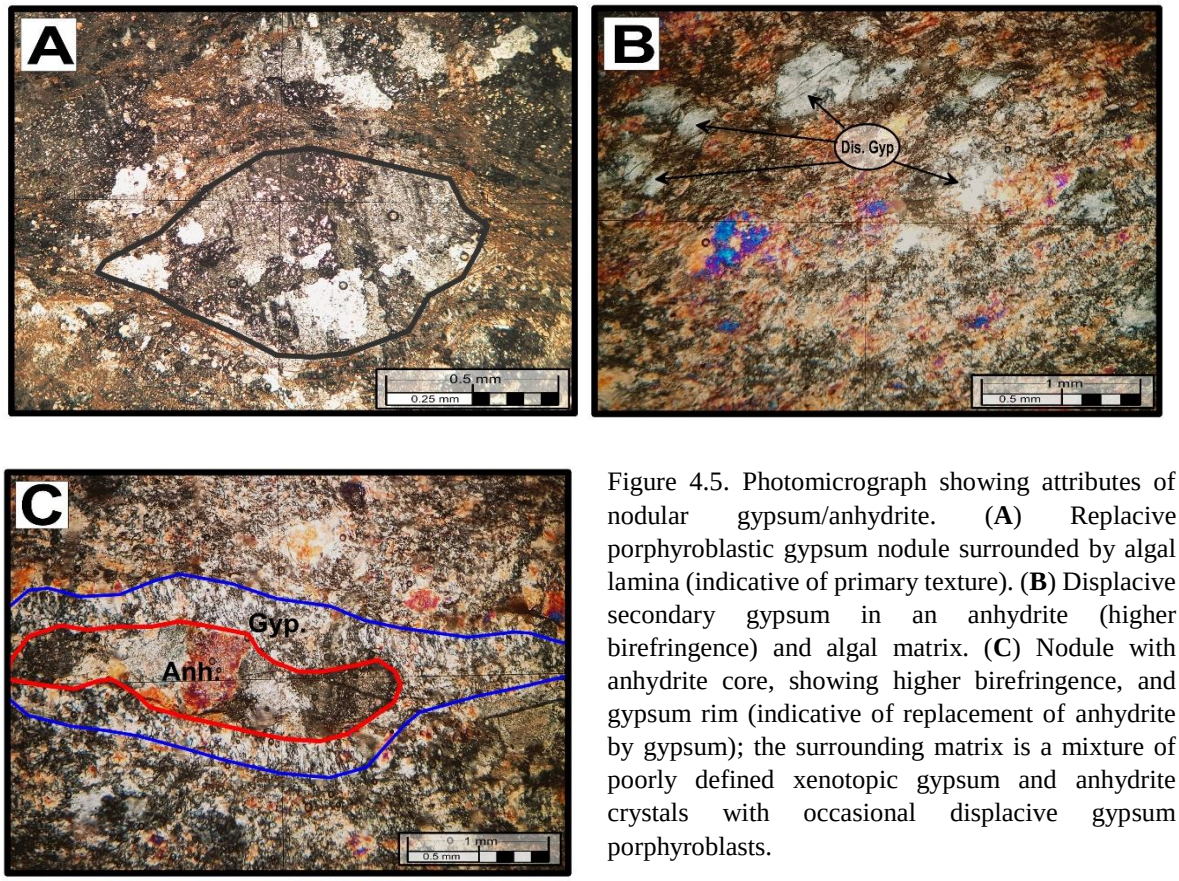

Figure 4.5. Photomicrograph showing attributes of nodular gypsum/anhydrite. (**A**) Replacive porphyroblastic gypsum nodule surrounded by algal lamina (indicative of primary texture). (**B**) Displacive secondary gypsum in an anhydrite (higher birefringence) and algal matrix. (**C**) Nodule with anhydrite core, showing higher birefringence, and gypsum rim (indicative of replacement of anhydrite by gypsum); the surrounding matrix is a mixture of poorly defined xenotopic gypsum and anhydrite crystals with occasional displacive gypsum porphyroblasts.

Selenitic Gypsum: though secondary selenite crystal growth is evident in almost all the analyzed thin sections, it is prominent in the sample from the Mugher section. In this thin section, the secondary selenitic crystals show a variety of fabrics including fracture filling equant mosaic of selenite crystals surrounded by carbonate mud (figure 4.6, D). The selenite crystals tend to form large, partly radiating crystals with nearly daisy like fabric. The crystals also form gradational to erratic contact with the surrounding microcrystalline alabastrine gypsum matrix (figure 4.6, A & C).

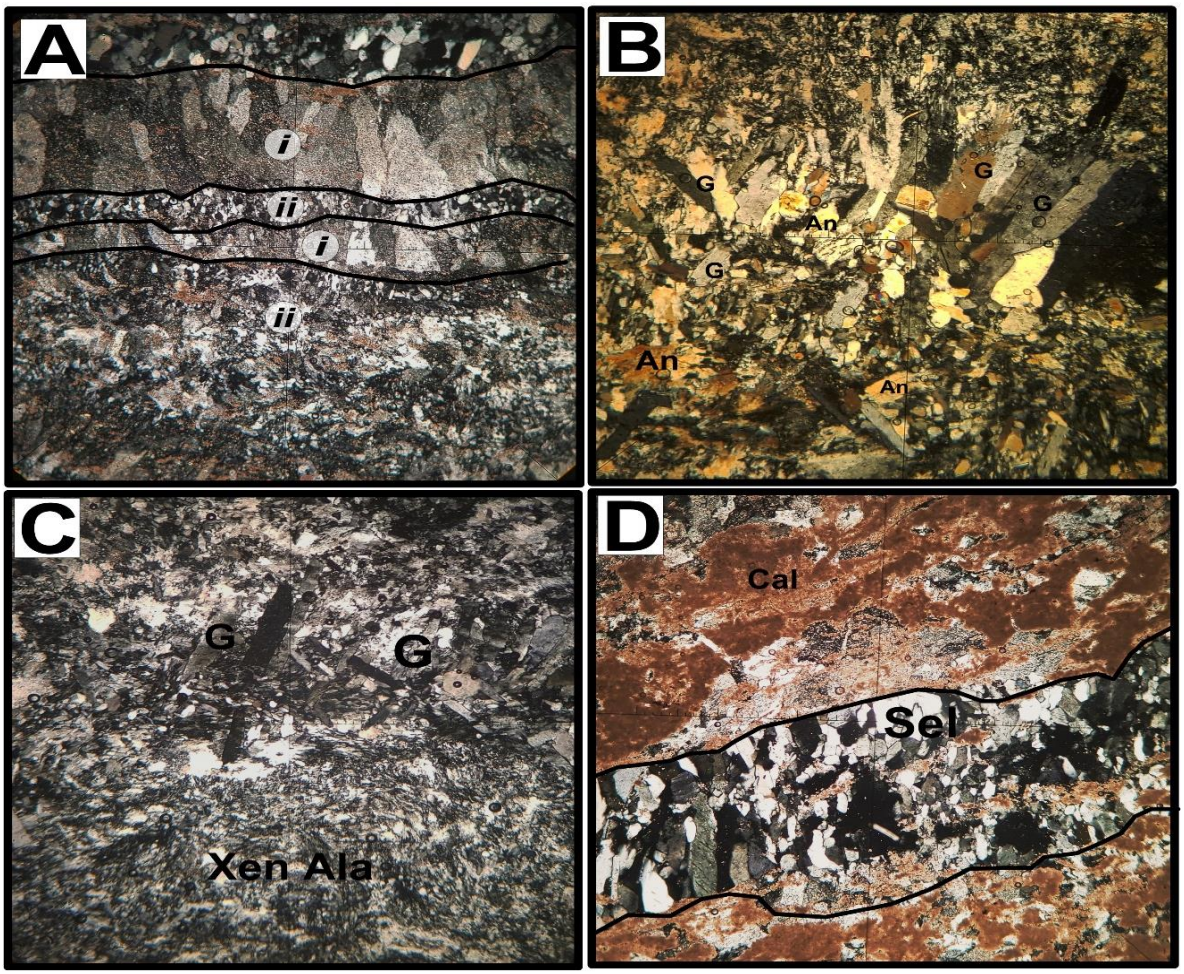

Figure 4.6. Photomicrographs of traits of selenitic gypsum. (**A**) Interlayering of radial roseate like selenitic crystals (*i*) and relatively fine equiangular granoblastic fracture filling selenite (*ii*) in a xenotopic alabastrine gypsum matrix. (**B&C**) secondary gypsum and anhydrite laths with semi-radial habit surrounded by granoblastic gypsum mosaic. (**D**) Fracture filling secondary selenitic gypsum with granoblastic texture surrounded by calcite matrix and secondary gypsum porphyroblasts.

It is often difficult to decipher primary evaporite textures of ancient evaporite deposits mainly due to the fact that evaporites undergo several diagenetic processes that alter the original texture. Nonetheless, careful observation reveals traces of textures that may give a clue to their origin. Although most of the alabastrine nodules observed in the thin sections show secondary growth (displacive growth), the presence of thin algal filaments surrounding coarse alabastrine nodules that also have anhydrite relics inclusions (figure 4.5, A) can be taken as indicative of primary anhydrite nodules formed under sabkha conditions (Warren, 2006). According to Aleali et al. (2013), microfacies analysis of evaporites (anhydrite and selenitic gypsum) from tidal flat and lagoon depositional environments may show lath shaped, acicular, equant and radial habit.

Gindre-Chanu et al. (2015) stated that formation of gypsum porphyroblasts and finer alabastrine, xenotopic gypsum mosaic happen in different hydration conditions of phreatic zone. The former forms by slow crystallization and near equilibrium hydration conditions under relatively stagnant phreatic zone (possibly when the rock passes under a stagnant aquifer during uplift) while the latter is formed under an active phreatic zone favoring rapid crystal growth. The presence of fluctuating dissolution and crystallization is also evident in: (i) etched grain contact between the gypsum nodules and porphyroblasts with the surrounding calcite matrix (figure 4.4, B), (ii) in relict anhydrite crystals within gypsum porphyroblasts that occur when abundant but slow leaching commences (Gindre-Chanu et al., 2015). The presence of various types of selenitic gypsum is also indicative of near equilibrium and slow hydration in isolated nucleation sites within pore spaces and fractures (figure 4.6, A). The presence of trans-granular fractures cross cutting each other and alabastrine mosaics (figure 4.4, C; 4.6, A &D) is indicative of both active and passive hydrological processes involving undersaturated water acting in episodes at different stages of uplift (Warren, 2006; Gindre-Chanu et al., 2015).There is also a possibility of forming satin spar gypsum at depth (perhaps at mesogenetic realm) sourced by overpressure and hyper-saline pore fluid waters (Shearman et al., 1972; Gindre-Chanu et al., 2015).

4.1.3. Dolomite and Calcitic Dolomites

Four representative thin sections were prepared from the Gohatsion, Dejen and Mugher sections. The samples range from dolomitic packstone to fine grained sugary calcitic dolomite (figure 4.7). Intraclasts observed in dolomitic packstone include bioclasts (bivalves and gastropods), ooids, peloids and rarely small fragments of quartz.

Fine grained calcitic Dolomite: this microlithofacies represents crystalline aggregates of dolomite with patchy micrite and rare clay patches. Dolomite crystals show anhedral to subhedral shape and xenotopic fabric. Void spaces irregularly and partially filled by dolomitic crystals are common. In some cases, rare secondary gypsum precipitation can also be observed (figure 4.7, C). Fine grained, sub-angular to angular quartz grains are dispersed in the matrix, while patchy micrites also envelope finer dolomitic crystals in specific spots. Spar calcite replacing the outline of shells of gastropods and elongated shapes (possibly fossil fragments) are also observed (figure 4.7, B).

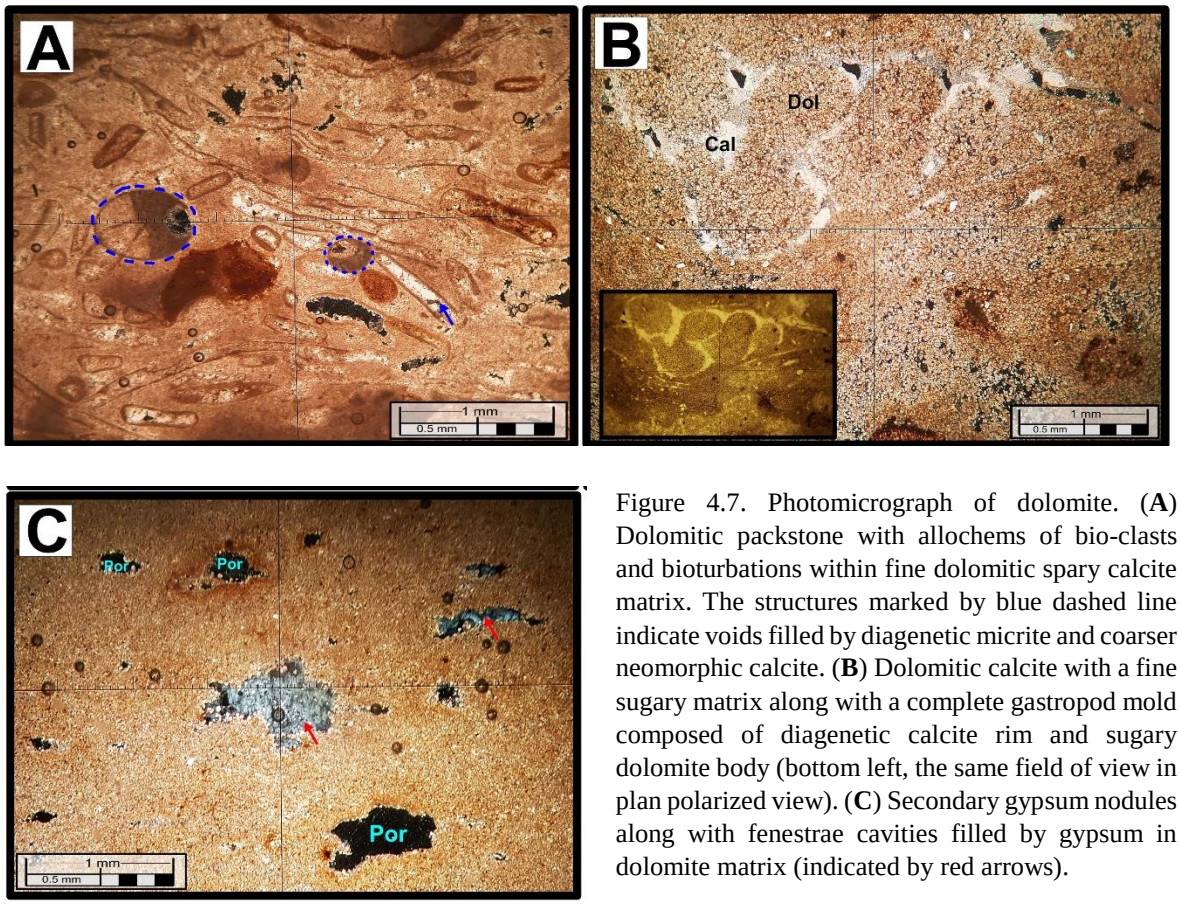

Figure 4.7. Photomicrograph of dolomite. (**A**) Dolomitic packstone with allochems of bio-clasts and bioturbations within fine dolomitic spary calcite matrix. The structures marked by blue dashed line indicate voids filled by diagenetic micrite and coarser neomorphic calcite. (**B**) Dolomitic calcite with a fine sugary matrix along with a complete gastropod mold composed of diagenetic calcite rim and sugary dolomite body (bottom left, the same field of view in plan polarized view). (**C**) Secondary gypsum nodules along with fenestrae cavities filled by gypsum in dolomite matrix (indicated by red arrows).

Dolomitic packstone: this microlithofacies represents a grain supported fabric full of peloids, bioclasts and occasional ooids. Bioclasts are highly affected by diagenetic process since the core of most bioclasts are replaced by neomorphic crystals (possibly calcite). The rims of these bioclasts have also been micritized. Calcite cement shows radial fibrous (isopachous fabric) habit along with micrite mud (figure 4.8, B). Some peloids and ooids show red stains, possibly indicating oxidized dolomite or clay inclusions. A close-up view of ooids showed their outer rings being completely micritized and their inner circles being replaced by fabric destructive idiotopic dolomitic crystals with the core showing red staining that possibly resulted from oxidization of dolomitic crystals (figure 4.8, D). One blue dyed thin section showed peloid grains having a ring of oxidized dolomite crystals, micritized rim and dull micritic matrix (figure 4.8, E). Heavily bioturbated zone with secondary drusy calcite fill and highly stained dolomitic patches are also observed (figure 4.8, F).

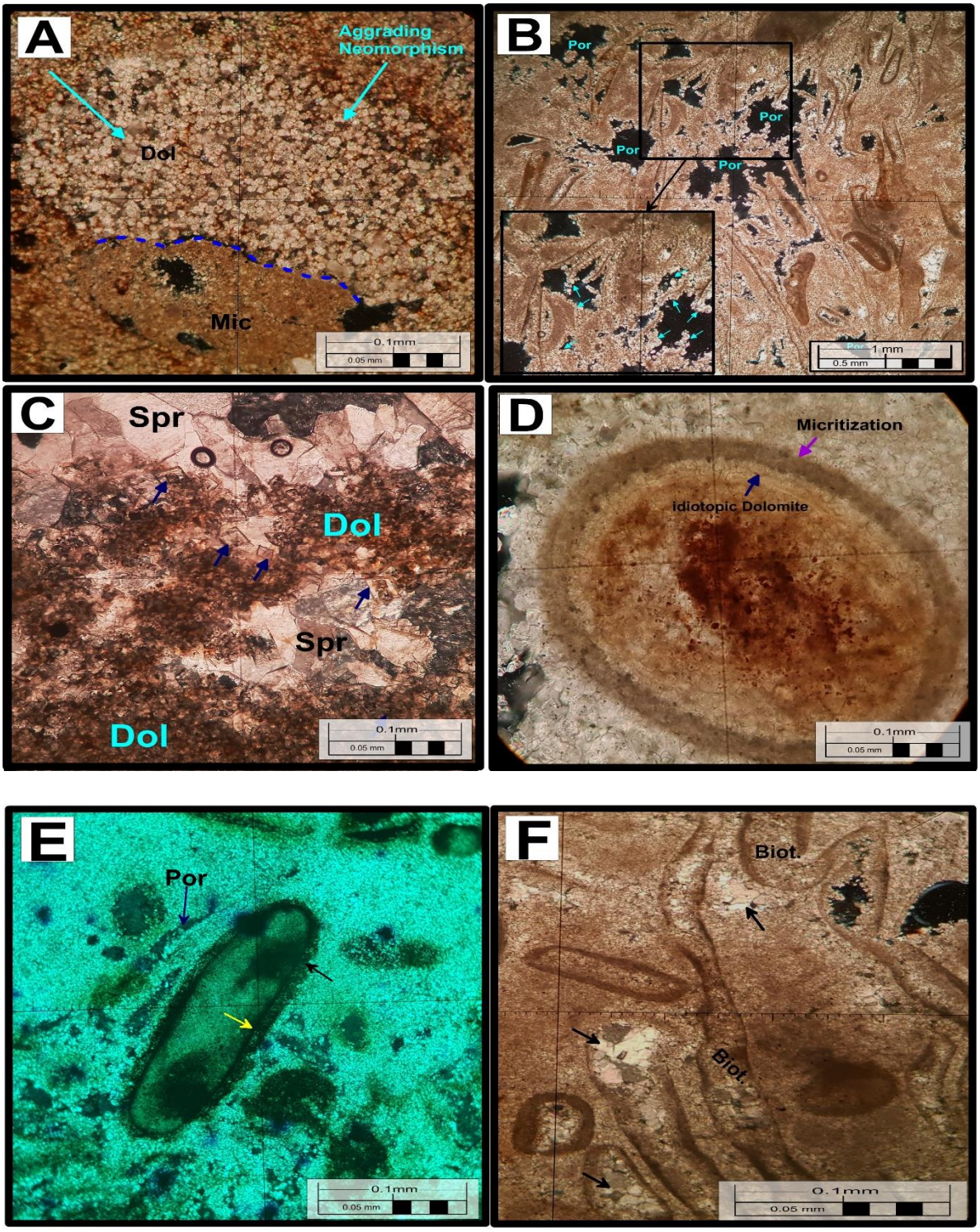

Figure 4.8. Photomicrograph of dolomite showing diagenetic textures. (**A**) 40x magnification of dolomitic limestone showing aggrading neomorphism (coarsening neomorphic crystals), as indicated by cyan arrows; the bottom part of the cavity is filled by micrite (*Mic*). (**B**) Dolomitic packstone showing isopacheous calcite cement attached to bioclasts within dissolution cavities (magnified and indicated by cyan arrows at bottom left corner). (**C**) Dolomite neomorphism (*Dol*) of cavity filling drusy calcite cement (*Spr*); dolomite rhombs indicated by blue arrows. (**D**) 40x magnification showing ooid with micritized rim; an idopatic dolomite (also mimetic) center of the ooid is red probably due to oxidation of dolomite. (**E**) Dyed thin section showing pelloid with micritized boundary (indicated by yellow arrow); in turn, covered by secondary calcite (fibrous

cements??). (**F**) 40x magnification of dolomitic packstone showing intraclasts and bioturbations filled by secondary blocky calcite cements (indicated by arrows).

Carbonate diagenesis can take place at different stages and locations of the rock's history, ranging from near surface and marine diagenesis to meteoric diagenesis and at deep burial environments (Freeman, 1997; Tucker, 2001). Marine diagenesis takes place in shallow and deep marine along with intertidal to supratidal zones. This process is marked by the presence of dissolution cavities, isopachous cement, and micritization along with anhydrite cementation (Tucker, 2001; Rahimpour-Bonab et al., 2010). Furthermore, Rahimpour-Bonab et al. (2010) also linked the presence of gypsum nodules and cavity fills as indicative of hypersaline diagenesis under salina to supratidal conditions. Meteoric diagenesis is associated with subaerial exposure during sea level lowstand in lagoon, shoal and offshoal facies. Since calcite is more reactive than dolomite in such conditions, dissolution cavities, drusy and blocky calcite cementation and calcite neomorphism is very common (Rahimpour-Bonab et al., 2010). Diagenesis due to burial causes replacive neomorphic dolomitization, minimizing porosity. In addition fenestric cavities also become flattened. Given that the analyzed samples show textural signatures form the above mentioned processes, the rock has undergone diagenetic process under hypersaline salina to sabkha settings in shallower depth and progressively affected by meteoric water introduced via groundwater system.

4.2. Mineralogical analysis

Mineralogy of three selected samples (two mudrocks from the Upper and Lower Mudrock Members and a gypsum from the Gypsum Member) was determined using semi-quantitative X-ray diffraction (XRD) analysis (table 4.2).

Table 4.2. XRD analysis result of selected samples (*quantitative results have been normalized to 100%, and it should be noted that the values represent the relative proportion of crystalline material in the sample. Total values greater than 100% are due to rounding errors*).

Minerals Detected	Sample codes		
	GS-2-3 (Gypsum Member)	GS-4-2 (Lower Mudrock Member)	GS-5-2 (Upper Mudrock Member)
Clay Minerals*	0	6	16
Palygorskite	0	7	5
Kaolinite	0	<1	3
Chlorite	0	0	1
Serpentine	0	0	1

Talc	<1	0	<1
Annite-Biotite-Phlogopite	0	2	5
Illite-Muscovite-Paragonite	0	18	28
Margarite group mica	0	0-	1
K-feldspar	0	1	4
Sodic Plagioclase	0	1	6
Alpha Quartz	2	24	19
Calcite	0	0	12
Dolomite-Ankerite	0	39	0
Anhydrite	8	0	0
Bassanite	74	0	0
Gypsum	15	<1	<1
Anatase	0	2	0

Amorphous material is abundant in the mudrock samples (estimated >20-25%). The gypsum sample contained less amorphous but crystalline material. The mineral bassanite in gypsum sample is slightly hydrated type ($CaSO_4 \cdot 0.6(H_2O)$). The mudrock samples contain micas in varying stages of alteration (hydromica) attributed to multiple stages of weathering/alteration. Their phases are quantified under the common name "*Clay mineral**". They are poorly crystalline with possible occurrence of zeolite and sepiolite. Polygorskite is not well crystalline and compositionally variable. Illite is also poorly crystalline and the associated muscovite is pengitic. K-feldspar is most likely microcline, and the sodic plagioclase closely resembles albite in composition. More than one distinct phase from the dolomite-ankerite solid solution series is also present.

The presence of high amount of quartz in the mudrocks may indicate their felsic source. The lower kaolin and higher amount of illite are indicative of diagenetic conversion of the former to latter. This observation is also shared by Getaneh Assefa (1979). According to this work, distribution of clay minerals in the Gohatsion Formation changes abrubtly form the underlain kaolinite rich sandstone formation to illite-chlorite dominant horizon. The formation of plygorskite and sepiolite in mudrocks may be indicative of high pH fluids rich in Mg occurring in pediogenic soils in arid climate with seasonal heavy rainfall and high evaporation rate (Golden et al., 1985; Xie et al., 2013). In the gypsum sample, the presence of minor quartz may

indicate continental brine influx besides marine water source. Large concentration of basanite in gypsum might suggest either the presence of basanite interlayered with gypsum in dissolution cavities and cave systems forming pseudomorphs after gypsum; or as a precursor phase of anhydrite and gypsum resulting from dehydration and rehydration related to telogenesis (Driessche et al., 2012).

4.3. Geochemical Analysis

4.3.1. Major element composition

Shales and Mudstones: analytical results of major elements from this study and comparative North American Shale Composite (NASC) (Gormet et al., 1984) and Post Archean Australian Shale (PAAS) (Cullers, 1995) values are listed in (appendix B).The major element compositions of shale and mudstones from different members show some variations. The average compositions of important major oxides in wt% are: SiO_2 (16.0-51.8, mean: 40.9), Al_2O_3 (3.1-16.2, mean: 11.9), Fe_2O_3 (2.1-9.8, mean: 6.23), MgO (3.3-15.8, mean: 7.3), CaO (0.9-23.2 mean: 7.9), Na_2O (0.1-0.3, mean: 0.2), K_2O (0.9-5.1, mean: 3.9), TiO_2 (0.1-0.9, mean: 0.7), P_2O_5 (0.1-0.2, mean: 0.1). The mean LOI value for the analyzed samples is 13.8% with the exception of one sample taken form the Gypsum Member having anomalously high value of 36.4%. This may be due to either higher content of sedimentary organic matter or mineral composition (eg. presence of carbon rich minerals like calcite) (Santisteban et al., 2004). SiO_2, Al_2O_3 values are similar to NASC and PAAS whereas significant depletion in Na_2O and enrichment of CaO and MgO values is observed (figure 4.10). Depletion of Na_2O may be related to ionic leaching during weathering and alteration of feldspars to clays whereas enrichment of CaO and MgO may be related to the calcareous nature of the rocks. A sandstone sample from the underlying Adigrat Sandstone Formation showed significant depletion in all major elements except in SiO_2,which is also the case in the Mekele Basin (Worash Getaneh, 2002), when compared with the mudrock samples and PAAS and NASC values (figure 4.10). This indicates higher degree of compositional maturity and the effect of sorting in the sandstones.

In a Log (SiO_2/Al_2O_3 vs Fe_2O_3/K_2O) plot (after Herron, 1988; Ejeh, 2016), the samples fall in the shale field (figure 4.9).

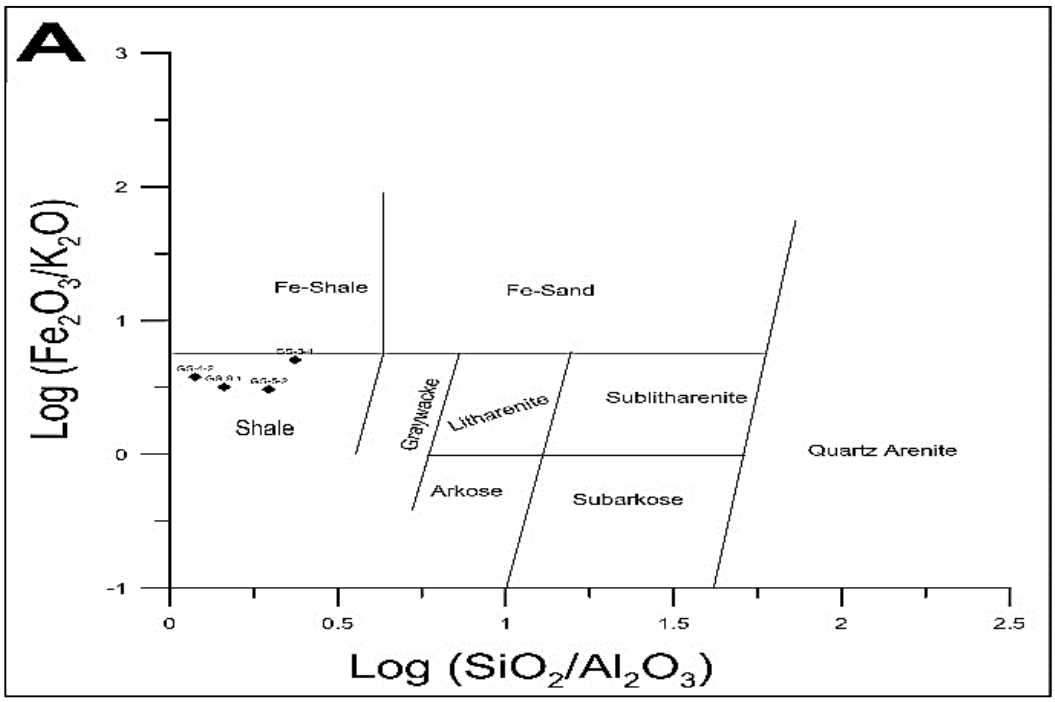

Figure 4.9.Chemical classification of mudrock samples (fields taken from Herron, 1988).

Gypsum and Limestone: in evaporite rocks (Gypsum), most major elements show very low concentration, while CaO is on average 31.4 wt%. The same trend can be seen in limestone sample taken from the Upper Mudrock Member (near the contact with the overlaying carbonate formation) with CaO values 37.7 wt%. Slight enrichment of MgO values (10.6%) also observed in this sample compared with evaporite and siliciclastic rocks. Enrichment in SiO_2 (5.11%) is also observed (figure 4.10).

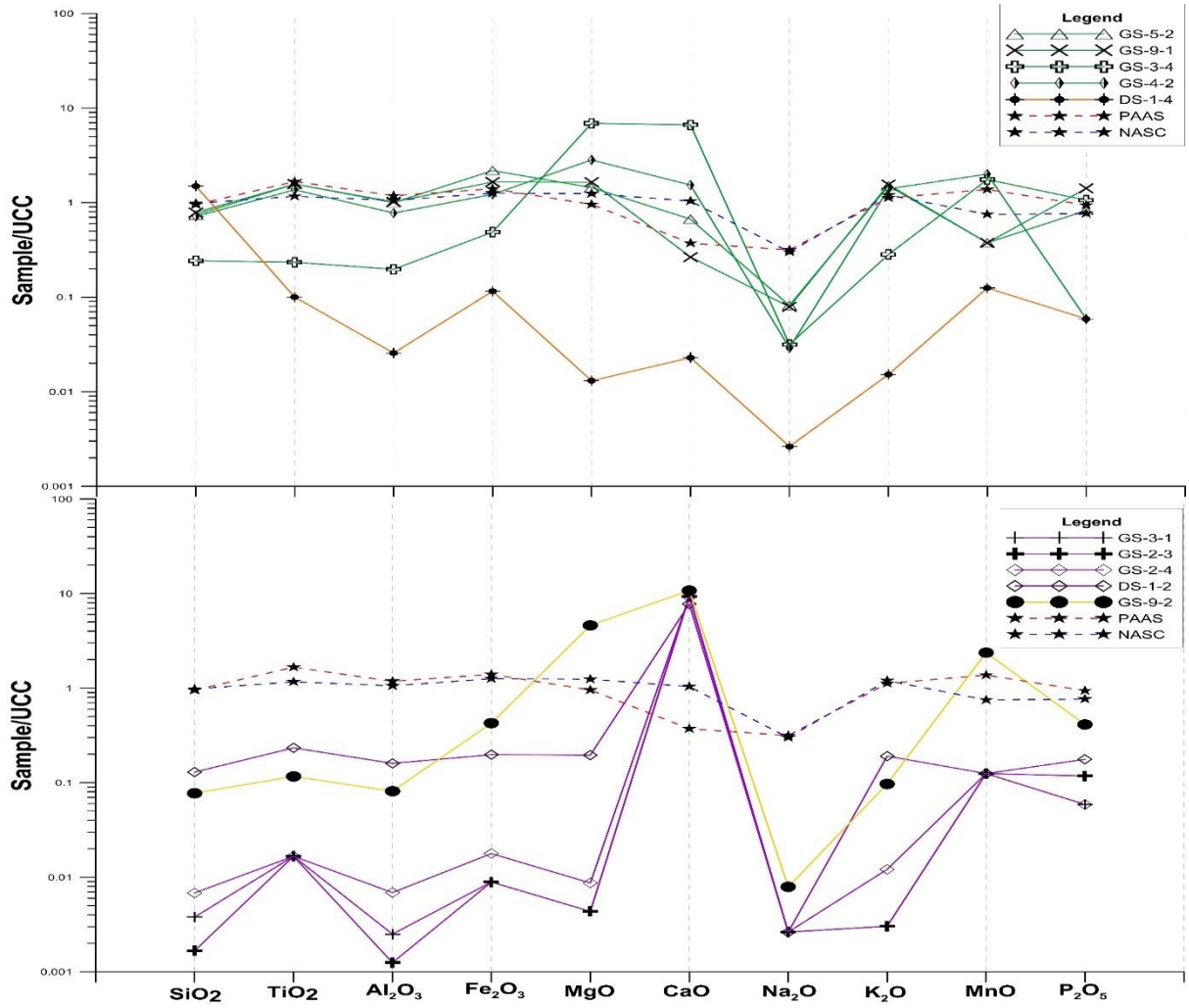

Figure 4.10. Major element oxide spider diagrams showing various attributes of the analyzed samples. (Top) UCC normalized major oxide distribution of mudrock (green lines) sandstone (brown line) samples; (Bottom) UCC normalized major oxide values for gypsum (blue lines) and carbonate (violate line) rocks. Reference values of PAAS and NASC after (Nance and Taylor, 1976) and UCC after (Taylor and Maclennan, 1995).

4.3.2. Trace element composition

Shales and Mudstones: analytical results of trace elements from this study and comparative PAAS, NASC and UCC values are given in (appendix B). All samples show slight depletion in Sc, Cr, Co, Ni and Ba compared with PAAS and NASC values whereas Zr, Y and Nb are enriched (figure 4.11). This might imply the presence of heavy minerals such as zircon associated with clay minerals (Herron, 1988; Descourvieres et al., 2011; Ejah, 2016). The Th/U ratio of the analyzed mudrocks show higher value than the average value of upper continental crust (UCC) (Condie, 1993) which is indicative of advanced weathering conditions (Descourvieres et al., 2011).

Gypsum: trace elements such as Ni, Co, V, Cu and Zn have values in the range of 1-5ppm with anomalously higher range seen in the sample from the Dejen section (values as high as 24-23 ppm) (figure 4.11). Such elements show strong positive anomaly during continental influx (Playa et al., 2007). Hence, wide variation in values in samples between Gohatsion and Dejen could be attributed to relatively different amount of continental input. The high concentration of Sr in gypsum samples (281-1280 ppm; mean: 1011.5ppm), might suggest greater marine influence although this cannot be the only reliable indicator of exclusively marine origin (Lu et al., 2002; Playa et al., 2007).

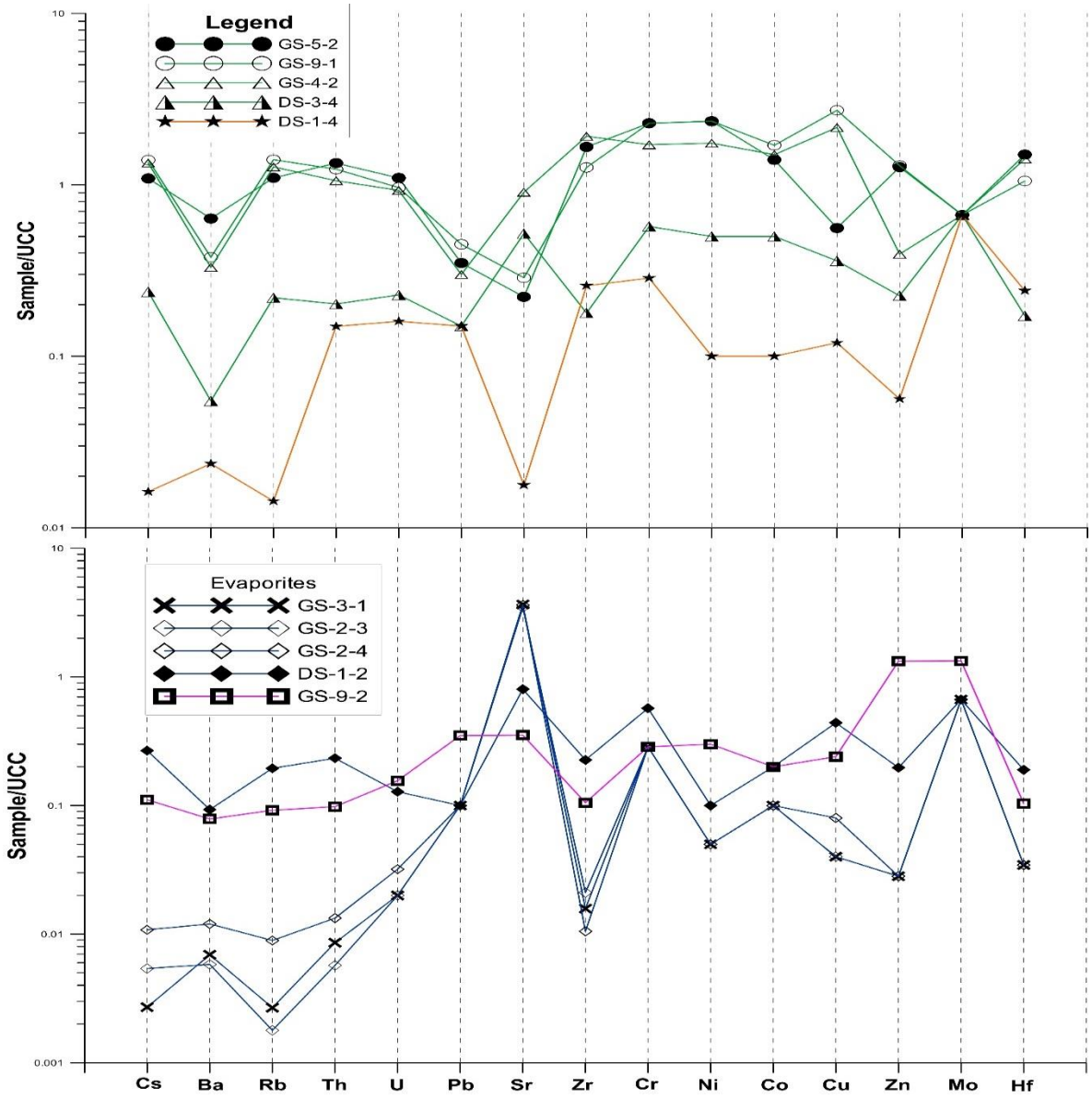

Figure 4.11. Trace element spider diagrams showing various attributes of the analyzed samples. (Top) UCC normalized element distribution of mudrock (green lines) sandstone (brown line) samples; (Bottom) UCC normalized trace element values for gypsum (blue lines) and carbonate (violate line) rocks.

REE in Shales, Mudrock, and Limestone: analytical results of REEs from this study and comparative PAAS and NASC values are given in appendix B. Chondrite normalized diagrams (figure 4.12) show enrichment of the light rare earth (LREE), slight negative Eu anomaly, and flat heavy rare earth (HREE) pattern. The average ΣLREE/ΣHREE for the analyzed samples have higher values than NASC and lower than PAAS. La_N/Yb_N values for the samples range between 4.3-11.3 (table 5.1). According to Andre et al. (1986), the two extreme 'end members' having La_N/Yb_N <4 and >14 along with a corresponding Th and La value could be regarded as having mafic and felsic protoliths, respectively. The intermediate values of these ratios for the analyzed sample might imply mixed sources. The limestone sample has similar REE pattern with the siliciclastic rocks, which is also indicative of the effect of continental input (eg. Worash Getaneh and Valera, 2002).

REE in Gypsum: Most of the samples show similar pattern (figure 4.12) with the exception of one sample from the Dejen section that have relatively higher REE concentration and smooth trend with the smallest amount of depletion or enrichment; which is also the general trend for the detrital samples.

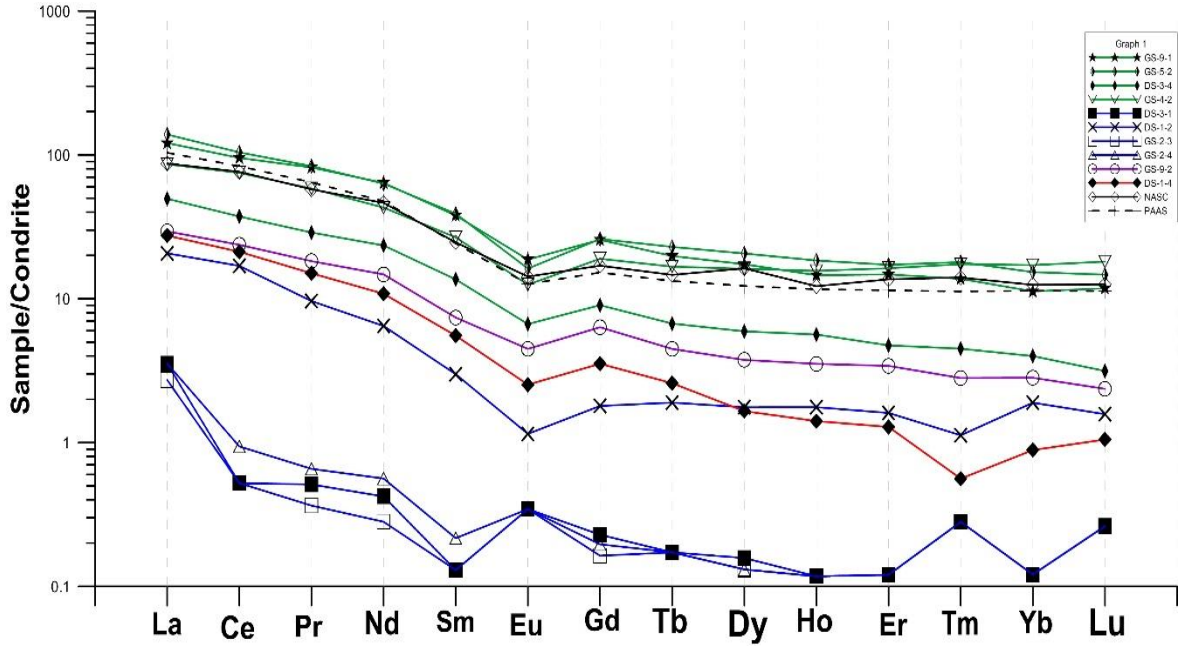

Figure 4.12. REE condrite normalized spider diagram of all the analyzed samples along with PAAS and NASC values for reference. Green lines are for mudrock samples, blue lines are for gypsum samples, violate line is for limestone sample whereas the sandstone sample is represented by the red line; references (PAAS and NASC) are dashed (after Nance and Taylor, 1976).

Bivariate and Discrimination Plots: bivariate plots of major oxides such as SiO_2, K_2O, Na_2O, TiO_2 and Fe_2O_3 show strong positive correlations against Al_2O_3 (figure 4.13). This implies that oxides derived from terrigenous sources are influenced either by sorting of primary and secondary minerals during weathering, reworking and transportation prior to deposition or by post depositional and in-situ weathering and diagenesis of primary alumino-silicates to clays (Descourvieres et al., 2011; Hoffer et al., 2013). MgO and CaO show negative trend. This is primarily due to the presence of carbonate minerals in some samples (especially in the sample form Gypsum Member) and not a result of element evolution. Carbonates (dolomites and calcite) along with evaporites (gypsum) are non-responsive to alteration of feldspars to clays (Hoffer et al., 2013). Positive correlation of CaO and LOI also observed which indicates the presence of either organic matter or carbonate mineral content (Santisteban, et al., 2003).

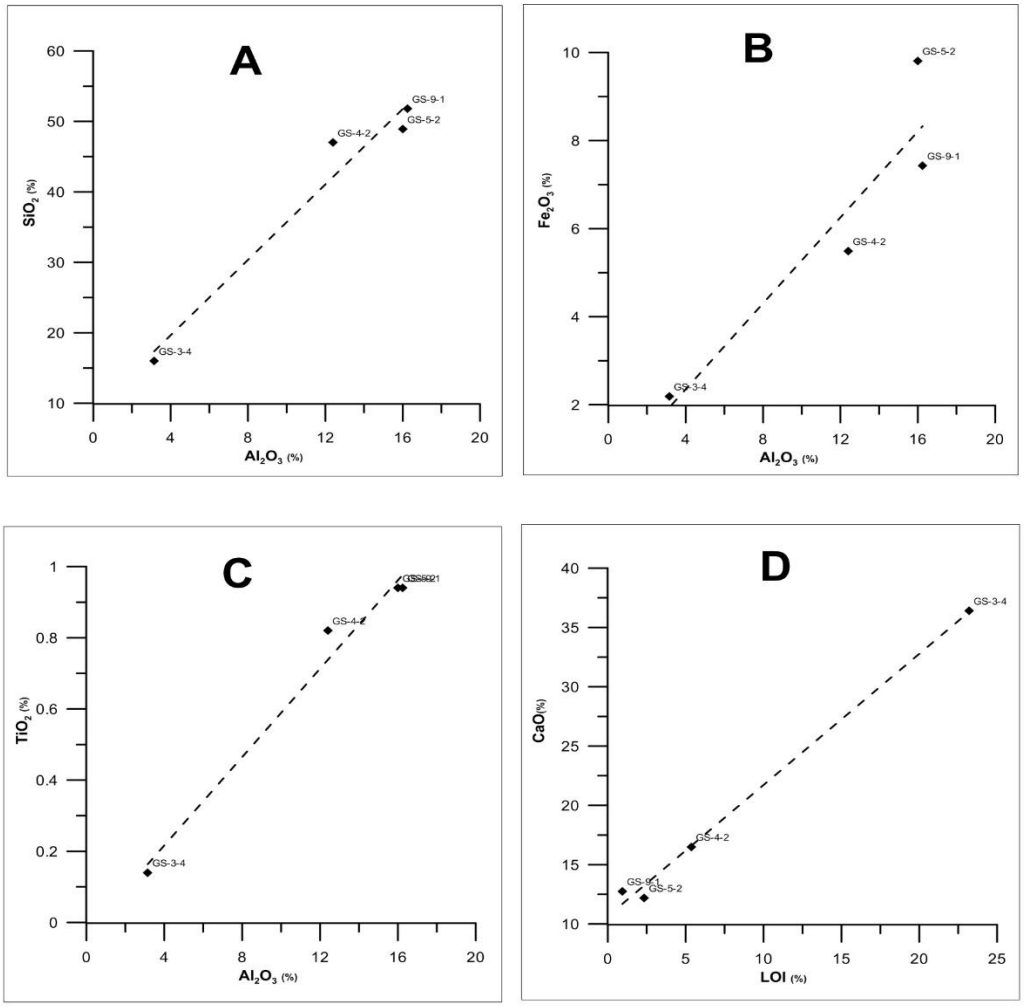

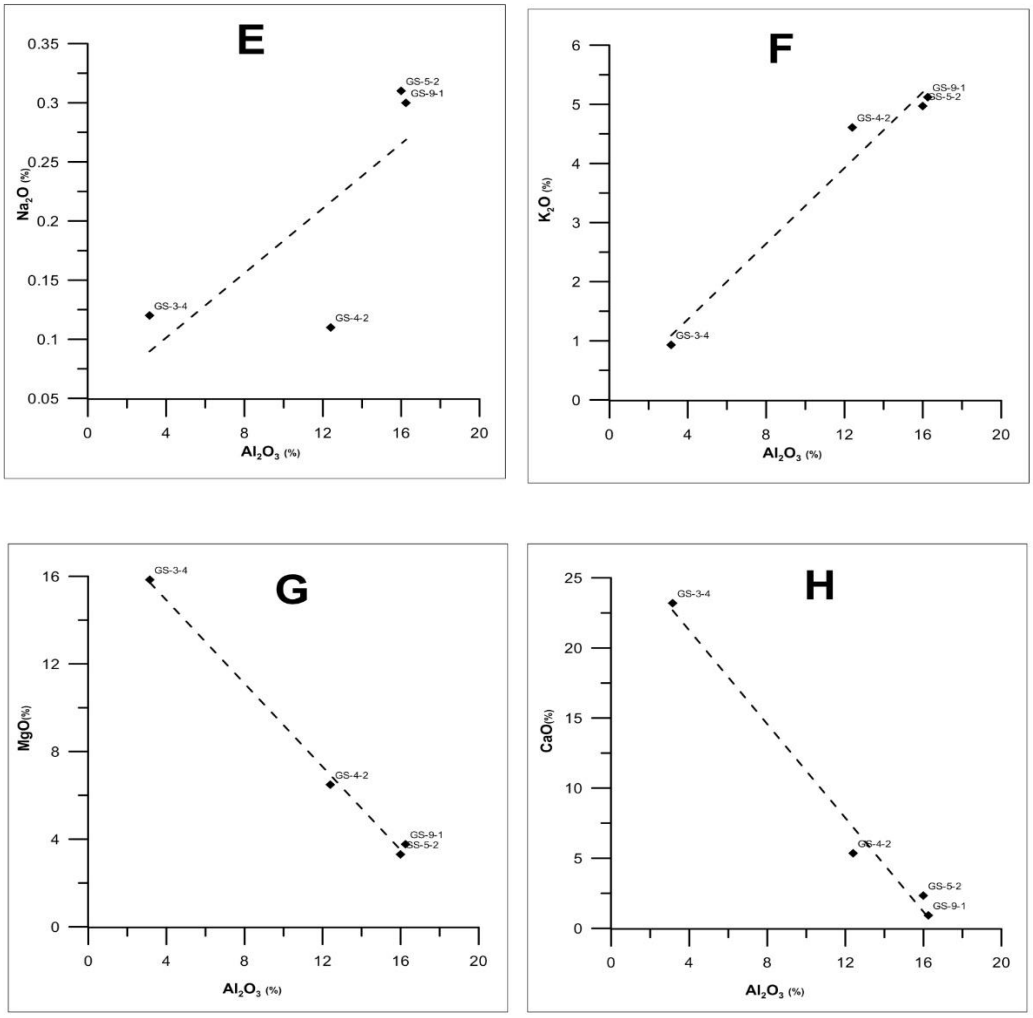

Figure 4.13. Bivarate diagrams of major elements verses Al2O3 (**A-C & E-H**) and LOI (**D**). Dashed lines show least square regression lines indicative of correlation trends.

Incompatible to compatible trace element raios such as those of Th/Sc vs. Zr/Sc can indicate the effect of mineral sorting in clastic sedimentary rocks (Hu et al., 2014). Th is generally incompatible while Sc is generally compatible in an igneous system, and their ratios with resistive elements such as Th and Zr could be powerful discriminants of provenance (Mclennan et al., 1993) and could help to determine whether sediments have undergone recycling processes (Mclennan et al., 1993; Khan and Khan, 2015). Zr becomes highly enriched during recycling process whereas Sc retains provenance signature, hence recycled sediments tend to have higher Zr/Sc ratio and would plot along the weathering trend profile (Critelli et al., 2008). The analyzed samples have Th/Sc value of an intermediate source with slightly increased Zr/Sc ratio which is indicative of enrichment of Zr due to recycling.

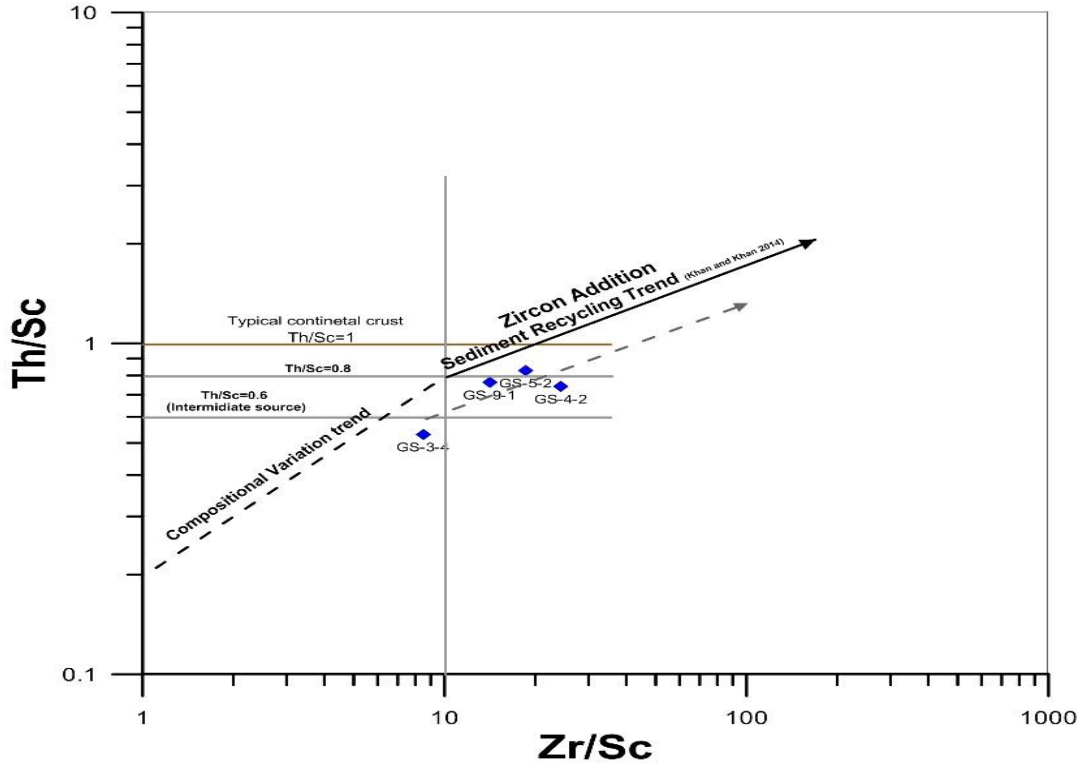

Figure 4.14. Th/Sc versus Zr/Sc plot for the analyzed samples showing intermediate source (on the basis of Th/Sc ratio after Condie, 1993). Enrichment in Zr is also shown in Zr/Sc showing higher variation than Th/Sc ratio which is indicative of sorting and recycling. Sediment recycling trend of siliciclastic rocks (after Khan and Khan, 2015).

4.4. Major oxides as paleoenvironment proxies

Major oxide can be used to infer the paleoenvironmental conditions affected by palaeoclimate and weathering conditions. Three types of major oxide relations (CIA and ICV) can be used.

The Chemical Index of Alteration (CIA) considers CaO from silica bound source only. Hence the correction method of Mclennan et al. (1983) is used to deduct the CaO from other minerals such as calcite, dolomite or apatite, and CaO* is calculated using:

$CaO^*=CaO-10/3P_2O_5$

The computed CIA values for the analyzed samples are given in (appendix B). One shale sample from the Gypsum Member show significantly lower value for CIA. This may be due to the presence of anomalously high amount of LOI. Samples from the Upper Mudrock Member have similar CIA values to those of the PAAS and NASC than samples from the Gypsum and Lower Mudrock Members (appendix B). This indicates such rocks were formed under relatively intense weathering conditions. This is also evident in the contrasting values of total alkali (Na_2O+K_2O+CaO) contents of the samples, which would also indicate the amount of feldspars relative to clay minerals (Potter et al., 2005). Examination of the analyzed samples in

relation to typical weathering trends of common rocks of the crust indicate that the samples show an affinity to granodiorite and granite trends (figure 4.15). Potential source rocks could have similar compositions to granite-granodiorite plutons within the basement rocks, such as those of Ujjikka and Guttin plutons (Tesfaye Kebede et al., 1999).

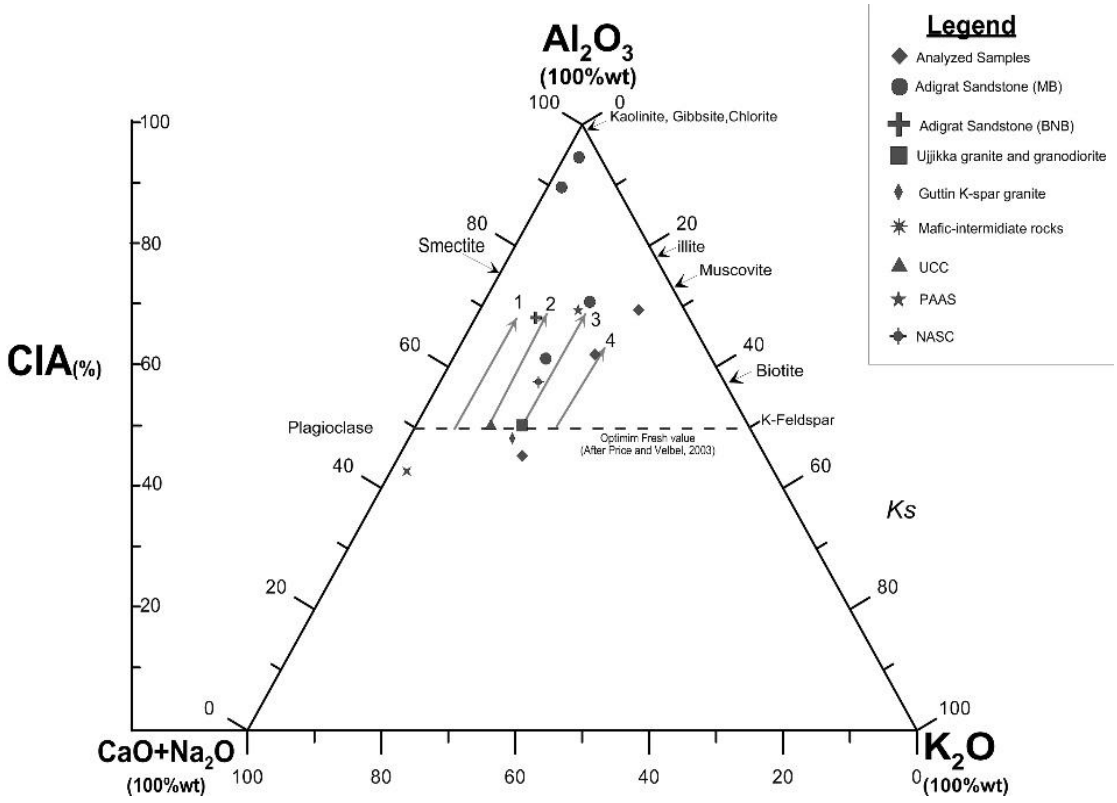

Figure 4.15. A-CN-K ternary plot (after Nesbitt and Young, 1984).black arrows indicate compositional trend of initial weathering profiles of different rock types (After Khan and Khan, 2015); *1:tonalite, 2:diorite, 3:granodiorite, 4: granite*; potential source rocks of granitic and intermediate rocks (Tesfaye Kebede, et al., 1999) and reference data UCC (Taylor and Maclennan, 1995) PAAS and NASC values from Nance and Taylor, (1976).

With the exception of the calcium enriched shale sample form the Gypsum Member, all the samples fall between typical basalt and granite weathering trend in the ICV trend (appendix B). This also possibly indicates intermediate composition source rocks. Clays are less dominant silicate phases in samples with increased ICV values (Lee, 2002). The XRD analysis also indicate significant amount of alpha quartz in mudstones (higher proportion seen in the sample from the Lower Mudrock Member). Median ICV value for the analyzed samples is 1.3 which surpasses the value for clay minerals (0.03-0.78) (Cox et al., 1995). Such result implies a first cycle detritus source for mudrocks (Lee, 2002). This is also in agreement with the presence of rock fragments in sandstones from similar horizons (see petrographic analysis in table 4.1 and figure 4.1, D; 4.2, C, D & E).

4.5. Provenance discriminations

Although most major elements are susceptible to changes during diagenesis, some elements such as Al and Ti are relatively immobile even under greenschist grade metamorphism (LaMaskin et al., 2008). Hence, Al, Ti and Zr could be good proxies for provenance. The average Al_2O_3/TiO_2 value is 3-11 for mafic rocks, 11-21 for intermediate rocks and 21-70 for felsic rocks (Paikaray et al., 2007). Average Al_2O_3/TiO_2 ratio of mudrock samples from the study area is 17.9 with 15.1-22.5 range. This suggests intermediate source. Furthermore, bivariate plot of two of the most immobile elements, Ti and Zr (Paikaray et al., 2007) also suggest intermediate source for the siliciclastic rocks (figure 4.16, A). Geochemical study of the underlying Adigrat Sandstone also indicated the ultimate source to be intermediate rocks (Worash Getaneh, 2002).

Inferred tectonic setting from major oxides can also be made by using discriminant function of ratios of mobile oxides such as CaO and Na_2O against SiO_2 and TiO_2 which are generally immobile under sedimentary system (Worash Getaneh, 2002). Increase in the ratio of immobile to mobile elements is observed in passive margin settings, primarily due to the fact that in such settings, high degree of weathering and recycling is common (Bhatia, 1983). Utilizing discriminate function analysis becomes a powerful tool in classifying samples in predefined fields on the basis of multiple variables (Bhatia, 1983). Hence, discriminant function in the form of $D_i=a_ix_1+b_ix_2+c_ix_3.....\pm C$ with x representing major oxides have been proposed by Bhatia (1983). Accordingly, the studied samples fall under 'intermediate igneous' source (figure 4.16, C).

The La/Th and Hf ratio (Floyd and Leveridge, 1987) is also useful proxy for provenance as they can discriminate sediment sources. Accordingly, the studied samples plot (figure 4.16, B) along the increasing old sediment component line between felsic island arc and passive margin sources. The sample form the Gypsum Member was omitted due to compositional bias that can arise from zircon assay which was anomalously low (see appendix B) (Worash Getaneh, 2002). According to Floyd and Leveridge (1987), progressive weathering of continental arc rocks and their plutonic roots along with ancient metasedimentary rocks facilitates release of Hf via its primary host mineral zircon. Hence, bias in zircon assay will affect the Hf content which will ultimately affect the discrimination ratio plot.

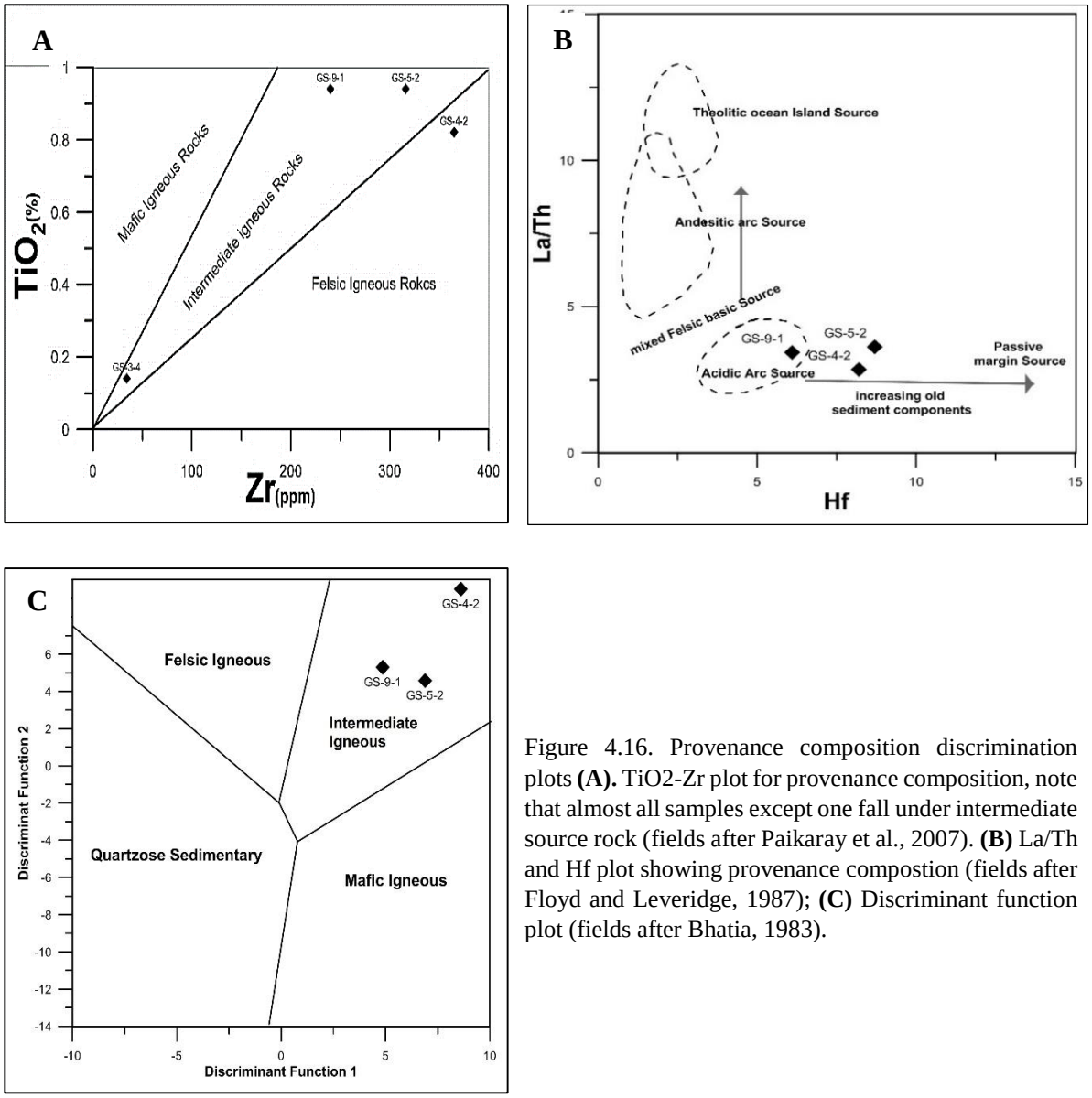

Figure 4.16. Provenance composition discrimination plots **(A).** TiO2-Zr plot for provenance composition, note that almost all samples except one fall under intermediate source rock (fields after Paikaray et al., 2007). **(B)** La/Th and Hf plot showing provenance compostion (fields after Floyd and Leveridge, 1987); **(C)** Discriminant function plot (fields after Bhatia, 1983).

Immobile trace elements ternary plot such as Th-Sc-La or Th-Sc-Zr/10 are excellent source of provenance indicators and have been used in may geochemical studies (eg. Cullers, 1994; Nyakairu and Koeberl, 2001; Worash Getaneh, 2002; Critelli et al., 2008; Hofer et al., 2013; Khan and Khan, 2015; Ejeh, 2016). Th and La are immobile elements and are relatively abundant in felsic rocks than basic rocks whereas Sc and Zr behave as immobile elements enriched in basic rocks (Nyakairu and Koeberl, 2001). Ternary plot of samples (figure 4.17) show that provenance of the samples is Continental Island arc setting. This discrimination is also mirrored by La-Th-Zr/10 plot as well.

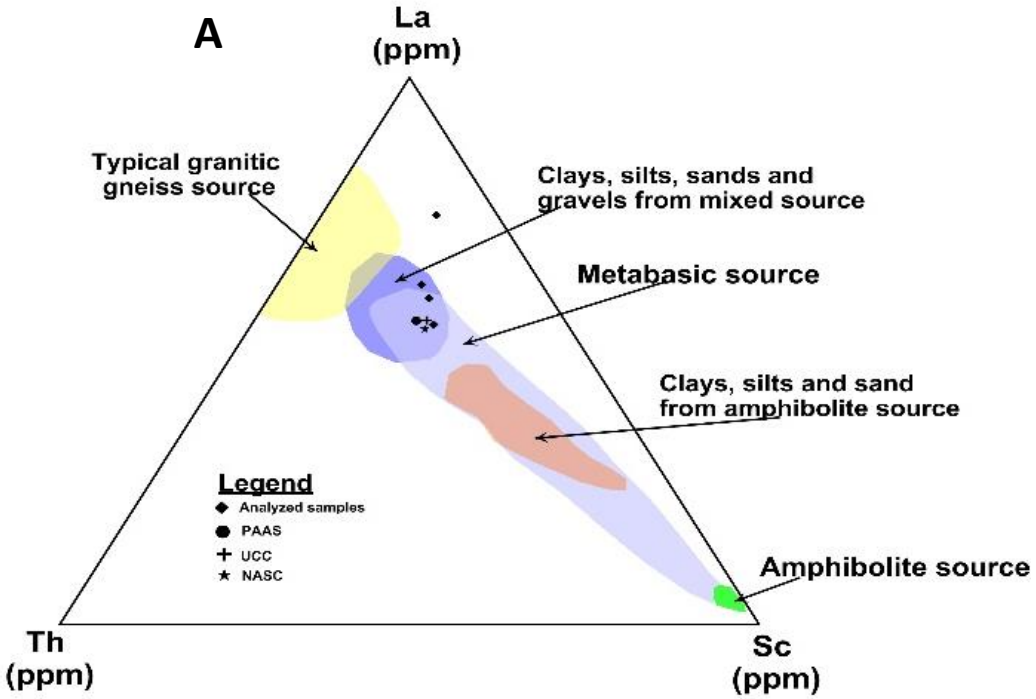
A
La
(ppm)
Typical granitic
gneiss source
Clays, silts, sands and
gravels from mixed source
Metabasic source
Clays, silts and sand
from amphibolite source
Legend
Analyzed samples
PAAS
UCC
NASC
Amphibolite source
Th
(ppm)
Sc
(ppm)

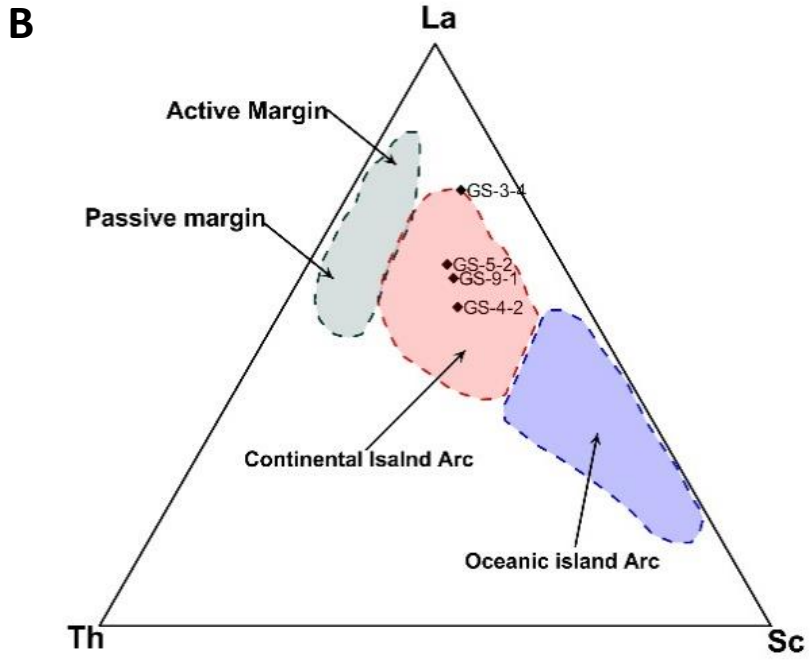
B
La
Active Margin
Passive margin
GS-3-4
GS-5-2
GS-9-1
GS-4-2
Continental Isalnd Arc
Oceanic island Arc
Th
Sc

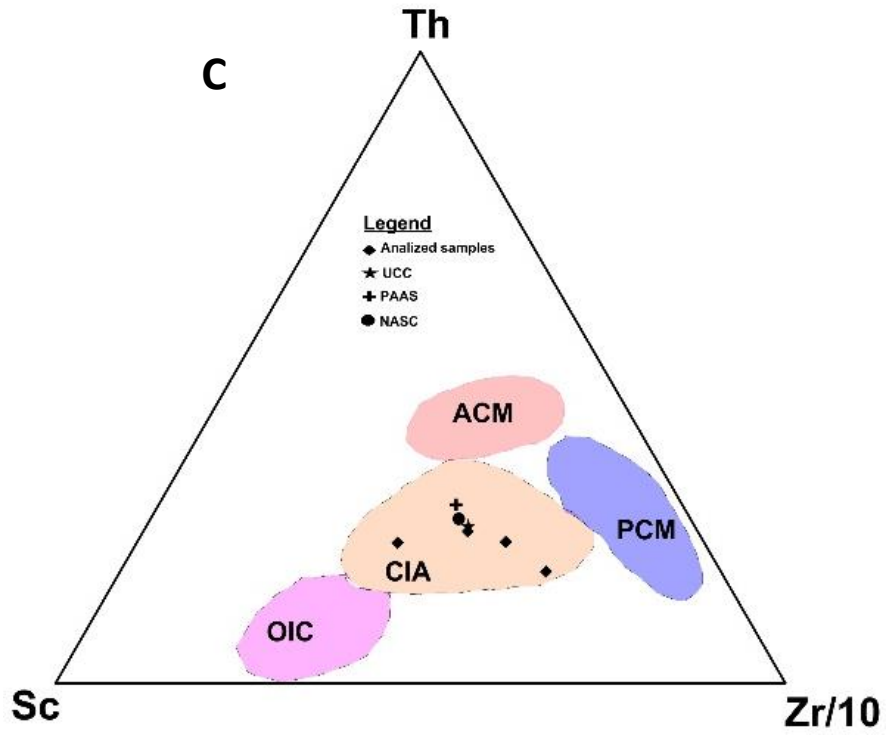

Fig 4.17.Provenance tectonic discrimination plots (**A and B**) La-Th-Sc diagrams showing source rock and tectonic discrimination for the analyzed samples. Discrimination fields taken form Cullers , 1994 for (A) and Khan and Khan (2015) for (B). (**C**) La-Th-Zr/10 discrimination diagram showing tectonic setting (discrimination field after Bhatia and Crook, 1986).

CHAPTER 5:

DISCUSSION

5.1. Lithostratigraphy and field relationship of members

Getaneh Assefa (1981) identified four informal members of the Gohatsion Formation on the basis of lithstratigraphy. However, this classification was not applied to other localities within the basin by subsequent workers, or even to the type locality in one case. Disregarding the 4 member subdivision of Getaneh Assefa (1981), Gani et al. (2008) proposed a different subdivision where the lower part of the unit is identified as 'Glauconitic Sandy Mudstone' and the remaining section including the gypsum beds as 'Lower Limestone'. Unpublished technical works by Geological Survey of Ethiopia (eg. Serawit Amene and Tamrat Mojo (1996, 1999); Tamrat Mojo and Tibebe G/Selassie, 1997) used 3 informal units in their description of the formation. Field observations, in this study, at different localities showed the successive recurrence of various types of fine siliciclastic units such as siltstone, shale and mudstone along with claystone. However, the relative proportion and abundance of siltstones, mudstones and shales seem to be higher than clay stones. This observation suggests classification of such members as 'Upper Mudrock Member' and 'Lower Mudrock Member' is more appropriate lithostratigraphic representation than 'Upper and Lower Claystone members' as previously proposed by Getaneh Assefa (1981). The 'Mudrock member' of Getaneh Assefa (1981) has not been identified as a prominent unit in the field observations in all localities, hence it has been incorporated in the 'Lower Mudrock Member' in this study.

Though the number of samples analyzed by XRD are very limited to draw definite conclusions, the XRD and petrographic analyses of mudstone and sandstone samples from the Lower Mudrock Member do not indicate the presence of glauconite. Furthermore, Getaneh Assefa (1979), in his assessment of clay mineral distribution in Mesozoic sediments, indicated the dominance of illite and chlorite in this Formation that drastically changes form the underlaying kaolinite rich Sandstone Formation. Hence, the proposed classification of 'Glauconitic Sandy Mudstone' by Gani et al. (2008) could not be confirmed. Further XRD analyses on more samples from diffrent localities are required. The prominent greenish colour of the mudstones, which, in most cases, is impacted by mineralogy could be related to the various K-rich micaceous minerals. Mineralogical analysis of samples indicated the presence of such minerals (eg. illite, pengite, hydromica) which may have an overlap with minerals having an affinity for ferric or ferrous oxidation states like chlorite with minor amounts of talc. Such minerals can

also give green color to clays (Odin, 1990; Velde, 2003). Furthermore, assigning the name 'Lower Limestone' (Gani et al., 2008) to a succession predominantly made of evaporites (gypsum and dolomitic limestones) and siliciclastic rocks may not be the exact representation of lithostratigraphic unit.

As noted by many of the previous works, the Gohatsion Formation as a whole and the individual members show considerable thickness variation among the different localities. This is confirmed by the logged sections in the current study (figure 5.1). Accordingly, there is an increasing abundance of Mudrock Members in the Jemma and Mugher sections in comparison with the Dejen and Gohatsion sections which implies significant clastic input to these localities.

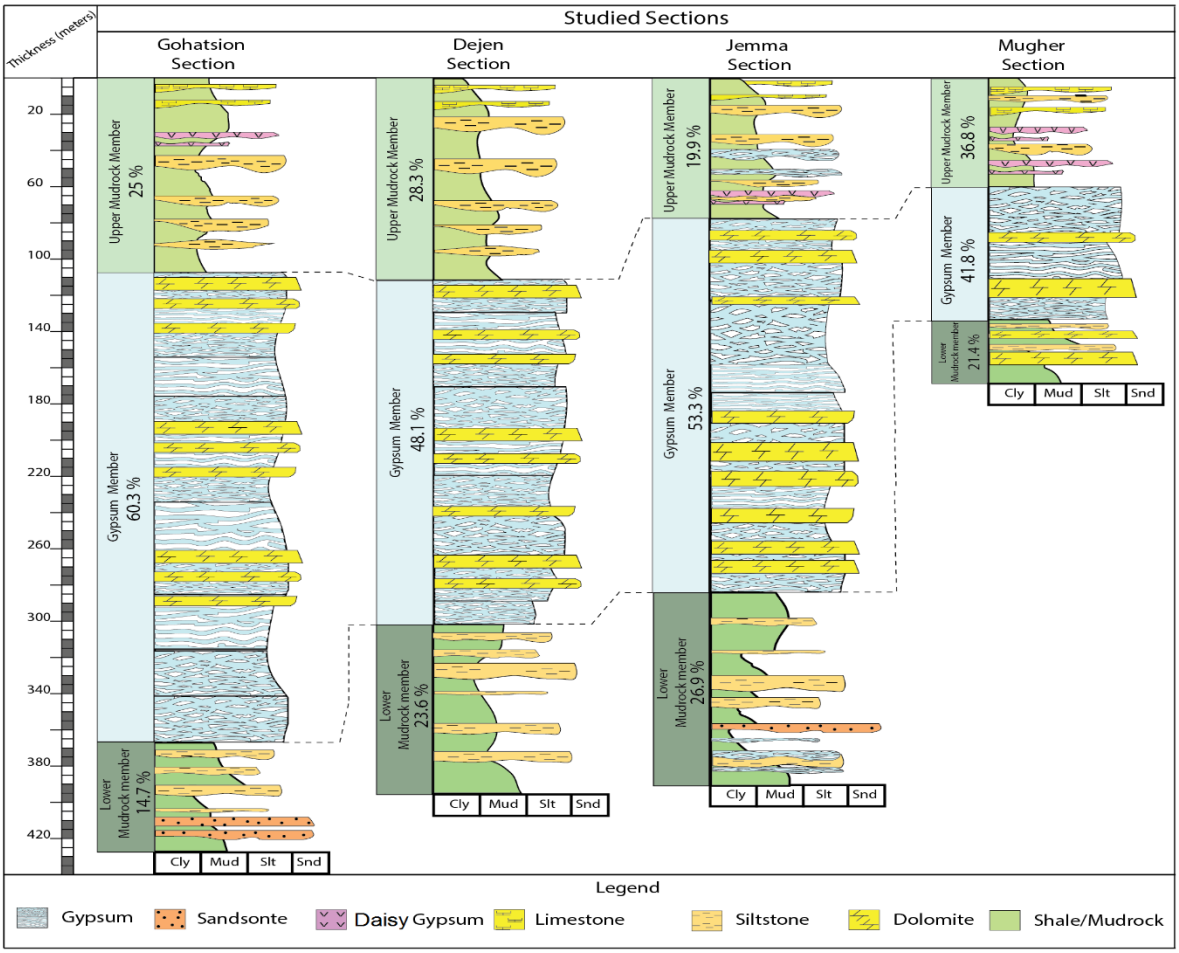

Figure 5.1. Simplified stratigraphic relationship of the studied sections and their respective members. Note that the percentages correspond to the thickness of individual members in percentage with respect to the measured thickness of the Gohatsion Formation in each locality. *(Details of each section is given in the appendix)*. The upper contact of each section with the overlaying Antalo Limestone Formation is taken as base of the correlation.

5.2. Implications for depositional setting

Significance of the variation in micro and macro facies of each member is discussed below.

The Lower Mudrock Member: This member is the oldest member of the Formation and has a gradational contact with the underlying siliciclastic fluviatile/deltaic to barrier/spit inlet deposit (*unit II* of Dawit Lebenie, 2010; Russo et al., 1994). This unit shows significant facies variations implying tide dominated estuary/ subtidal signatures in the Gohatsion and Dejen sections (Facies 1 and 2). Tide dominated estuary system having fluvial influence from Dejen side affected by tides from Gohatsion section may be the implied depositional setting based on the following observations: (i) Progressive decrease in grainsize from Dejen to Gohatsion section from silt dominated to sandy beds, (ii) The dominance of mudrock and silty shale with abundant channel scour in the Dejen Section that progressively coarsen towards the Gohatsion section showing typical tidal sandbars indicating a SE flowing direction. In Adigrat Sandstone Formation, the upper beds show paleo-current directions show dipping towards SE (Dawit Lebenie, 2010). According to, Dalrymple et al. (1992), in tide dominated estuary system, transgression can cause an abrupt emplacement of cross bedded sandbars over mudflat and/or saltmarsh sediments; a case observed in the Gohatsion section (figure 5.2; appendix A) whereas in the central mixed energy zone, meandering sediments accommodate finer sediments; mirrored by cross bedded and hetrolitic interlayering of sandy silt and mudstones that progressively decrease in grain size towards Dejen Section. Furthermore, Potter et al. (2005) noted the difference in mudstone lithology between estuary mudstone and flood plain mudstones. Floodplain mudstones in transitional environments show predominantly silty and sandy textures with olive drab to green color deposited as overbank splays, as observed in all the studied sections. On the other hand, estuary mudstones show predominantly micaceous siltstones with seaward ripples, as observed near the contact with the Gypsum Member in the Gohatsion section.

The drawback of this interpretation is the lack of evidence of alluvial channel facies in the studied sections that can represent the tidal limit to the estuary system. An alternative model could be a siliciclastic back-barrier tidal flat system. In such system, shoreward decrease in grainsize from sandy mud to muddy sand, wave dominated ripples, bioturbation and hetrolitic bedding are common (Flamming, 2012). Back-barrier tidal systems can be formed in non-vegetated settings, hence, salt marsh type deposits may not necessarily be formed, which seems to be the case in the studied area. However, it’s very difficult to differentiate ancient tidal

systems (in this case mesotidal and macrotidal systems) because of the ubiquitous nature of facies architecture in the subsystems. The depositional model of this unit is given in figure 5.2. The gradual transition from mud dominated facies to evaporitic facies at the top of this unit indicates transgression process may have been hindered by global sea level fall and subsequent arid climate in the formation of the arid belt beyond 40^0 lattitude (Russo et al., 1994; Wolela Ahmed, 2008; Berra and Angiolini, 2014).

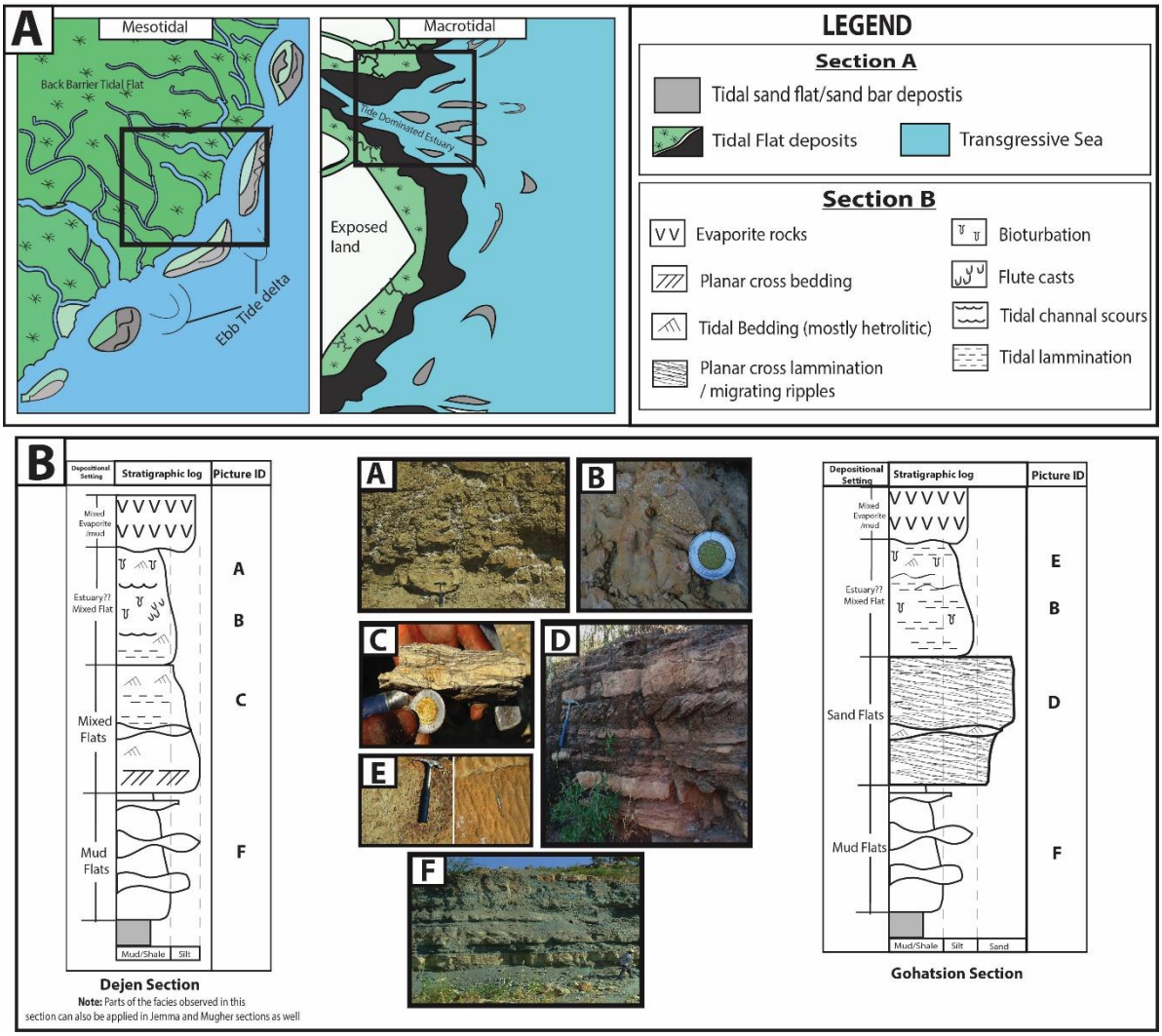

Figure 5.2. Simplified model for depositional conditions of the Lower Mudrock Member. (**A**) Two possible depositional models siliciclastic back-barrier tidal flat depositional setting having mesotidal energy (after Flamming, 2012) and tide dominated estuary formed under microtidal environment (after Dalrymple et al., 2012 ; Tessier, 2012). The boxes represent the possible setting of the Gohatsion (bottom left corner of the box) and Dejen sections (top right corner of the box). (**B**) Facies associations in the observed sections related to the proposed depositional setting.

Gypsum Member: Textural contrast between the Gohatsion section and the other sections is observed in Gypsum Member. Variety in textures of gypsum are indicative of depositional and post-depositional history. Aside from the localized variability of textures, the overall texture seems to be uniform throughout the sections with majority of textures falling under laminated or nodular textures. This is a key characteristics of evaporites (in this case, gypsum) formed under tectonically inactive settings such as passive margin basins (Schreiber et al., 2007).

Close relationship between gypsum textures and hydrography has been the point of interest recently (Babel, 2007). In the Gohatsion section, laminated gypsum facies showed typical stratified facies of deeper basins such as salina. Such succession also represents fining upward in bedding thickness which is indicative of increasing salinity (Warren, 2006). In ancient evaporite platforms, such facies can be identified with a facies association of poorly bedded/massive anhydrite, capped by bedded nodular anhydrite with preferential elongation overlain by laminated nodular anhydrite (Warren and Kendall, 1985). This is observed in Gohatsion section (figure 3.7, B). Truncated contact between laminated and nodular layers, pseudomorphs or 'gypsum ghosts' of bottom grown gypsum crystals with truncated or brecciated texture could also indicate seasonal exposure or change in brine chemistry as a result of mixing and the effect of pycnocline fluctuation (Babel, 2007; Schreiber et al., 2007). This reflects the presence of holomictic brine which allowed brine mixing between stratified water horizons (Babel, 2007). The presence of wavy beds of gypsum (figure 3.9, F) that are dominant in the Dejen and Gohatsion section are also indicators of shallow subaqueous system prone to turbulence /storm (Boggs, 2009; Warren, 2016). In clastic gypsum layers, most of the clasts observed show less reworking indicating proximal source (figure 3.11, A).

The Dejen, Jemma and Mugher sections show dominantly nodular gypsum facies in comparison to the Gohatsion section. The presence of nodular and entrolitic anhydrite/ gypsum in association with lagoonal and tidal flat carbonates with fenestral fabric and microbial laminations indicate a peritidal to supratidal sabkha setting (Warren and Kendall, 1985). According to Perri et al. (2017), growth structure of stromatolitic laminae along with uniform arrangements of algal filaments indicates autochthonous origin.

Considering the paleogeography of the region (eg. Schandelmeier et al., 1997, Scotese, et al., 1999; Dawit Lebenie, 2010; Berra and Angiolini, 2014), full separation of the east and west Gondwana that led to the formation of 'Karoo rifts' proceeded in the form of a 'failed arm' (Russo et al., 1994) in central Ethiopia. At the same time, Neo-Tethyan Sea was in transgressive

phase. In the studied area, marine transgression came from SE direction (Russo et al., 1994; Dawit Lebenie, 2010). The combination of the observed facies in the various sections indicate that marine influence was grater in the Gohatsion section while continental influence is greater in the others. Variations observed in trace element and REE data from Gohatsion and Dejen sections (REE and trace element depletion of Gohatsion section and enrichment in Dejen section) is also in agreement with this statement. The proposed model for depositional setting for Gypsum Member is given in figure 5.3.

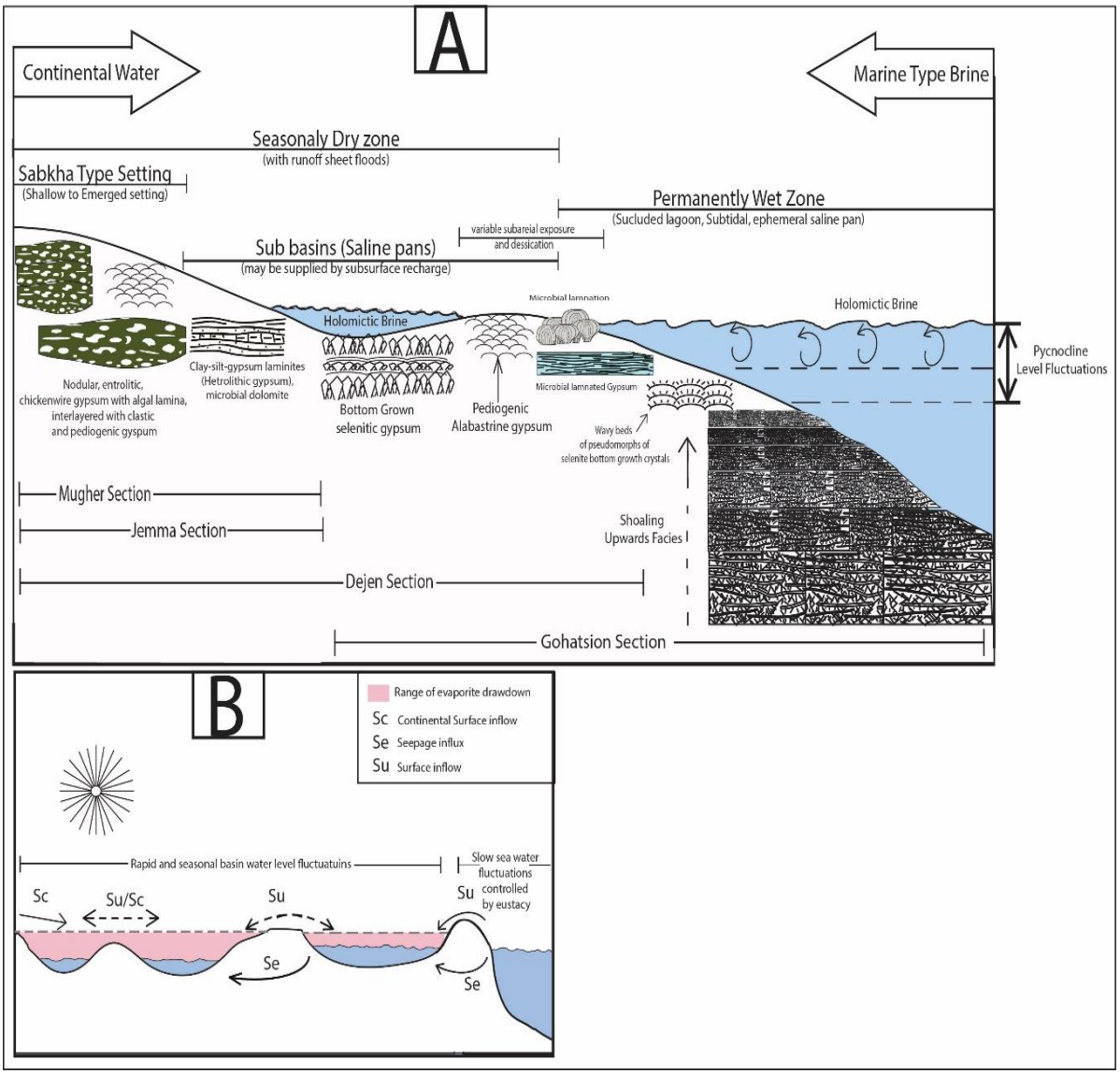

Figure 5.3. Simplified model for depositional conditions for the Gypsum Member **(A)** Integration of the observed facies with depositional settings (after Schreiber et al., 2007). **(B)** model showing the possible mechanism of brine influx and reflux and deposition of gypsum/carbonate in the basin (after Babel, 2007)

Upper Mudrock Member: Lithofacies in this member is dominated by mudrock and shales. Carbonate and evaporite rocks become common interlayers at the top and bottom contact of this member. According to Potter et al. (2005), deposition of mud in coastal environment can occur under a protected setting where destructive wave and coastal currents are weak. This dominance of very fine sediments was interpreted to be a result of deposition under an environment of lesser energy by Getaneh Assefa (1981), who suggested these sediments were deposited in restricted lagoon or coastal lakes. This led to the formation of thick beds of shale and mudstone with rare sedimentary structures (Facies 2) along with siltstones showing predominantly fining upwards sequence and background sedimentation (figure 3.14, B: the red bar in the figure indicates a bed formed from background sedimentation and suspension settling). On the other hand, field observations show the presence of tidal bedding (flaser, lenticular and hetrolitic beddings in figure 3.14, A) which imply the presence of tide related processes (Potter et al., 2005; Davis, 2012; Fagherazzi et al., 2013). However, Didu (2013) noted that such structures can also form in non-tidal zones but the presence of associated fining upwards bedding may also be indicative of intertidal flat deposition. The presence of evaporite (mainly gypsum and subordinate carbonate) indicates either seasonal climate shift to arid conditions in a supratidal setting or ephemeral saline pond (Warren, 2006). The scarcity of fossil in this unit is noted by Getaneh Assefa (1981) and Russo et al. (1994). The influence of localized arid conditions or removal of organic matter by bacteria is proposed by Getaneh Assefa (1981) for such scarcity. The lithofacies of this member shows generally similar stratigraphic evolution in all the measured sections. The presence of evaporite carbonate and gypsum rocks at the bottom suggests supratidal setting. The presence of massive shale and mudstone beds with no sedimentary structures in the middle suggest lagoonal setting, whereas presence of tidal facies also indicates a broad intertidal mud flat setting. The absence of salt marsh type facies may indicate that the mudflat was non-vegetated. At the top, interlayering of partly fossiliferous limestone and marl also indicates seasonal sea level rise and flooding of the basin by marine water (Getaneh Assefa, 1981). Furthermore, Russo et al. (1994) noted the presence of gastropods and bivalves (eg. *Arcomytilus* and Protocerithium) and gave an interpretation of mixed marine setting with fresh water influences form adjenecet areas.

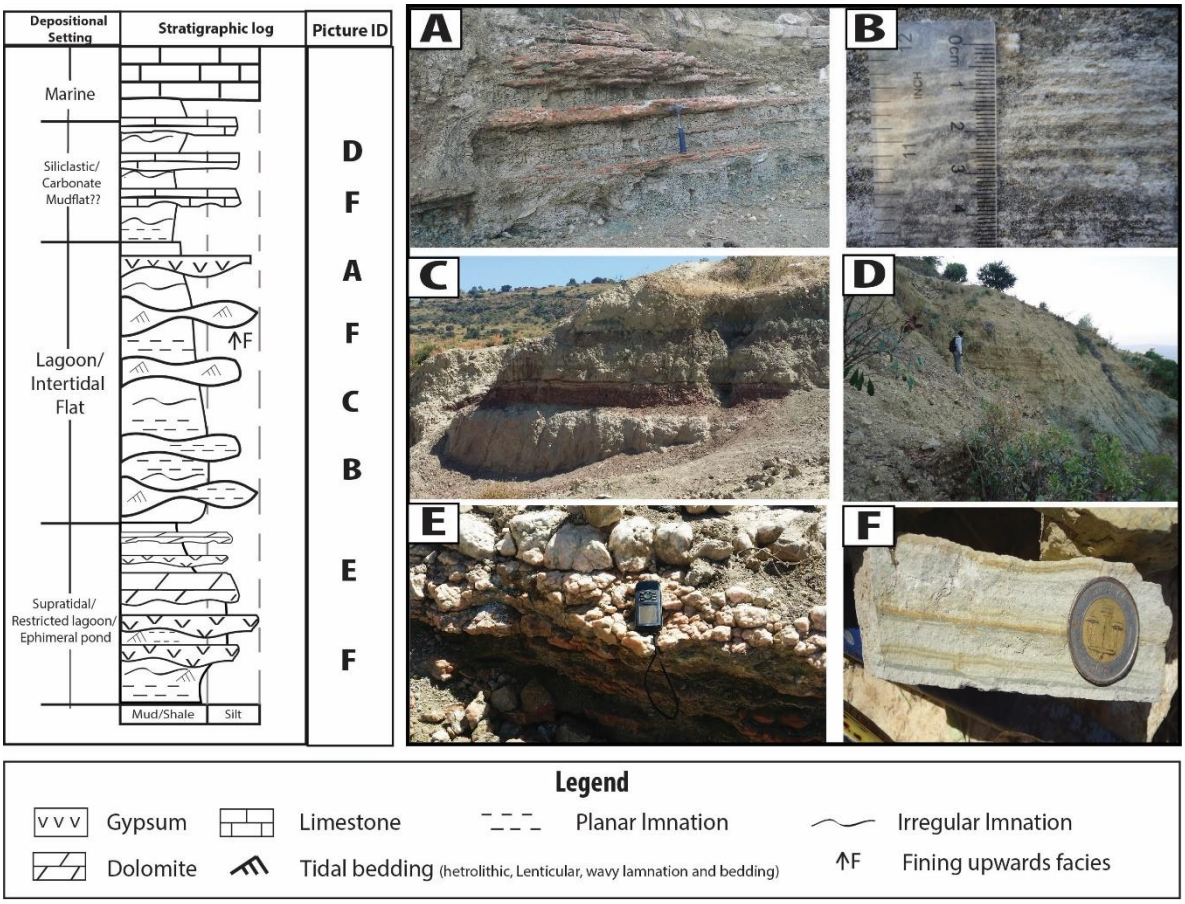

Figure 5.4. Simplified Lithostratigraphic depositional model for Upper Mudrock Member

5.3. Implications for provenance and paleoclimate

Provenance of the upper and Lower Mudrock Members can be seen from different angles, mineralogical and petrographic analysis of samples (both mudrock and sandstone) from these members indicate proximal source. Petrographic analysis of sandstone generally show sub angular to sub rounded grain shape along with the presence of not reworked and unaltered feldspar grains which indicates proximal source.

Most mudrock deposits of the world are products of sediment reworking and recycling of older sediments (Potter et al., 2005). Hence, mudrocks formed form recycled sediments undergo repeted sorting that enables them to have comporitional maturity. Mineralogy of mudrock samples also show the presence of significant amount of non-clay silica (alpha quartz, and feldspars) which suggests compositionally immature mudrock. This is also in agreement with ICV values of major oxides that tend to be affected by clay silicate mineral relative to non-clay silicate mineral phases (Cox et al., 1995). Alternatively Zr/Sc ratio of mudrock (appendix B) showed lower value than UCC and slight enrichment than PAAS. Th/Sc-Zr/Sc discrimination plot also shows weak recycling signature (figure 4.14). This indicates minimal effect of

recycled component which is indicative of first cycle deposition (Ullah et al., 2015). Geochemical attributes of the underlaying sandstone formation show higher degree of weathering and sorting (Worash Getaneh, 2002; Barsisa Bekele, 2011). The analyzed mudstone samples have lower weathering intensity than the Adigrat Sandstone Formation which is indicative of less weathering and reworking conditions. According to Ullah et al. (2015), fractionation of Th and U increases with weathering intensity and sediment recycling. During weathering, U turns its oxidation state from +4 to +6 and forms a highly soluble uranyl ion whereas Th remains relatively insoluble. As such, Th/U ratio should increase as rocks experience intensive weathering and sediment recycling. Comparison of Th/U ratio with PAAS yielded lower values (appendix B) along with lower CIA values. This, in turn, suggests that mudrock were formed from first cycle deposition rather than recycled products of the underlying sandstone formation. Though, it should be noted that the sediments also have higher values (Th/U) than UCC which may implicate the presence of recycled components. This is not surprising as fine siliciclastic sediments tend to be homogenized from different sources and show mixed provenance signatures (Cillers, 1994; Potter et al., 2005; figure 4.17, A).

Comparison of the analyzed samples with Neoproterozoic intrusive rocks found in western parts of the basin (see table 5.1 *data after Tesfaye Kebede et al., 1999*) show good affinity towards felsic and intermediate intrusive rocks than mafic intrusive rocks. Geochemical attributes that reflect felsic to intermediate source include low Eu/Eu*, Cr/Th and high LREE/HREE, $(La/Yb)_N$ and La/Sc along with the general REE pattern (eg. Worash Getaneh, 2002; Ejah, 2016). This is also the case in the underlying sandstone formation, as interpreted by Worash Getaneh, (2002), having an ultimate provenance of intermediate source. Moreover, Potter et al. (2005) also suggests muds originating from Precambrian shield settings tend to be formed from recycled muscovite, illite and quartzo-feldspatic composition under moderate weathering conditions, which coincides with the mineralogy of the analyzed samples (table 4.2). petrographic analysis of sandstone samples show the presence of sutured and foliated polycrystalline quartz (figure 4.2, C) along with fragments with random and aligned internal fabric (figure 4.1, D) indicate metamorphic and associated intrusive rocks as provenance for the formation.

Tectonic discrimination diagrams (figure 4.17, B & C) also show continental island arc signatures which may be related to signatures shown by the granites from Wallega area reported in Tesfaye Kebede et al. (1999). According to this paper, intermediate granitic intrusive bodies showed geochemical signature of A_2 type granite which are related to post orogenic

environments in continental arc settings (Eby, 1992). Considering the proximal signatures observed in the mudstones along with their geochemical affinity, the possible source of the fine siliciclastic sediments must have similar geochemical attributes as the plutonic rocks of Wollega.

Table 5.1. Geochemical attributes of the analyzed samples in comparison with potential provenance rock types.

	This Work	Worash Getaneh, 2002	Data from Tesfaye Kebede et al., 1999		
	Gohatsion Formation	Adigrat Sandstone	Ujjikka granite and granodiorite	Guttin k-spar granite	mafic intermediate Rocks
$(La/Yb)_N$	12.4	17.54	15.49	14.72	4.55
Eu/Eu*	0.56	0.51	0.66	0.90	1.20
Th/Co	0.73	2.48	0.89	2.03	0.04
Cr/Th	6.67	22.68	0.74	0.72	58.79
Th/Sc	0.71	3.31	1.65	3.27	0.04
La/Th	4.62	3.65	4.87	1.93	12.72
La/Sc	3.06	9.76	8.04	6.29	0.48
La/Co	3.00	8.13	4.35	3.90	0.50
K_2O/Na_2O	20.69	7.24	0.99	0.98	0.30
Al_2O_3/SiO_2	0.28	0.06	0.21	0.21	0.34
$Al_2O_3/(CaO+Na_2O)$	5.41	14.06	2.46	2.19	1.35

5.4. Implications for diagenetic evolution

A combination of field observation and petrographic data have been used to identify the major diagenetic processes in the various rocks (table 5.2).

Early diagenesis related to syndepositional processes is mainly featured in the evaporite rocks (dolomite and gypsum). The presence of early calcite cements, associated with fenestral cavities, micritized grain boundaries and solution cavities filled with micrite along with isopacheous calcite cement was used as an indication for syndepositional diagenesis under either lagoon environment or shoal facies (Tunik, et al., 2009; Rahimpour-Bonab et al., 2010). Syndepositional dehydration of gypsum to anhydrite (currently affected by rehydration and is only found in the form of relic crystals floating in gypsum) can also be interpreted as sabkha type diagenesis where surface temperatures are high enough to dehydrate gypsum and form primary anhydrite (Warren, 2006, 2016). In dolomites, dissolution cavities filled by secondary

gypsum is also interpreted as typical supratidal/sabkha environment (Getaneh Assefa, 1981; Rahimpour-Bonab et al., 2010).

In later stages of early diagenesis, textural examinations showed that meteoric water influence was greater. In carbonate rocks, the formation of dissolution cavities partially or fully filled by drusy calcite cement and neomorphic crystals (eg., Moore, 1989; Tunik, et al., 2009; Rahimpour-Bonab et al., 2010; Perri et al., 2017). In sandstones, shallow burial compaction caused grain suturing and small overgrowth textures along with the formation of calcite cement via the introduction of meteoric water. Calcite cements seem to prohibit alteration of feldspars to clay minerals hence, autogenetic clay minerals are not that common. In some cases early dissolution resulted in the formation of secondary poikilotopic calcite cement (Cal 2 in figure 4.2, H). This processes precedes quartz overgrowth, evident form trapped calcite relics between the boundaries of detrital quartz and autogenetic quartz (eg. Xiong et al., 2016; Yuan et al., 2017). Leaching and replacement of feldspar grains by poikilotopic calcite as a result of introduction of acidic meteoric water rich in CO_2 is common at this diagenetic stage (Serra, 1986; Milliken, 2005). Vuggy dolomite beds (figure 3.12, B) are results of leaching via meteoric water as well. Conversion of primary gypsum to anhydrite via the process of dehydration is also evident at this stage (mostly observed at an outcrop level that resulted in the formation of chicken wire and entrolitic textures in most of the laminated gypsum beds).
Late stage diagenesis includes intermediate to deep burial. In the carbonate rocks, dolomite neomorphism is the main process observed whereas in sandstones, autogenetic clay minerals forming cements (possibly Kaolinite in figure 4.2, F; matrix component at the bottom of *Qs* grain showing different birefringence than calcite matrix labeled *Cal*) occur. In gypsum, formation of anhydrite pseudomorphs and nodules after gypsum as pore fluid from dehydration possibly acted as hyper saline fluids that enabled the precipitation of secondary satin spar gypsum in fractures and voids (eg. Warren, 2006; 2016; Gindre-Chanu et al., 2015).

Gypsum rocks show various textures that mark telogeneitic processes. Displacive and replacive (eg. Figure 4.5, B & C) tertiary gypsum textures that mark rehydration via fluids from phreatic water or dehydrated fluid are common in the rocks. Large granoblastic/poikilotopic, replacive or displacive gypsum crystals are indicators of near equilibrium solution (Gindre-Chanu et al., 2015; Warren, 2016). Such growth textures often occur when anhydrite is subjected to stagnant phreatic water-table during the early stages of uplift (Warren, 2006). Leaching of such crystals

is also indicative of the presence of hypersaline solvent. On the other hand, formation of xenotopic mosaic of gypsum can be used as an indicator for the presence of an active phreatic zone where the water table changes seasonally, leading to a rushed rehydration and precipitation state that forms finer microcrystalline aggregates of gypsum or roseate gypsum (Gindre-Chanu et al., 2015). At this stage, formation of satin spar gypsum is also possible through the actions of active and passive hydrological processes with respect to the formation of fractures that enable the precipitation of satin spar (Warren, 2016). When the gypsum horizon reaches vadose zone, formation of karst and dissolution breccia may commence (Warren, 2006; Gandin and Wright, 2007; Gindre-Chanu et al., 2015), leading to the formation of clastic gypsum and localized slumps that are filled by the overlaying sediments.

Table 5.2. Summary of diagenetic processes observed in the various rocks

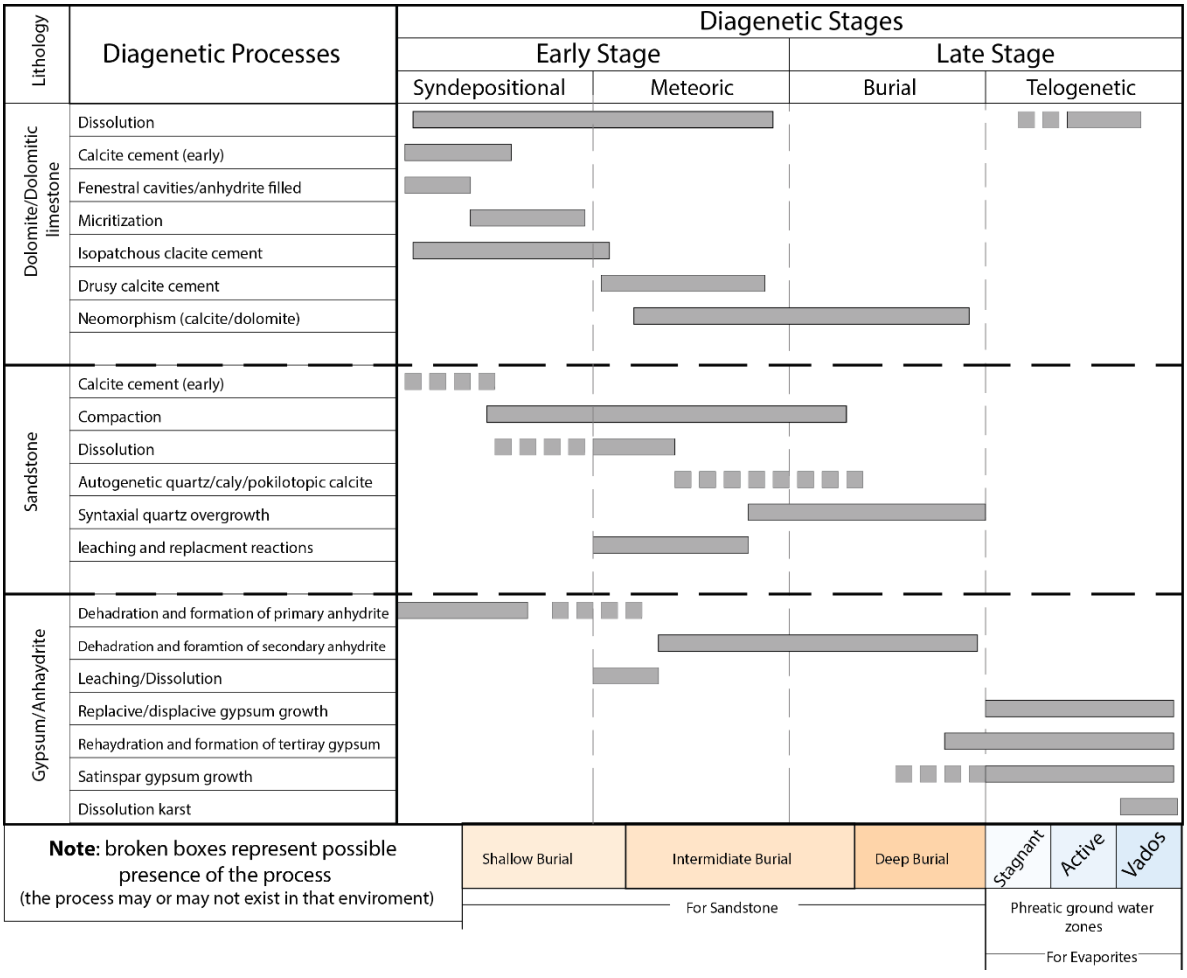

CHAPTER 6:

CONCLUSION AND RECOMMENDATION

6.1. Conclusion

- The Gohatsion Formation in the Blue Nile Basin was previously regarded as a marker formation for basin evolution from continental to transgressive marine setting. Detailed lithofacies analysis coupled with petrographic and geochemical analysis suggests that the Formation has complex and diverse geological setting than previously thought.
- Lithostratigraphic sections studied throughout the basin (including the type section) showed variation in terms of facies and thickness of individual members.
- Lithofacies analysis was done by informally classifying the Formation into the Upper Mudrock Member, Gypsum Member and Lower Mudrock Member.
- Lithofacies of the Lower Mudrock Member, specifically between the Gohatsion and Dejen section, shows mesotidal to macrotidal signatures that indicates siliciclastic back-barrier tidal flat setting or estuary depositional conditions.
- Lithofacies of the Gypsum Member shows subaqueous and subaerial signatures. The Gohatsion section showed salina type facies with frequent erosive contacts and abundant intra-sediment layering indicative of brine mixing and seasonal subaerial exposure under holomictic brine conditions. Subaerial (sabkha type) facies dominates the remaining sections.
- Lithofacies of the Upper Mudrock Member shows a gradational facies change from supratidal and restricted lagoon to intertidal flat that eventually evolve to the overlaying marine facies.
- Petrographic, mineralogical and geochemical attributes of fine siliciclastic sediments indicate first cycle deposit. Geochemical comparison with the underlying sandstone formation show difference in degree of recycling and compositional maturity which rules out the sandstone formation as potential source rock for fine siliciclastic sediments. Instead, the siliclastic rocks show geochemical affinity to nearby Neoproterozoic intrusive rocks exposed in western side of the basin. This implies potential source rock for the sediments may have similar geochemical and geological attributes as the intermediate intrusive rocks.

- Evidence form major/trace element bivariate and multi element plots indicate intermediate to felsic source rock. Trace element tectonic discrimination plots indicate continental island arc setting as an ultimate provenance for siliciclastic sediments.
- Petrographic analysis of dolomitic packstone and sandstones shows the prevalence of syndepositional and meteoric diagenesis than late stage diagenesis whereas gypsum recorded telogenetic textures resulting from interaction with active phreatic water.

6.2. Recommendation

- The studied lithostratigraphic sections reveal facies variation in the basin with respect to the Gohatsion Formaton. Hence, more detailed lithostratigraphic studies in other localities such as Kachise and Chancho areas will confirm and elaborate the facies variation very well. Hence, further lithostratigraphic study in such localities is recommended.
- Recent palynological and paleontological studies on the underlaying sandstone foramtion yielded good results in establishing age contraints. Construction of bio-stratigraphic profile (age constraints) for the siliciclastic and carbonate rocks of this Formation will enhance and strengthen the results and interpretations postulated thus far. Hence, bio-stratigraphic study on such rocks is also recommended.
- Although geochemical signatures in this study provided valuable information when they are integrated with stratigraphic and facies analysis, the number and scale of the geochemical analysis was very limited. Hence, detailed geochemical sampling and analysis is recommended.
- Regarding brine source for evaporite rocks, recent works utilize isotope geochemical analysis of Sr, S, O and C. Although variation in geochemical attributes of REE and trace element have been utilized to investigate continental or marine influence in brine chemistry, isotope analysis gives a definitive answer to this question. Hence, such study is recommended.

REFERENCE

Abbate, E., Bruni, P. and Sagri, M. (2015). Geology of Ethiopia: A Review and Geomorphological Perspectives. **In:** Billi, P. *Landscapes and Landforms of Ethiopia, World Geomorphological Landscapes*. Springer Science+Business Media Dordrecht .33-64

Adams, A.E., MacKenzie, W.S. and Guilford, C. (1984). *Atlas of Sedimentary rocks under microscope*, Longman Group Limited, Burnt mill, Harlow, England, 110pp.

Alberto, W., Giardino, C.M. and Tiranti, D. (2007). Genesis and evolution of 'pseudocarniole': preliminary observations form the Susa Valley (Western Alps), **In**: Schreiber, B.C., Lugli, S. and Babel, M. (2007). *Evaporites through space and time*, Geological Society, London, Special Publications, **285**:155-169.

Aleali, M., Rahimpour-Bonab, H., Moussavi-Harami, R. and Jahani, D. (2013). Environmental and sequence stratigraphic implications of anhydrite textures: A case from the Lower Triassic of Central Persian Gulf, *Journal of Asian Earth Sciences*, **75:** 110-125.

Al-Juboury, A.I., Al-Tarif, A.M. and Al-Eisa, M. (2007). Basin Analysis of Burdigalian and Early Langhian successions, Kirkuk Basin, Iraq. **In**: Schreiber, B.C., Lugli, S. and Babel, M. (2007). *Evaporites through space and time*, Geological Society, London, Special Publications, **285**:335-376.

Andre, L., Deutsch, S. and Hertogen, J. (1986). Trace element and Nd isotopes in shales as indexes of provenance and crustal growth: the early Paleozoic from Brabant Massif (Belgium), *Chemical Geology*, **57**: 101-115.

Aref, M.A.M. (2003). Classification and depositional environments of Quaternary pediogenic gypsum crusts (gypcrete) from east of the Fayum Depression, Egypt, *Sedimentary Geology*, **155**: 87-108.

Asfawossen Asrat, Barbey, P. and Gleizes, G. (2001). The Precambrian geology of Ethiopia: a review. *African Geosciences Review*, **8**: 271-288.

Aster Denekew and Sileshi Bekele (2009). Characterization and Atlas of the Blue Nile basin and Its Sub Basins. Unpublished technical report, International Water Management Institute, Addis Ababa, Ethiopia, 253pp.

Bach, W., Roberts, S., Vanko, D.A., Binna, R.A., Yeats, C.J. and Craddock, P.R. (2003). Controls of fluid chemistry and complexation on rare earth element contents of anhydrite from the Pacmanus sub sea floor hydrothermal system, Manus basin, Papua New Guinea, *Mineralium Deposita*, **38**: 916-935.

Barsisa Bekele (2011). Geochemistry of Lower sandstone in Blue Nile gorge Mesozoic sedimentary sequences: Implication for provenance composition and paleoclimate, Unpublished MSc Thesis, Addis Ababa University, Addis Ababa, Ethiopia, 103pp.

Bekele Abebe, Acocella, V., Tesfaye Korme, and Dereje Ayalew (2007). Quaternary faulting and volcanism in the Main Ethiopian Rift, *Journal of African Earth Sciences*, **48**: 115-124.

Berra, F. and Angiolini, L. (2014). The evolution of the Tethys region throughout the Phanerozoic: a brief tectonic reconstruction. **In**: Marlow, L., Kendall, C. and Yose, L. eds, *Petroleum systems in the Tethyan region*, AAPG Memoir, 106, 1-27.

Bhatia, M.R. (1983). Plate tectonics and geochemical composition of sandstones, *The Journal of Geology*, **91(6)**: 611-627.

Bhatia, MR. and Crook, K.A.W. (1986). Trace element characteristics of greywackes and tectonic setting discrimination of sedimentary basins, *Contributions to Mineral and Petrology*, **92 (2):** 181-193.

Binks, R.M. and Fairhead, J.D. (1991). A plate tectonic setting for Mesozoic rifts of West and Central Africa. *Tectonophysics*, **213**: 141-151.

Boggs, S.(Jr) (2009). *Petrology of Sedimentary rocks (2nd ed)*, Cambridge University Press, New York, 612pp.

Bosellini, A. (1992). The continental margins of Somalia: structural evolution and sequence stratigraphy. **In:** Watkins, J.S., Zhiqiang, F and McMillen, K.J. eds, *Geology and Geophysics of Continental Margins*, **53:** 185-205.

Condie, K.C.(1993). Chemical composition and evolution of the upper continental crust: contrasting results from the surface samples and shales, *Chemical Geology*, **104**: 1-37.

Conforto, L., Calderoni, G., Ferrini, V. and Masi, U. (1993). Element abundances in the Mesozoic neritic limestone from the Abbai (Blue Nile) river valley (Western Ethiopia) and geologic implications, *Geologica Romana*, **29**: 263-275.

Cox, R., Lowe, D.R. and Cullers, R.L. (1995). The influence of sediment recycling and basement composition on evolution of mudrock chemistry in the southwestern United States, *Geochemica et Cosmochemica Acta*, **59(14)**: 2919-2940.

Critelli, S., Mongelli, Giovanni, G., Perri, F., Martin-Algarra, A., Martin-Martin, M., Perrone, V., Dominici, R., Sonnino, M. and Zaghloul, M.N. (2008). Compositional and geochemical signatures for the sedimentary evolution of the Middle Triassic-Lower Jurassic continental red beds form wester-central Mediterranean Alpine chains, *The Journal of Geology*, **116**: 375-386.

Cullers, R.L. (1994). The chemical signature of source rocks in size fractions of Holocene stream sediment derived from metamorphic rocks in the wet mountains region, Colorado, U.S.A., *Chemical Geology*, **113**: 327-343.

Cullers, R.L. (1995). The controls on major and trace element evolution of shales, siltstones and sandstone of Ordovician to Tertiary age in the Wet Mountains region, Colorado, U.S.A. *Chemical Geology*,**123**: 107-131.

Daidu, F. (2013). Classifications, sedimentary features and facies associations of tidal flats, *Journal of Palaeogeography*, **2(1)**: 66-80.

Dalrymple, R.W. (1992). Estuarine facies models: conceptual basis and stratigraphic implications, *Journal of Sedimentary Petrology*, **62 (6):** 1130-1146.

Dalrymple, R.W., Mackay, D.A., Ichaso, A.A. and Choi, K.S. (2012). Process, morphodynamics and facies of tide dominated estuaries (Chapter 5) **In**: Davis, R.A. (Jr) and Dalrymple, R.W (2012). *Principles of Tidal Sedimentology*, Springer Science+Business Midea B.V. DOI 10.1007/978-94-007-0123-6_10.

Dalrymple, R.W., Zaitlin, B.A. and Boyd, R. (1991). Estuarine facies models: conceptual basis and stratigraphic implications, *Journal of Sedimentary Petrology*, **62(6)**: 1130-1146.

Davis, B.L., Kath, R. and Spidle, M. (1990). The Reference Intensity Ratio: its measurement and Significance, *Powder Diffraction*, **5**: 76-78.

Davis, R.A. (2012). Tidal signatures and their preservation potential in stratigraphic sequences (Chapter 3) **In**: Davis, R.A. (Jr) and Dalrymple, R.W (2012). *Principles of Tidal Sedimentology*, Springer Science+Business Midea B.V. DOI 10.1007/978-94-007-0123-6_10.

Dawit Lebenie Enkurie and Bussert, R. (2009). Stratigraphy and facies architecture of Adigrat Sandstone, Blue Nile basin-central Ethiopia, *Zbl.Geol.Palaont.Teil I*, **3 (4)**: 217-232.

Dawit Lebenie Enkurie (2010). Adigrat Sandstone in Northern and Central Ethiopia: stratigraphy, facies, depositional environments and palynology. Unpublished Ph.D. thesis Technische Universität, Berlin. 166 pp.

Dawit Lebenie Enkurie (2016). Paleoclimatic records of Late Triassic plaeosols from central Ethiopia. *Palaeogeography, Palaeoclimatology, Palaeoecology*, **449**:127-140.

Driessche, A.E.S.V., Benning, L.G., Rodriguez-Blanco, J.D., Ossorio, M., Bots, P. and Garcia-Ruiz, J.M. (2012). The role and implications of bassanite as a stable precursor phase to gypsum precipitation, *Science*, **336**: 69-72.

Eby, G.N. (1992). Chemical subdivision of A type granitoids: petrogenetic and tectonic implications, *Geology*, **20**: 641-644.

Ejeh, O.I. (2016). Geochemical discriminant for provenance characterization and paleogeography of shales form Dahomey Embayment, South East Nigeria, *Journal of Geosciences and environment protection*, **4**: 56-68.

Fagherazzi, S., FitzGerald, D.M., Fulweiler, R.W., Hughes, Z., Wiberg, P.L., McGlathery, K.J., Morris, J.T., Tolhurst, T.J. Deegan, L.A. and Johnson, D.S. (2013).Ecogeomorphology of tidal flats. **In**: Shroder, J., Butler, D.R. and Hupp, C.R. (Eds), *Treatise on Geomorphology*, Academic Press, San Diego, CA, **12**: 201-220.

Flemming, B.W. (2012). Silicicalstic back-barrier tidal flasts (Chapter 10), **In:** Davis, R.A. (Jr) and Dalrymple, R.W (2012). *Principles of Tidal Sedimentology*, Springer Science+Business Midea B.V. DOI 10.1007/978-94-007-0123-6_10.

Floyd, P.A. and Leveridge, B.E. (1987). Tectonic environment of the Devonian Gramscatho Basin, South Cornwall: framework mode and geochemical evidence from turbiditic sandstone, *Journal of the Geological Society*, **144**: 531-542.

Freeman, T. (1997). Sedimentary and Dolomitization of Muschelkllk carbonates (Triassic), Iberian range, Spain, *American Association of Petrolium Geologists Bull*, **56**: 434-453.

Gandin, A. and Wright, D.T. (2007). Evidence of vanished evaporites in Neoarchean carbonates of South Africa. **In**: Schreiber, B.C., Lugli, S. and Babel, M. (2007). Evaporites through space and time, *Geological Society, London, Special Publications*, **285**:335-376.

Gandin, A. and Wright, D.T., (2007). Evidence of vanished evaporites in Neoarchean carbonates of South Africa, **In**: Schreiber, B.C.m, and Babel, M. (eds) 2007. *Evaporites through space and time*. Geological Socity of London, Special Publications, **285**:285-308

Gani, N. DS., Abdelsalam, M. G., Gera, S. and Gani, M. R. (2008). Stratigraphic and structural evolution of the Blue Nile basin, northwestern Ethiopian plateau: www.interscience.wiley.com DOI: 10.1002/gj.1127.

Garzanti, E. (2016). From static to dynamic provenance analysis- sedimentary petrology upgraded, *Sedimentary Geology*, **336**: 3-13.

Gebrehiwot, S. G., Ilstedt, U., Gardenas, A. I. and Bishop, K. (2010). Hydrological characterization of watersheds in the Blue Nile Basin. *Hydrol. Earth Syst. Sci. Discuss*. **7**: 4089–4111

Geological Survey of Ethiopia (2016). Geotectonic setting and evolution of sedimentary basins in Ethiopia. Retrieved from www.gse.gov.et/index.php/2016/09/03/petrolium-exploration, on 12.02.2018.

Getaneh Assefa (1979). Clay mineralogy of the Mesozoic sequence in the Upper Abbay (Blue Nile) River valley region, Ethiopia. *Sinet,Ethiop.J.Sci.,***3** (2): 37-65.

Getaneh Assefa (1981). Gohatsion Formation. A new Lias-Malm lithotratigraphic unit from the Abay River basin, Ethiopia. *Geosci. J.* **2**: 63–68.

Gindre-Chianu, L., Warren, J.K., Puigdefabregas, C., Sharp, I.R., Peacock, D.C.P., Swart, R., Poulsen, R., Ferreira, H. and Henrique, L. (2015). Diagenetic evolution of Aptian evaporites in the Namibe Basin (South West Angola). *Sedimentology*, **62**, 204-233.

Golden, D.C., Dixon, J.B. Shadfan, H. and Kippenberger, L.A. (1985) Palygorskite and sepiolite alteration to smectite under alkaline conditions, *Clays and Clay Minerals*, **33**: 44-55.

Gromet, L.P. Dymek, R.F., Haskin, L.A. and Korotev, R.V. (1984). The North American shale composite: its composition, major and trace element characteristics, *Geochimica et Cosmochimica Act*a, **48**: 2469-2482.

Handford, C.R. (1991). Marginal Marine Halite: Sabkhas and Salinas.**In**: Melvin, J.L. (ed.) (1991). *Evaporites, Petroleum and Mineral Resources*, Developments in Sedimantology, **50**, 1-66.

Headberg, D. Hollis. (1976).*International Stratigraphic Guide: A Guide to stratigraphic classification, Terminology and Procedure*. John Wiley & Sons. Inc, Canada, 200 pp.

Herron, M.M. (1988). Geochemical classification of terrigenous sands and shales from core or log data, *Journal of sedimentary Petrology*, **58**: 820-829.

Hofmann, C., Courtillot, V., Feraud, G., Rochette, P., Gezahegn Yirgu, Ketefo, E. and Pik, R. (1997).Timing of the Ethiopian flood basalt event and implications for plume birth and global change, *Nature*, **389**: 838-841.

Hovorka, S.D., Holt, R.M. and Powers, D.W. (2007). Depth indicators in Permian Basin Evaporite. **In**: Schreiber, B.C., Lugli, S. and Babel, M. (2007*). Evaporites through space and time*, Geological Society, London, Special Publications, **285**,335-376.

Hu, J., Li, Q., Fang, N., Yang, J. and Ge, D. (2014). Geochemistry and characteristics of the low Permian sedimentary rocks form central uplift zone, Qiangtang Basin, Tibet: insights into source area weathering, provenance, recycling and tectonic setting, *Arab. J.Geosci.*, **8 (8):** 5373-5388.

Janssen, M.G., Stephnson, R.A. and Cloetingh, S. (1993). Changes in plate motions and their control on the subsidence of rifted basins in the African plate. *Geodynamics of Rifting, TectonoPhysics* **213**: 141-151.

Jepsen, D.H. and Athearn, M.J. (1961).General geology map of the Blue Nile River basin Ethiopia. Unpublished geological map, U.S. Department of Interior/Department of water resources Ethiopia, Addis Ababa, Ethiopia.

Kazmin, V. (1975). Explanation of the Geological Map of Ethiopia. Unpublished technical report, Geological Survey of Ethiopia, Addis Ababa, Ethiopia, 18 pp.

Khan, T. and Khan, M.S. (2015). Clastic rock geochemistry of Punagarh basin, trans-Aravalli region, NW Indian Shield: implications for paleoweathering, provenance and tectonic setting, *Arab J Geosci*, **8**: 3621-2644.

Kieffer, B., Arndt, N., Lapierre, H., Bastien, F., Bosch, D., Pecher, A., Gezahegn Yirgu, Dereje Ayalew, Weis, D., Jerram A.D., Keller, F. and Meugniot, C. (2004). Flood and shield basalts from Ethiopia: magmas from the African super swell. *Journal of Petrology*, **45**: 793-884.

Krumbein, W.C. and Sloss, L.L. (1950). *Stratigraphy and Sedimentation*. W.H. Freeman & Co., San Fransisco, USA, 497 pp.

Lee, Y.I. (2002). Provinance derived from the geochemistry of late Paleozoic-early Mesozoic mudrocks of Pyeongan Supergroup, Korea, *Sedimentary Geology*, **149**, 219-235.

Lentz, D.R. (2003). Geochemistry of sediments and sedimentary: historical to research perspectives, *Geological association of Canada, Geo Text*, **4**, 1-6.

Lonoy, A., Akselsen, J. and Ronning, K. (1986). Diagenesis of deeply buried sandstone reservoir: Halid Field, Northern North Sea, *Clay Minerals*, **21**: 497-511.

Lu, F.H., Meyers, W.J. and Hanson, G.N. (2002). Trace elements and environmental significance of Massinian gypsum deposits, the Nijar Basin, southeastern Spain, *Chamical Geology*, **192**: 149-161.

Matter, A. (1967). Tidal flat deposits in the Ordovician of western Maryland, *Jour.Sed.Petrology*, **37**: 601-609.

McLennan, S.M., Hemming, S. and McDaniel, D.K. (1993). Geochemical approaches to sedimentation, provenance and tectonics, *Geological Society of America special paper*, **284**: 21-40.

McLennan, S.M., Tylor, S.R. and Kroner, A. (1983). Geochemical evolution of Archean shale from South Africa: I. the Swaziland and Pongola Supergroups. *Precambrian Res*., **22**: 93-124.

McLennan, S.M., Simonetti, A. and Goldstein, S.L. (2000). Nd and Pb isotopic evidence for provenance and post-depositional alteration of the Paleoproterozoic Huronian Super group, Canada, *Precamberian Research*, **102**: 263-278.

Mengesha Tefera, Tadiwos Chernet and Workineh Haro (1996). Explanation of the geological map of Ethiopia (Scale 1:2,000,000) 2nd ed. Unpublished technical report, Ethiopian Institute of Geological Surveys, Addis Ababa, Ethiopia, 85pp.

Merla, G., Abbate, E., Azzaroli, A., Bruni, P., Canuti, P., Fazzuoli, M., Sagri, M. and Taacconi, P.(1979). A geological map of Ethiopia and Somalia (1:2,000,000) and comment with a map of major landforms, Unpublished technical report, University of Florence, Italy, 98pp.

Milliken, M.L. (2005). Late diagenesis and mass transfer in sandstone-shale sequences. **In**: Mackenzie, F.T. (ed). *Sediments, diagenesis and sedimentary rocks*, Treatise on Geochemistry, Elsevier, Oxford, United Kingdom, **7**: 159-190.

Mills, R,A, and Elderfield, H. (1995). Rare earth element geochemistry of hydrothermal deposits form the active TAG Mound, 26^0N Mid Atlantic Ridge, *Geochemica et Cosmochemica Acta*, **59**: 3511-3524.

Mogessie, A., Krenn, K., Schaflechner, J., Koch, U., Egger, T., Goritchnig, B., Kosednar, B., Pichler, H., Ofner, L., Bauernfeind, D., Tadesse, S., Hailu K., and Demessie, M. (2002). Geological excursion to the Mesozoic sediments of the Abay Basin (Blue Nile), recent volcanics of the Ethiopian Main Rift and basement rocks of the Adola area, Ethiopia. *Mitt.Österr.Miner.Ges*. **147**: 43-74.

Mohr, P.A. (1962). *The geology of Ethiopia*. University College of Addis Ababa Press, Addis Ababa, Ethiopia.

Moore, C.H. (1989). *Carbonate diagenesis and Porosity, Developments in sedimentology 46*, Elsevier Sciences B.V., Amsterdam, Netherlands, 351pp.

Muir, M.D. (1987). Facies models for Australian Precambrian evaporites. **In**: Peryt, M.T. (ed.) (1987). *Evaporite Basins, Lecture notes in Earth Sciences*, Springer-Verlag, Berlin, Germany, 5-21.

Nasbitt, H.W. and Young, G.M. (1984). Prediction of some weathering trend of plutonic and volcanic rocks based on thermodynamic and kinetic consideration, *Geochem. Acta*, **48**: 1523-1534.

Nesbitt, H.W. and Young, G.M. (1982). Early Proterozoic climates and plate motions inferred from major element chemistry of lutites, *Nature*, **299**: 715-717.

Nyakairu, G.W.A. and Koeberl, C. (2001). Mineralogical and chemical composition and distribution of rare earth elements in clay rich sediments from central Uganda, *Geochemical Journal*, **35**: 13-28.

Odin, G.S. (1990). Clay mineral formation at the continent-ocean boundary: the verdine facies, *Clay Minerals*, **25**: 477-483.

Ogawa, Y. and Shikazono, N. (2006). REE behaviors during anhydrite and gypsum formations of the Kuroko Type massive sulfide-sulfate deposit. **In:** *Water Dynamics: 3rd international Workshop on water Dynamics,* pp.162-166. Tohoku University, Sendai, Japan.

Paikaray, S., Banerjee, S., Mukherji, S. (2007). Geochemistry of shales from the Paleoproterozoic to Neoproterozoic Vindhyan Supergroup: Implications on provenance, tectonics and paleoweathering, *Journal of Asian Earth Sciences*, **32(1)**: 34-48.

Perri, E., Gindre-Chanu, L., Caruso, A., Cefala, M., Scopellti, G. and Tucker, M. (2017). Microbial-meditated pre-salt carbonate deposition during the Massinian salinity crisis (Calcare di Base fm., Southern Italy), *Marine and Petroleum Geology*, **88**: 235-250.

Pettijohn, F.J., Potter, P.E., and Siever, R. (1987). *Sand and Sandstone*, Springer-Verlag, NewYork, 553pp.

Pik, R., Daniel, C., Coulon, C., Gezahegn Yirgu, Hofmann, C. and Dereje Ayalew (1998). The northwestern Ethiopian plateau flood basalts: classification and spatial distribution of magma types. *Journal of Volcanology and Geothermal Research*, **81**: 91-111.

Playa, E., Cendon, D.I., Trave, A., Chivas, A.R. and Garcia, A. (2007). Non-marine evaporites with both inherited marine and continental signatures: the Gulf of Carpentaria, Australia, at ~70ka, *Sedimentary Geology*, **201**: 267-285.

Rahimpour-Bonab, H., Esrafili-Dizaji, B. and Tavakoli, V. (2010). Dolomitization and anhydrite precipitation in Permo-Triassic carbonates at the south pars gas field, offshore Iran: controls on reservoir quality, *Journal of Petroleum Geology*, **33(2)**: 1-24.

Rahimpour-bonab, H., Shariatina, Z. and Siemann, M.G. (2007). Role of rifting in evaporite deposition in the Great Kavir Basin, Central Iran, **In**: Schreiber, B.C.m, and Babel, M. (eds) 2007. *Evaporites through Space and Time*, Geological Socity of London, Special Publications, **285**:69-86

Roser, B.P. and Korsch, R.J. (1988). Provenance signatures of sandstone-mudstones suites determined using discriminant function analysis of major elemental data, *Chem Geol*. **67**: 119-139.

Rouchy, J.M., Laumondals, A. and Groessens, E. (1987). The Lower Carboniferous (Visean) Evaporites in northern France and Belgium: depositional, diagenetic and deformational guides to reconstruct a disrupted evaporite basin. **In:** Peryt, M.T. (ed.) (1987). *Evaporite Basins, Lecture notes in Earth Sciences*, Springer-Verlag, Berlin, Germany, 25-31.

Russo, A., Getaneh Assefa, and Balemwal Atnafu (1994). Sedimentary evolution of the Abbay River (Blue Nile) basin, Ethiopia. *N. Jb. Geol. Paläont. Mh*. **5**: 291–308.

Santisteban, J.I., Mediavilla, R., Lopez-Pamo, E., Dabiro, C.J., Zapata, M.B.R., Glrcia, M.J.G., Castano, S. and Martinez, E. (2004). Loss of ignition: a quantitative or qualitative method for organic matter and carbonate mineral content in sediments?, *Journal of Paleolimnology*, **32(3)**: 287-299.

Schandelmeier, H. and Reynolds, P.-O., (eds) (1997). *Palaogeographic-Palaotectonic atlas of north eastern Africa, and adjacent areas*, A.A Balkema, Rotterdam, Netherlands, 160pp.

Schandelmeier, H., Reynolds, P.O. and Semtner, A.K. (1997). Chapter 8. The Late Triassic (Norian, Ca.220Ma). In*:* Schandelmeier, H., Reynolds, P.O. and Semtner, A.K.(eds.).*Paleogeographic-Paleotectonic Atlas of North Eastern Africa and Adjecent areas*, Rotterdam, A.A. Balkema, 45-50.

Schieber, J., (1999).Distribution and deposition of mudstone facies in the upper Devonian Sonyea Group of New York, *Journal of Sedimentary Research*, **69**: 909-925.

Schmidt. D. & Werner, C. (1998). Early Cretaceous coastal plain sediments of the Mugher Mudstone Formation. Abay River Basin, Ethiopia. *Zbt. Geol. Palaont*. **1**: 293–309.

Serawit Amene and Tamrat Mojo (1996). The geology of Gundo Meskel and Ejere Areas: Abay Basin, North Shoa. Unpublished technical report, Ministry of Mines and Energy Petroleum Operations Department, Addis Ababa, Ethiopia. 61pp

Serawit Amene, and Tamrat Mojo (1999). The geology of Mugher Cement Factory Area: Abay Basin, north Showa. Unpublished technical repot, Ministry of Mines and Energy Petroleum Operations Department, Addis Ababa, Ethiopia. 25pp

Serra, O. (1986). Fundamentals of well-log interpretation 2.the interpretation of logging data; Chapter 7: information on diagenesis (transformation of rocks and sediments), *Developments in Petroleum Sciences*, **15 (B)**: 3-679.

Shearman, D.J., Mossop, G., Dunsmore, H. and Martin, H. (1972). Origin of gypsum veins by hydraulic fracture, *Trans.Inst.Min.Met all*, **82(B):** 65-67.

Solomon Tadesse, Milesi, J.P. and Deschamps, Y. (2003). Geology and mineral potential of Ethiopia: a note on geology and mineral map of Ethiopia. *J. of Afr. Earth sci.*, **36**: 273-313.

Tamrat Mojo and Tibebe G/Selassie (1997). The Geology of Gindeberet-Jeldu and Amuru-Jarti Areas: eastern Wollega and western Shoa. Abay Basin, north Showa. Unpublished technical report, Ministry of Mines and Energy Petroleum Operations Department. Addis Ababa, Ethiopia.27pp.

Tamrat Worku and Astin, T.R. 1992. The Karroo sediments (Late Palaeozoic to early Jurassic) of Ogaden Basin, Ethiopia. *Sediment. Geol*. **76**: 7–21

Tao, H., Sun, S., Wang, Q., Yang, X. and Jing, L. (2014). Petrography and geochemistry of Lower Carboniferous greywacke and mudstones in Northeast Junggar, China: Implications for provenience, source weathering and tectonic setting, *Journal of Asian Earth Sciences*, **87:** 11-25.

Taylor, S.R. and McLennan, S.M. (1995). The geochemical evolution of the continental crust, *Reviews in Geophysics*, **33**:241-265.

Tesfaye Kebede, Koeberl, C. and Koller, F. (1999). Geology, geochemistry and petrogenesis of intrusive rocks of the Wollega area, western Ethiopia, *Journal of African Earth Sciences*, **29 (4)**: 715-734.

Tessier, B. (2012). Stratigraphy of tide dominated estuaries (Chapter 6) **In**: Davis, R.A. (Jr) and Dalrymple, R.W (2012). *Principles of Tidal Sedimentology*, Springer Science+Business Midea B.V. DOI 10.1007/978-94-007-0123-6_10.

Totten, M.W. and Hanan, M.A. (2007). Heavy minerals in shales, *developments in sedimentology*, **58**: 323-341

Tunik, M.A., Pazos, P.J., Impiccini, A., Lazo, D. and Aguirre-Urreta, M.B. (2009). Dolomitized tidal cycles in the Agua De la Mula member of the Agrio Formation (Early Cretaceous) Neuquen Basin, Argentina, *Latin American Journal of Sedimentology and Basin Analysis*, **16(1):** 29-43.

Ullah, K., Arif, M. and Tahir Shah, M. (2015). Petrography and geochemistry of Kamlial Formation, southwestern Kohat plateau, Pakistan: implications for paleoclimate of Western Himalayas, *Turkish Journal of Earth sciences*, **24**: 276-288.

Verde, B. (2003). Green clay minerals In: Sediments, Diagenesis and Sediemtary Rocks (ed. Macknzie, F.T.). **In**: *Treatise on Geochemistry* 488pp. (eds. Holland, H.D. and Turekian, K.K), Elsevier-Pergamon, Oxford, England.

Warren, J.K. (1991). Sulfate dominated sea marginal and platform evaporative settings: Sabkhas and Salinas, mudflats and salterns. **In**: Melvin, J.L. (ed.) (1991). *Evaporites, Petroleum and Mineral Resources*, Developments in Sedimantology,**50**, 1-66.

Warren, J.K. (2006). *Evaporites: sediments, resources and hydrocarbons*, Springer Verlag, Berlin Heidelberg, Germany. 1041 pp.

Warren, J.K. (2016). *Evaporites: a geological compendium,* 2nd ed., Springer International Publishing, Switzerland. 1822 pp.

Wolela Ahmed (2008). Sedimentation of the Triassic–Jurassic Adigrat Sandstone Formation, Blue Nile (Abay) basin, Ethiopia, *J. Afr. Earth Sci*. doi:10.1016/j.jafrearsci.2008.04.001.

Worash Getaneh (2002). Geochemistry provenance and depositional tectonic setting of Adigrat Sandstone northern Ethiopia. *Journal of African Earth Sciences*, **35**: 185-198.

Worash Getaneh and Valera, R. (2002). Rare earth element geochemistry of the Antalo supersequence in the Mekele Outlier (Tigray region, northern Ethiopia), *Chemical Geology*, **182**: 395-407.

Xiaosong, X., (1987). Characteristic and environments of Sinan evaporites in Southern Sichuan, China. **In:** *Evaporite Basins, Lecture notes in Earth Sciences*, (Peryt, M.T. ed.), pp.25-31.Springer-Verlag, Berlin, Germany,

Xie, Q., Chen, T., Zhou, H., Xu, X., Xu, H., Lu, H. and Balsam, W. (2013). Mechanism of palygorskite formation in the Red Clay Formation on the Chinese loess plateau, northwest Chania, *Geoderma*, **192**: 39-49.

Xiong, D., Azmy, K., Blamey, N.G.F. (2016). Diagenesis and origin of calcite in Flemish Pass Basin sandstone reservoir (Upper Jurassic): Implications for porosity, *Marine and Petroleum Geology*, **70**: 93-118.

Yuan, G., Cao, Y., Zhang, Y. and Gluyas, J. (2017). Diagenesis and reservoir quality of sandstones with ancient 'deep' incursion of meteoric fresh water- an example in the Nanpu sag, Bohai Bay Basin, East China, *Marine and Petroleum Geology*, **82**: 444-464.

Zelalem Shiferaw (2005). Lithological and structural mapping of the central and north western parts of central and north western part of Ethiopia in view of petroleum exploration. Unpublished MSc thesis, Addis Ababa University, Addis Ababa, pp 110.

APPENDIX

Appendix A: Lithostratigraphic sections

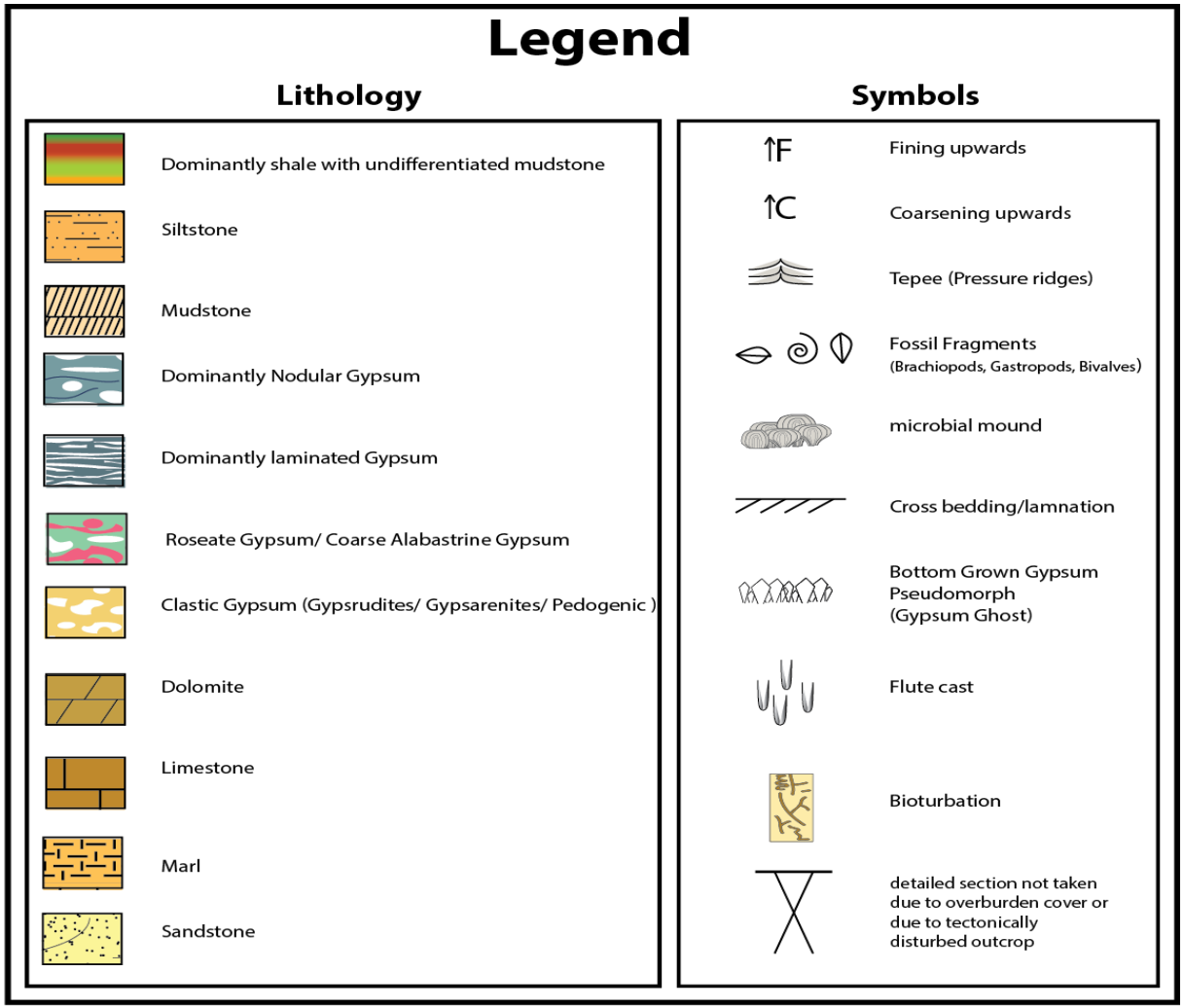

1: Gohatsion Section

GOHATSION SECTION	TOTAL SECTION : 433 meters	

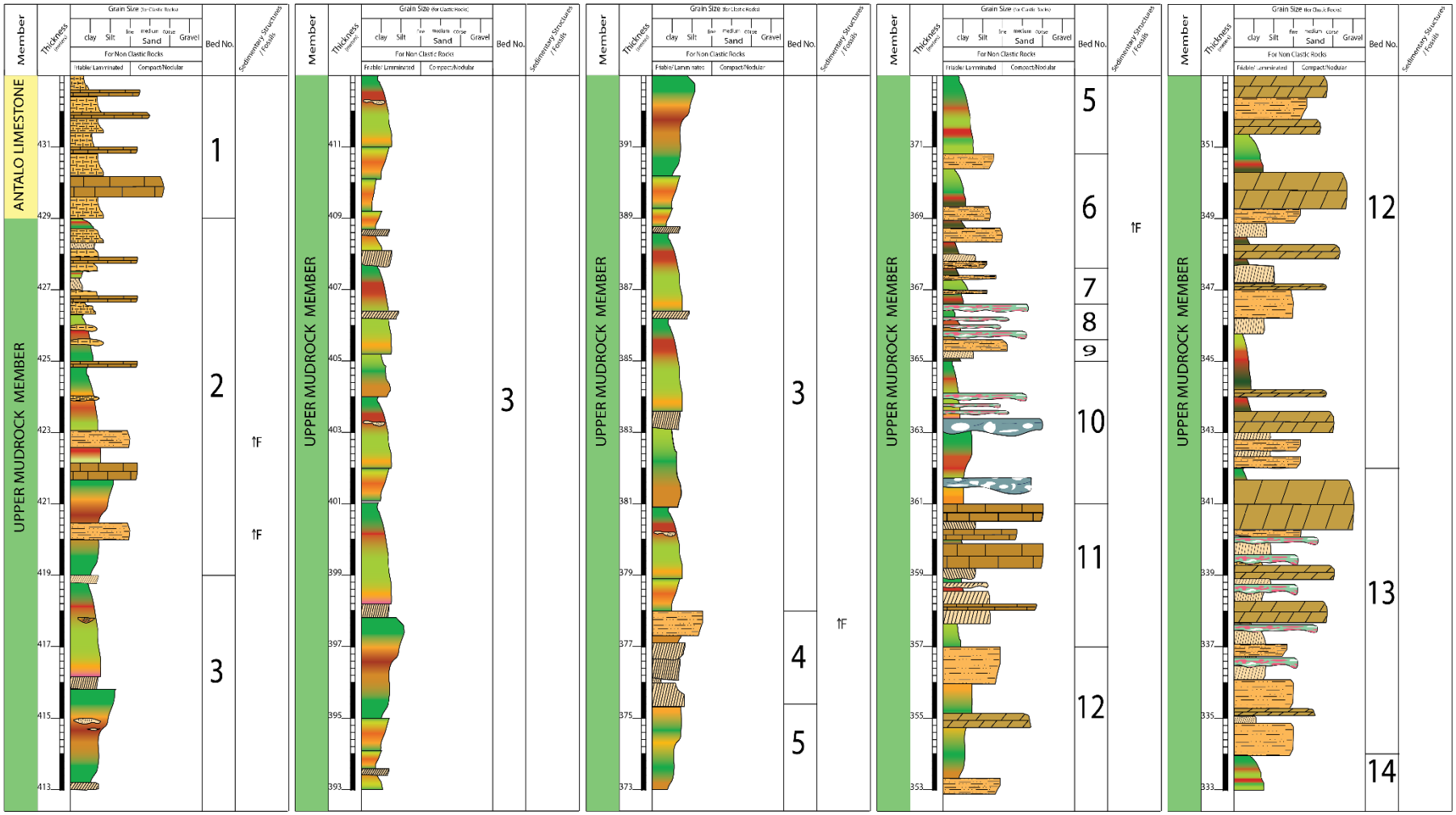

GOHATSION SECTION	TOTAL SECTION : 433 meters	

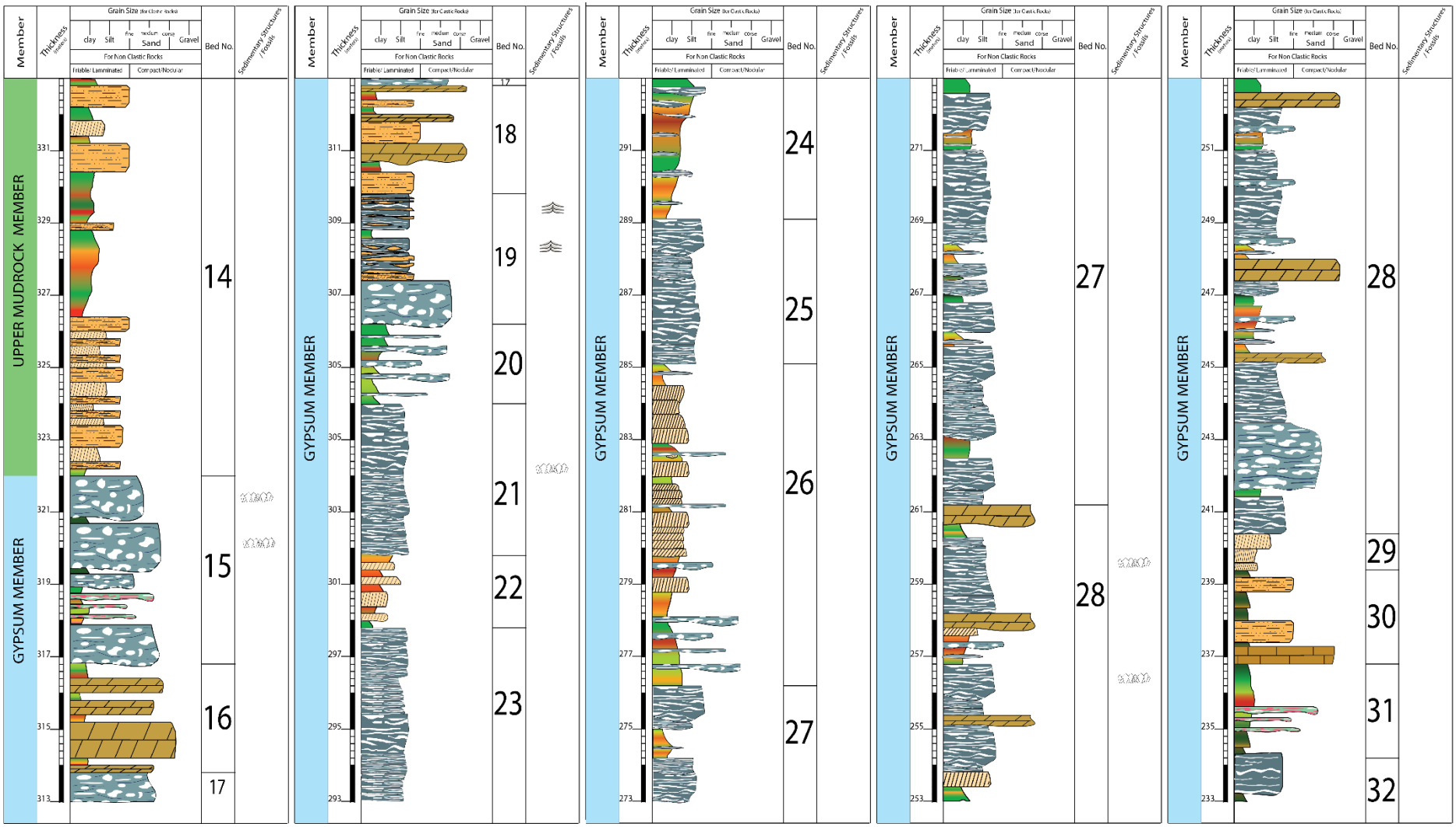

GOHATSION SECTION	TOTAL SECTION : 433 meters	

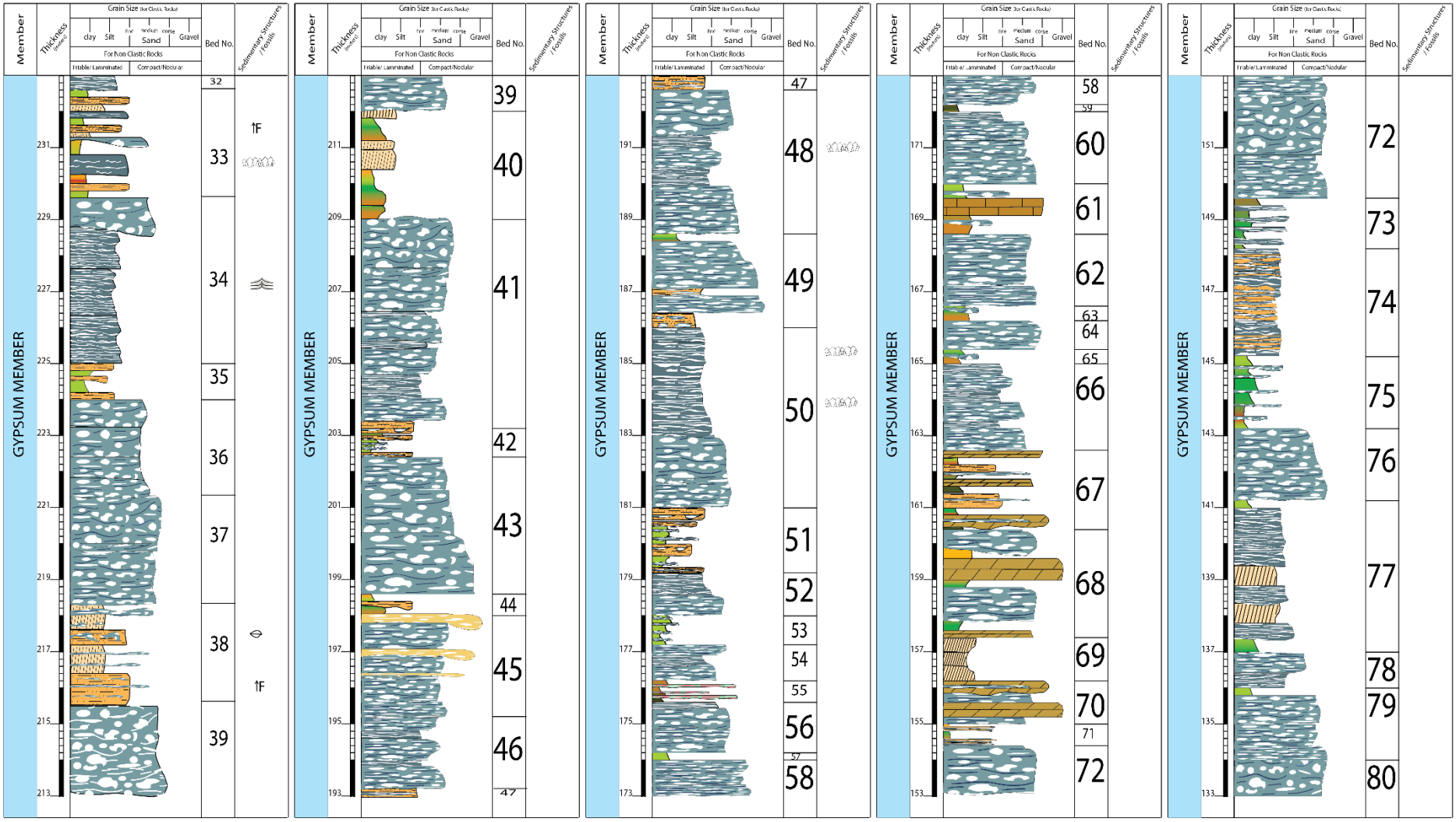

GOHATSION SECTION	TOTAL SECTION : 433 meters	

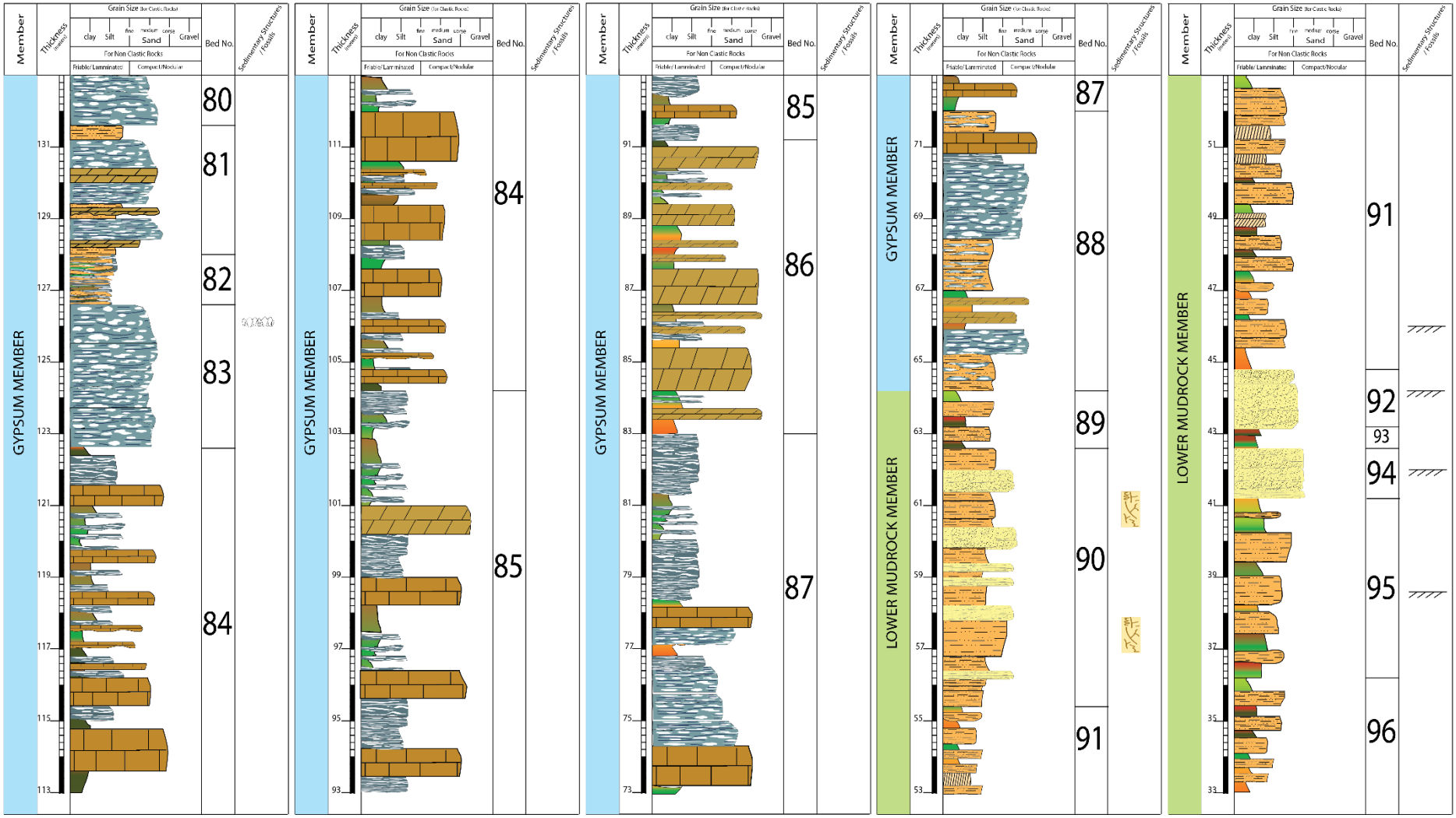

GOHATSION SECTION	TOTAL SECTION : 433 meters	

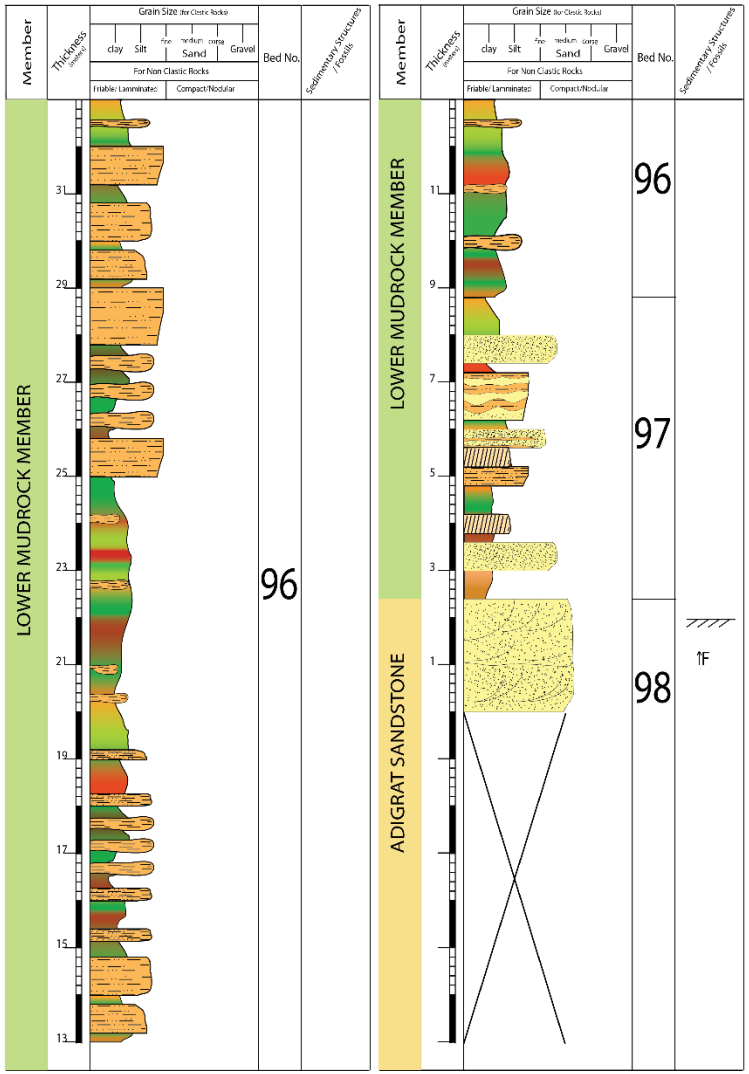

Lithostratigraphic Description of Gohatsion Section

Bed No.	Description
1	• **Marl inter bedded with limestone**: light gray to yellowish gray, massive marl beds with occasional thin beds of limestone (0.2-0.6m thick). Limestone beds are generally micritic. Some fossil fragments observed towards the top. Cavities often filled with secondary calcite.
2	• **Inter bedded Marl, limestone Mudstone and Shale:** Marl and Limestone similar to bed 1, shale beds are greenish gray in color, mostly fissile but also compact in other observation sites and are heavily inter Layard with greenish gray mudstone beds especially south of Filiklik town. Wavy laminations and beds of calcareous silty beds with fining upwards sequence observed towards the bottom.
3	• **Variegated Shale, mudstone and clay stone:** Both shale and mudstone show shades of green and gray along with reddish and brownish gray color. Clay stone beds tend to be more compact and occasionally contain lenticular beds of silt. Dark green clay stone laminations with uniform to irregular bedding can be found along with flame structures and wavy bedding.
4	• **Inter Layard Mudstone and Siltstone and Shale:** Light greenish to brownish gray. Shale beds are similar to bed 3 in description, mudstone is dominant towards the bottom whereas, siltstone is dominant at the top. Siltstone is calcareous and also shows fining up wards sequence. In both mudstone and siltstone beds, laminations of green clay stones with irregular and discontinuous bedding can be found.
5	• **Variegated Shale and Mudstone:** description of this bed is similar to Bed 3 with the exception of absence of lenticular beds of siltstone
6	• **Inter bedded muddy siltstone and shale:** Light greenish to brownish gray, muddy siltstone shows thin lamination towards the bottom whereas, bed thickness increases towards the top (0.4m). Also fining upwards sequence is observed towards the bottom including rip up clasts of clay stone can be observed. Shale beds are similar to bed 3.

Bed No.	Description
7	• **Inter bedded Mudstone and Shale:** description of both Mudstone and Shale Similar to bed 4
8	• **Intercalation of Desert Rose Gypsum, shale and Mudstone:** shale and mudstone have various shades of greenish gray color. Mudstone is compact and also show thin irregular laminations of green claystone in the middle. Gypsum crests also observed near the contact to desert rose beds. Desert rose gypsum show shades of pink to red color and becomes more nodular towards the bottom.
9	• **Inter bedded Mudstone and Shale:** description similar to bed 4
10	• **Desert rose Gypsum inter layered with Shale:** Shale beds show dominantly greenish gray color but also have minor variegated colored layers towards the bottom, shale horizons at the middle of this unit are also gypsified especially near the contact to gypsum beds. Desert rose gypsum beds are mostly thinly bedded range from deep pink to white in color. The degree of nodules increase towards the bottom to the point that beds become chicken wire gypsum beds.
11	• **Inter Layard limestone and Variegated Mudstone.** Description of limestone beds similar to bed 1. Mudstone shows greenish gray at the top and reddish to brownish gray color at the bottom of this unit. Limestone unit is dominant at the top with minor intercalations of calcareous brownish gray mudstone (0.2-0.4m).
12	• **Inter Layard Shale, Mudstone, Siltstone, Dolostone and Clay Stone:** description of variegated shale and mudstone similar to bed 10. Layers are partly dissected by satin spar semi conjugate to erratic satin-spar veins. Siltstone description similar to bed 4 with the exception that majority of siltstone layers are sandy with thickness ranging from 0.4-0.8m. dolostone layers show light yellowish to brownish gray color, partly fossiliferous, cavities and veins filled with secondary calcite and gypsum with thickness ranging from 0.2-1m.
13	• **Alternating Dolostone, mudstone and Desert Rose Gypsum:** Description of Dolostone similar to bed 12. Description of mudstone and desert rose gypsum similar to bed 12

Bed No.	Description
14	• **Variegated Silty mudstone and Shale:** mudstone shows multitude of colors ranging from reddish gray to greenish and yellowish gray color. Calcareous with rare irregular laminations of clay stone. Shale description similar to bed 8, is more dominant at the top. Towards the bottom, inter Layard sequence of siltstone, mudstone and shale is very intensive.
15	• **Inter bedded Gypsum and shale along with laminations of desert rose:** gypsum beds are light bluish gray to light gray color nodular texture with uniform bedding (0.4-1.5m) various textures observed such as abrupt truncated surfaces, pseudomorph of anhydrite after gypsum, relict textures of bottom growth crystals, degree of nodularity increases towards the bottom to the point that it becomes chicken wire gypsum. Shale and desert rose gypsum description similar to bed 8. Shale units also dissected by thin irregular satin-spar gypsum veins.
16	• **Alternating Dolostone and shale layers:** shale show variegated color (light greenish to brownish and reddish gray) partly calcareous, Dolostone description similar to bed 14. Some Dolostone beds show vugg structures and intense and irregular satin spar veins.
17	• **Gypsum:** massive Albastrine type, light pinkish to bluish gray color with irregular and scattered laminations of white gypsum also present.
18	• **Siltstone inter layered with gypsiferous shale and Dolostone:** silt beds description similar to bed 4. Shale are light greenish to brownish gray color, gypsified (selenitic gypsum fragments having coarse sand to pebble grain size) and highly friable. Dolostone description similar to bed 16.
19	• **Laminated Gypsum, silt and shale:** Gypsum shows light bluish to light gray color, highly laminated and intercalated with calcareous silt and shale units. Silt and shale description similar to bed 4. Gypsum beds also show tepee and enterolithic folds. Displasive gypsum growth also observed within these layers.
20	• **Interlayered Shale, Gypsum:** Shale beds are dominantly light greenish color, partly silty towards the bottom, calcareous and gypsiferous. Gypsum, light bluish gray to light gray, thinly bedded and highly intercalated with shale, secondary satin spar veins irregularly cross cut both shale and gypsum units.

Bed No.	Description
21	• **Gypsum:** Light Bluish Gray, laminated, laminations are uniformly wavy with irregular thickness, enterolithic white layers of gypsum also present, microbial gypsum also observed towards the bottom. At the top, white wavy beds with gypsum ghosts showing bottom growth textures can also be observed.
22	• **Interlayered Shale and mudstone:** shale shows various shades of greenish gray color. Mudstone is compact and also show thin irregular laminations of green claystone in the middle. Gypsum crests also observed. Mudstone and calcareous and dominantly shows light yellowish to brownish gray color,
23	• **Gypsum:** description similar to bed 21, with the exception that in this unit, laminations is less wavy and intensified and there is no microbial gypsum within this unit.
24	• **Interlayered Shale and Gypsum:** Shale and gypsum description similar to bed 20, with the exception that gypsum beds are thinner in this sequence.
25	• **Gypsum:** Description of this unit similar to bed no 21.
26	• **Inter Layard Shale, Mudstone, and Gypsum:** description of Shale and Gypsum Similar to bed 24, Mudstone description similar to bed no 22.
27	• **Interlayered Gypsum, Shale and Mudstone:** Description of Gypsum similar to bed 21 (the alteration between wavy laminated beds and microbial gypsum texture also observed here). Towards the bottom of this succession, the texture of gypsum also becomes nodular (the change of texture is gradational). Shale and Mudstone description Similar to bed no 22 and 24 respectively
28	• **Interlayered Gypsum, Shale, Dolostone and Mudstone:** Description of Gypsum similar to bed 27. Beds become more coarse and nodular along with some enterolithic layers in the middle. Gypsum ghosts also observed. Shale and Mudstone description Similar to bed no 22 and 24 respectively. Dolostone beds are uniformly and thinly bedded partly fossiliferous and distributed throughout the succession, forming and intercalation with both gypsum and shale beds.

Bed No.	Description
29	• **Sandy Mudstone:** Greenish to brownish gray, very friable, calcareous and gypsiferous (selenite gypsums with fine to coarse crystal size) consolidated claystone layers with 0.05-0.1m thickens also present.
30	• **Inter layered siltstone, clay stone and mudstone:** description of this unit similar to bed 4 with the addition of satin spar veins. At the bottom, there is a 0.5m thick sandy limestone bed having a yellowish Brown to yellowish gray color that is dissected by irregular satin spar veins
31	• **Shale:** description of this bed similar to bed 8 with the addition of a network of satin spar veins along with some minor laminations of desert rose gypsum
32	• **Gypsum with minor intercalation of mudstone:** gypsum dark gray to greenish gray laminated, displacive gypsum crystals along with occasional nodules show sub-horizontal alignment towards the bottom of the bed. Mud layers (0.2m thick) are gypsified and clasts of them can also be found within gypsum layers near the contact of the bed.
33	• **Inter Layered Gypsum, Shale and Siltstone:** Gypsum description similar to bed 32 with the exception that beds become nodular in comparison with the above bed and gypsum ghosts showing a bottom growth texture in contorted and bent beds. Shale beds are also similar to bed 31. Siltstone layers are brownish gray in color, having an irregular beds with fining upwards sequence also observed.
34	• **Gypsum:** reddish brown to brownish gray, massive, top 1m is nodular while the rest of the bed is massive to laminated bed with some occasional gypsum nodules that form albastrine texture. The nature of contact between these beds is sharp and truncated (erosive surface). Laminated beds of the second layer show tepee structure while the upper nodular bed is affected by local dissolution cavity filled with the overlaying shale unit from bed 33.
35	• **Inter Layered Siltstone and Shale:** description of this bed similar to bed no 14.
36	• **Gypsum:** Description of Gypsum beds similar to bed 32. Uniformly layered, Bedding thickness increases towards the top.

Bed No.	Description
37	• **Gypsum:** White to light gray, shows chicken wire texture, at the top, laminations of gypsum crests matrix alabastrine gypsum nodule. Relatively friable when compared to the other gypsum beds. Towards the bottom the beds become calcareous (gypsum nodules with calcareous matrix)
38	• **Inter bedded gypsified Mudstone and Siltstone:** Mudstone shows light greenish gray to dominantly yellowish gray color, selinitic crystals (sand to pebble size) occur, it is also calcareous. Siltstone shows brownish to yellowish gray color, indurated, fossiliferous (brachiopods and other fossil fragments), it also shows fining upwards sequence, gypsum veins along with voids filled by secondary selenite crystals also occur.
39	• **Gypsum:** Description similar to bed no 37 with the exception that this bed is more pink and no calcareous matrix in this unit
40	• **Inter bedded Mudstone and Shale:** description similar to bed 22
41	• **Gypsum:** light bluish to pinkish gray, massive, wavy laminations occasionally observed throughout the bed, cracks and dissolution voids filled by secondary selenitic gypsum also observed.
42	• **Interlayered Gypsiferous Siltstone and Shale:** Description of this bed similar to bed no 38 with the exception that neither siltstone nor shale are fossiliferous. Veins of secondary satin spar also affect both beds.
43	• **Gypsum:** description of this bed similar to bed no 41. Although In this case, chicken wire texture dominates instead of irregular wavy laminations.
44	• **Interlayered Shale and Siltstone:** Description of this bed similar to be 38 with the addition of lenticular beds within siltstone beds.

Bed No.	Description
45	• **Gypsum:** light Bluish to deep Bluish gray, massive irregular beds in the middle. At the top and middle part of this bed, thin clastic beds having gypsum (Pebble to Cobble sized, sub rounded) and silt clasts matrixed by gypsum and organic matter observed.
46	• **Gypsum:** description of this unit similar to bed 41.
47	• **Gypsified siltstone:** Brownish to reddish gray, normal graded bedding, occasional clasts of gypsum observed towards the bottom, cavities filled with secondary selenitic gypsum also observed.
48	• **Gypsum:** layered, light bluish gray to light gray, bed thickness decreases towards the top, gypsum ghosts forming bottom growth textures, dissolution surface between layers partly filled by fibrous and selenitic secondary gypsum, some layers tend to have both laminated and nodular bed within them. Nodular texture dominates the bottom.
49	• **Inter layered Gypsum, Silt and mudstone:** gypsum shows dark gray and massive bed at the top that gradually change in to nodular and chicken wire texture towards the bottom. Siltstone and shale beds are calcareous and gypsiferous and show light brownish to greenish gray color.
50	• **Gypsum:** deep blue to bluish gray, layered, bed thickness decreases when going from bottom to top, a mixture of textures between nodular and laminated texture exist. The bottom layers are dominated by nodular gypsum whereas the top layers show distinct lamination and layering. Gypsum ghosts showing bottom growth texture, erosive surfaces between beds and some enterolithic folds.
51	• **Intercalated Shale, gypsum and gypsiferous siltstone:** Gypsum shows laminated texture, bluish gray to violate color, sporadic clasts of gypsum (dispalcive or clastic??) also observed. Description of Shale and gypsiferous silt similar to bed no 14 and 49 respectively.
52	• **Gypsum:** description of this bed similar to bed no 50, with the exception that no erosive surface was observed.

Bed No.	Description
53	• **Shale:** light greenish gray to reddish gray, partly gypsiferous, also affected by secondary vein filling satin spar gypsum
54	• **Gypsum:** Description Similar to bed 50 with the exception that individual beds don't show change in thickness
55	• **Shale:** description of this unit similar to bed no 53 except in this case, the thickness of gypsum increases and forms desert rose and shale is more variegated
56	• **Gypsum:** description of this unit similar to bed no 50 with the exception that Nodular texture dominates in this unit.
57	• **Shale:** Description of this unit is similar to bed no 53 with the exception that this bed is dominantly greenish gray in color
58	• **Gypsum:** light gray to white, gypsum shows chicken wire texture, separated by a thin lamination of gypsified shale from the underlain unit.
59	• **Shale:** Description of this unit similar to bed no 53
60	• **Gypsum:** Description of this bed similar to bed 56
61	• **Interlayered Shale, Gypsum and Limestone:** Shale, description Similar to bed no 57 with intense dissection of veins filled by secondary satin spar gypsum instead of Desert rose gypsum, it's also calcareous. Limestone, light brownish to yellowish gray. Gypsum is light gray to violate laminated with some displacive gypsum crystals.

Bed No.	Description
62	• **Gypsum:** Light gray to white, coarse alabastrine nodules form chicken wire texture, at the top this unit also show irregular microbial lamination.
63	• **Shale:** Description of this unit similar to bed no 53 and more gypsiferous
64	• **Gypsum:** Description of this unit similar to bed no 56
65	• **Shale:** Description of this unit similar to bed 63
66	• **Gypsum:** Description of this bed Similar to bed 50
67	• **Interlayered Dolostone, Siltstone and Shale:** Dolostone, description of this unit similar to bed 28 and it also becomes vuggy near the contact with gypsiferous shale beds. Shale, light greenish gray, calcareous and gypsiferous, intensely intruded by secondary satin spar veins. Siltstone, light brownish to yellowish gray, void spaces filled by secondary alabastrine and selenitic gypsum, veins are also filled bay secondary satin spar gypsum as well, partly calcareous, rip up clasts of red clay can also be found at the base.
68	• **Interlayered Gypsum and Dolostone:** Dolostone, description Similar to bed 28, description of Gypsum similar to bed no 58.
69	• **Interlayered Mudstone and shale:** light brownish to greenish gray, calcareous, interlayered with shale unit at the bottom.
70	• **Interlayered Gypsum and Dolostone:** light bluish gray to light yellowish gray, shows nodular gypsum cemented by carbonaceous matrix. Dolostone description similar to bed 67.

Bed No.	Description
71	• **Inter layered Shale and laminated silty Gypsum:** Description of shale similar to bed no 67, laminated gypsum is light gray, laminations are separated by microbial lamina and sandy and silty cumulates.
72	• **Gypsum:** Massive, show chicken wire texture, displacive gypsum laths forming a random fabric dominate this bed
73	• **Interlayered Shale and Gypsum:** Description of this unit similar to bed 71
74	• **Gypsum:** light bluish gray to gray, Laminated, highly inter laminated with siltstone, also show wavy laminations especially when its intercalated with siltstone. Secondary veins filled by satin spar gypsum.
75	• **Shale:** Light bluish gray, gypsiferous, highly dissected by secondary satin spar veins
76	• **Gypsum:** gray, massive, alabastrine grains dominate the bed
77	• **Interlayered Gypsum, Shale and Mudstone:** gypsum description similar to bed no 74 with the exception that the gypsum beds are significantly thicker than bed 74. Shale and mudstone are light greenish gray, calcareous and partly gypsiferous.
78	• **Gypsum:** light Bluish gray, gradational change in texture from nodular top to laminated bottom observed in this unit.
79	• **Gypsum and Shale:** Nodular gypsum showing light bluish gray to gray color capped by thin 0.2m thick shale at the top.
80	• **Gypsum:** description of this bed similar to bed no 76

Bed No.	Description
81	• **Interlayered Gypsum, Dolostone and Siltstone:** Description of Gypsum similar to bed no 79, with the exception that this bed is calcareous and thin layers of Dolostone exist between thick uniform gypsum layers. Siltstone shows similar trend as Dolostone in terms of layering, shows reddish to brownish gray color, partly vesiculated. Dolomite beds also show vuggy texture as well.
82	• **Interlaminated Siltstone, Shale and gypsum:** Shale, light greenish to brownish gray, calcareous, gypsiferous and dominant at the top. Siltstone, light brownish gray, highly laminated and lithified by gypsum laminations and crests, shows soft sediment deformation. Both shale and siltstone have been affected by secondary vein filling satin spar and alabastrine gypsum
83	• **Gypsum:** light bluish gray to light gray, uniformly and thinly bedded, gypsum ghosts showing bottom growth textures can be seen in layers found at the top. Teppe structures can also be seen at the bottom pf this unit.
84	• **Interlayered Limestone, Shale and Gypsum:** Limestone is light brownish to yellowish gray, micritic, thick and uniformly bedded, parlty fossiliferous, gypsiferous (voids and cracks filled with secondary gypsum), shale, light greenish to khaki colored, calcareous, gyspsiferous, massive, gypsum rarely exist above 0.2m thick beds, highly interlayered with shale and limestone, when found forming thicker beds, it shows laminated texture with displacive secondary gypsum crystals.
85	• **Interlayered Gypsum, Dolostone, Limestone and Shale:** Gypsum, Limestone and Shale Description Similar to bed 84, Dolostone, light brownish to yellowish gray, massive, partly vuggy, partly argillaceous, the proportion of bedding in this unit is 1:1 for all units except shale which is subordinate.
86	• **Dolostone interlayered with shale:** Dolostone and shale description similar to bed no 85. Shale beds are subordinte
87	• **Interlayered Gypsum, Shale and Limestone:** Description of Shale and Limestone Similar to bed no 84. Gypsum light bluish gray, massive beds having a microbial gypsum texture at the top that gradually becomes nodular and chicken wire texture in beds found at the bottom of this unit.

Bed No.	Description
88	• **Interlayered Gypsum, Siltstone, Limestone, Dolostone and shale:** Description of Dolostone, limestone and shale similar to bed no 85, gypsum description similar to bed no 87, siltstone, light brownish gray, calcareous and gypsiferous, voids filled with secondary selenitic gypsum
89	• **Interlayered Shale and siltstone:** Shale light greenish gray to brownish gray color, massive, siltstone, light brownish gray color, partly gypsiferous, longitudinal ripple marks are common, coarsening upwards sequence also observed.
90	• **Siltstone:** Light brownish gray color, massive, partly calcareous at the top, sandy siltstone and fine sandstone thin to laminated beds can be found in the middle. At the bottom, beds become micaceous and highly bioturbated
91	• **Interlayered Shale and Siltstone:** Shale description similar to bed 89, Siltstone unit description similar to bed no 90 with the exception that most of the siltstone beds show cross bedding.
92	• **Sandstone:** Light brownish to reddish gray, fine, shows planar cross bedding, bed thickness decreases towards the bottom, climbing ripples also observed in one bed at the bottom. Thin red mudstone beds separate the beds towards the bottom.
93	• **Shale:** Reddish gray, massive, thin laminations of sandy siltstone exist forming wavy beds.
94	• **Sandstone:** light reddish gray to pinkish gray, massive, fine grained, cross laminated towards the bottom.
95	• **Interlayered Shale, Siltstone and mudstone:** Shale and mudstone show variegated color, massive, siltstone, light brownish gray, also show cross bedding towards the bottom of this unit
96	• **Interlayered Siltstone and Shale:** Shale dominantly show greenish gray color but at the top part, it becomes variegated, massive, lenses and wavy beds of siltstone and mudstone common within shale beds. Sitstone, light brownish to greenish gray, massive, bed thickness is not uniform, thin irregular laminations of clay stone also present in some siltstone beds, also found forming lenticular and wavy beds within thick undifferentiated shale and mudstone beds, mudstone, description similar to shale with the exception that it doesn't show fissility.

Bed No.	Description
97	• **Interlayered Sandstone, Siltstone Mudstone and Shale:** Description of Silt stone and Shale similar to bed no 96, Sandstone, uniformly layered, light gray, fine, argillaceous, partly calcareous, massive. Mudstone, light brownish gray to greenish gray, massive, thin laminations of siltstone and clay stone forming irregular laminations can be found in some beds.
98	• **Sandstone:** light brownish gray to reddish gray, fine, cross bedded, cliff forming, fining upwards bedding, fractures and veins filled with secondary chert can also be found.

2: Dejen Section

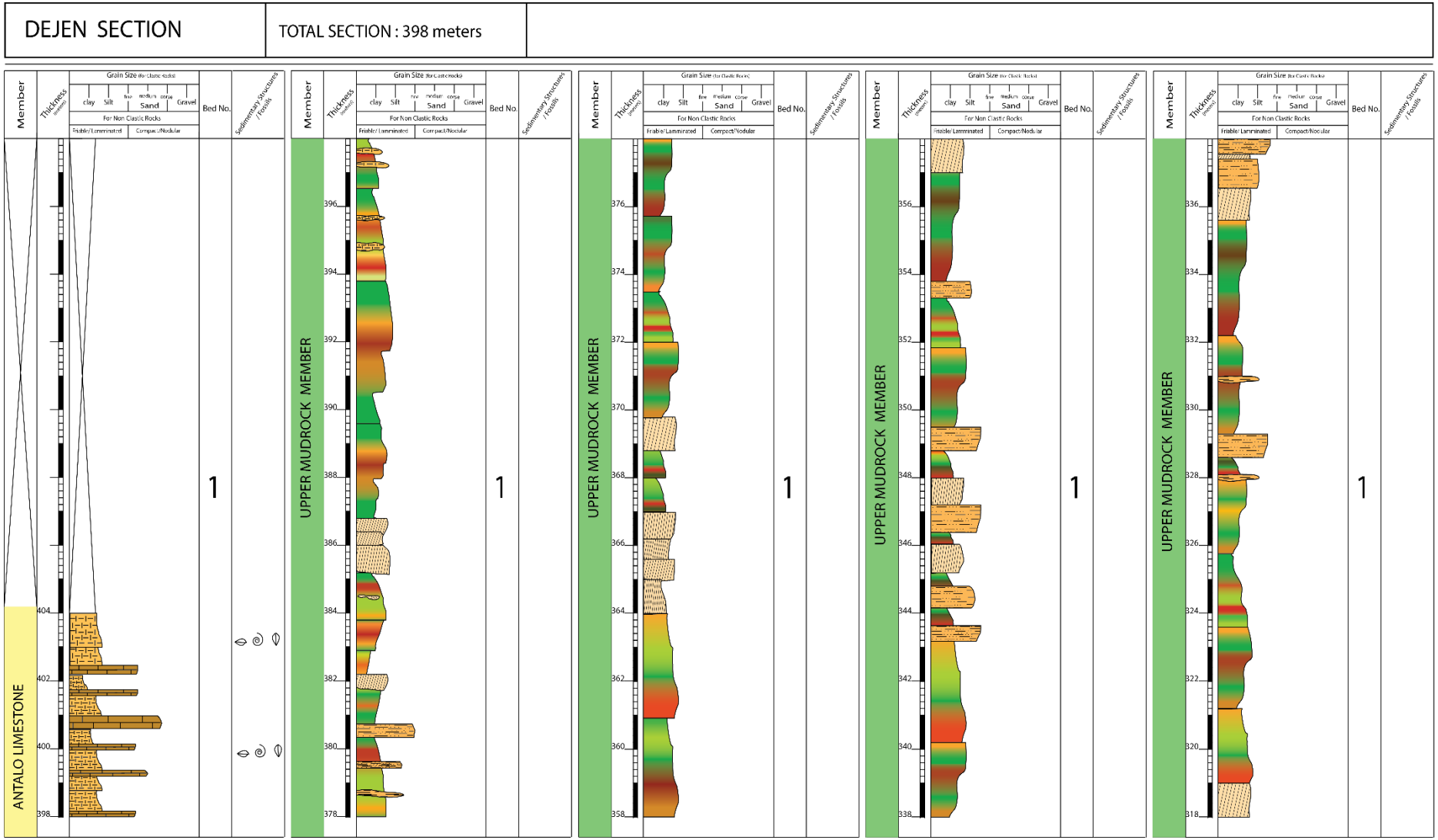

DEJEN SECTION	TOTAL SECTION : 398 meters	

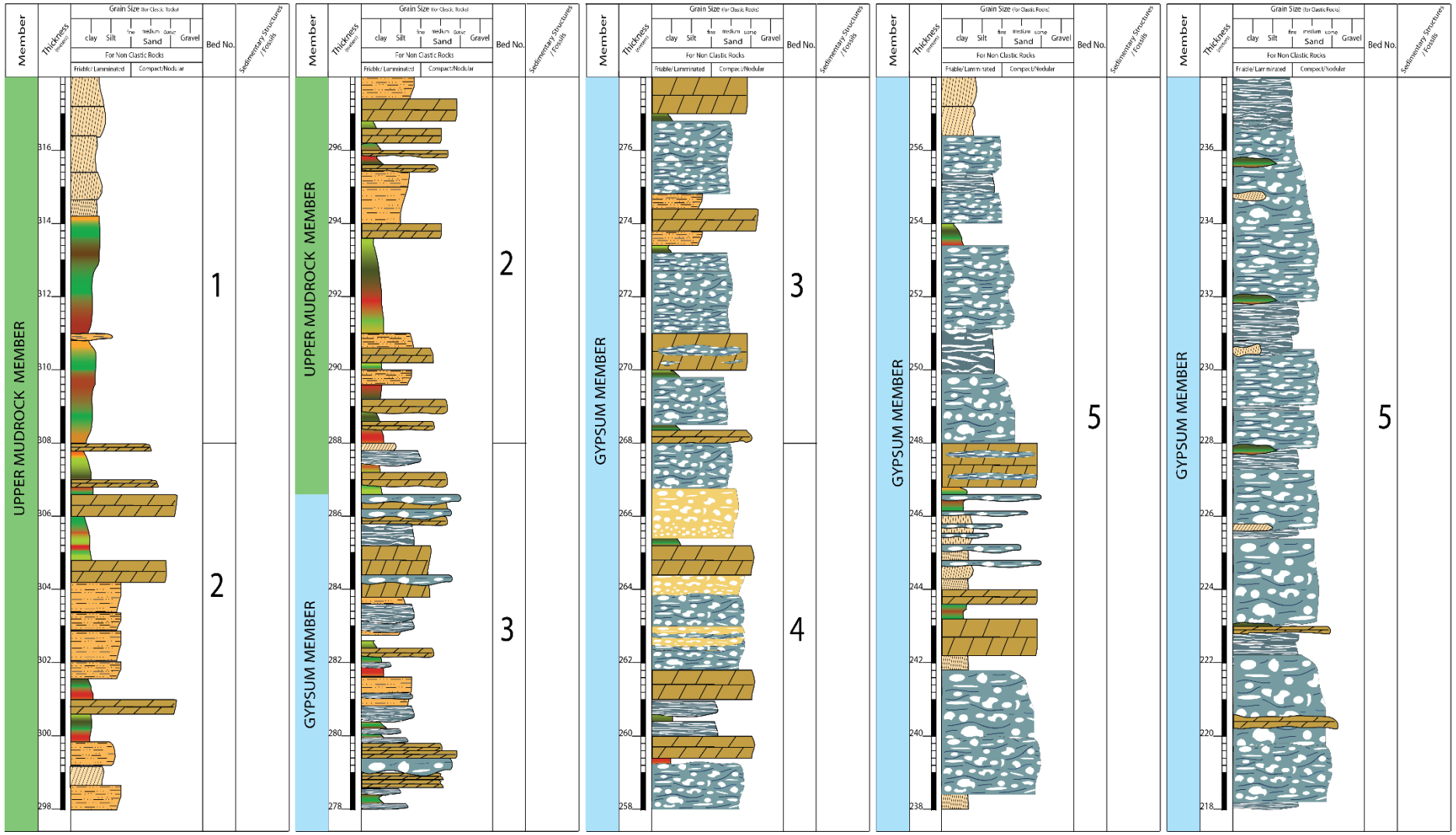

DEJEN SECTION	TOTAL SECTION : 398 meters	

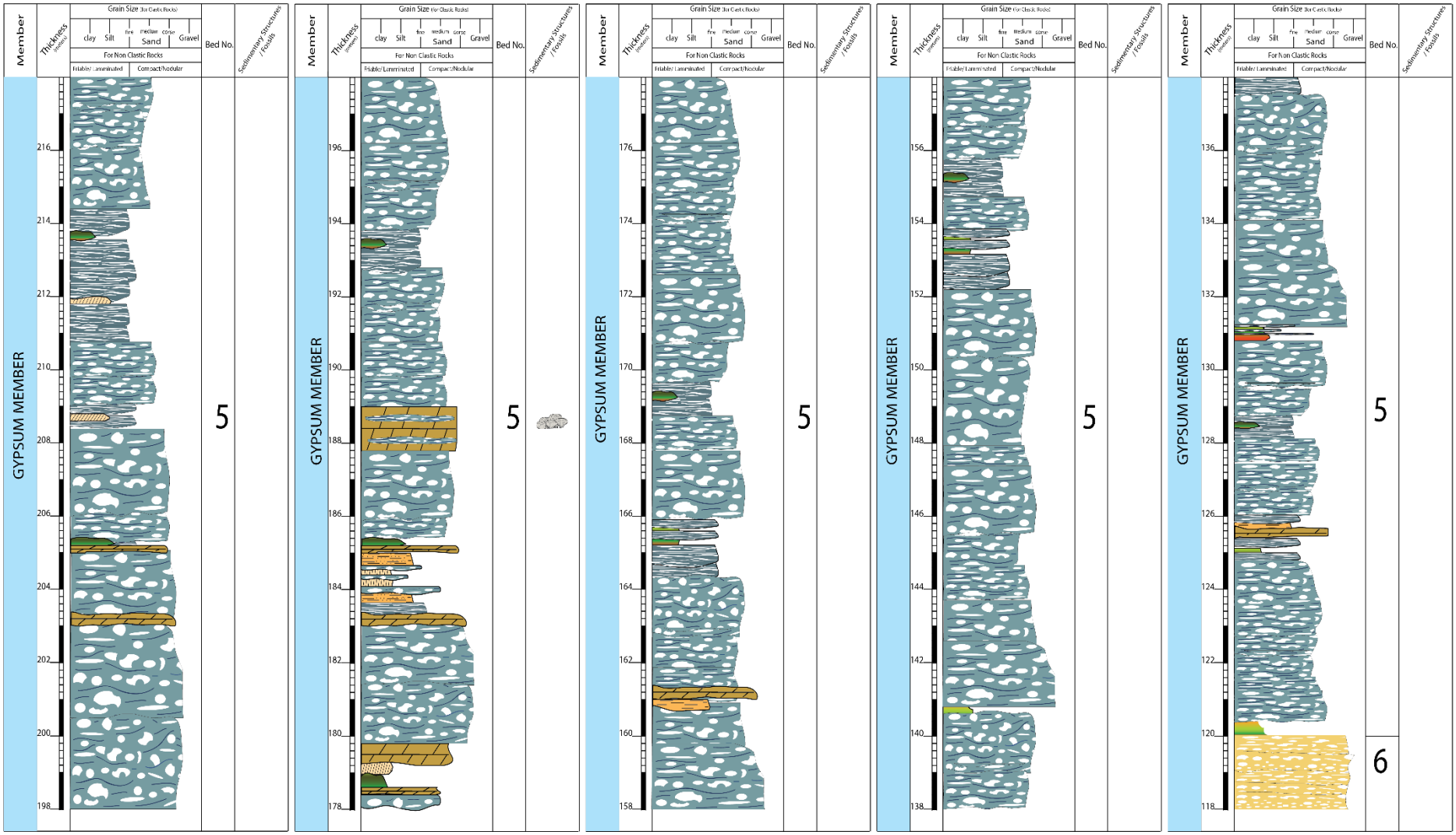

DEJEN SECTION

TOTAL SECTION : 398 meters

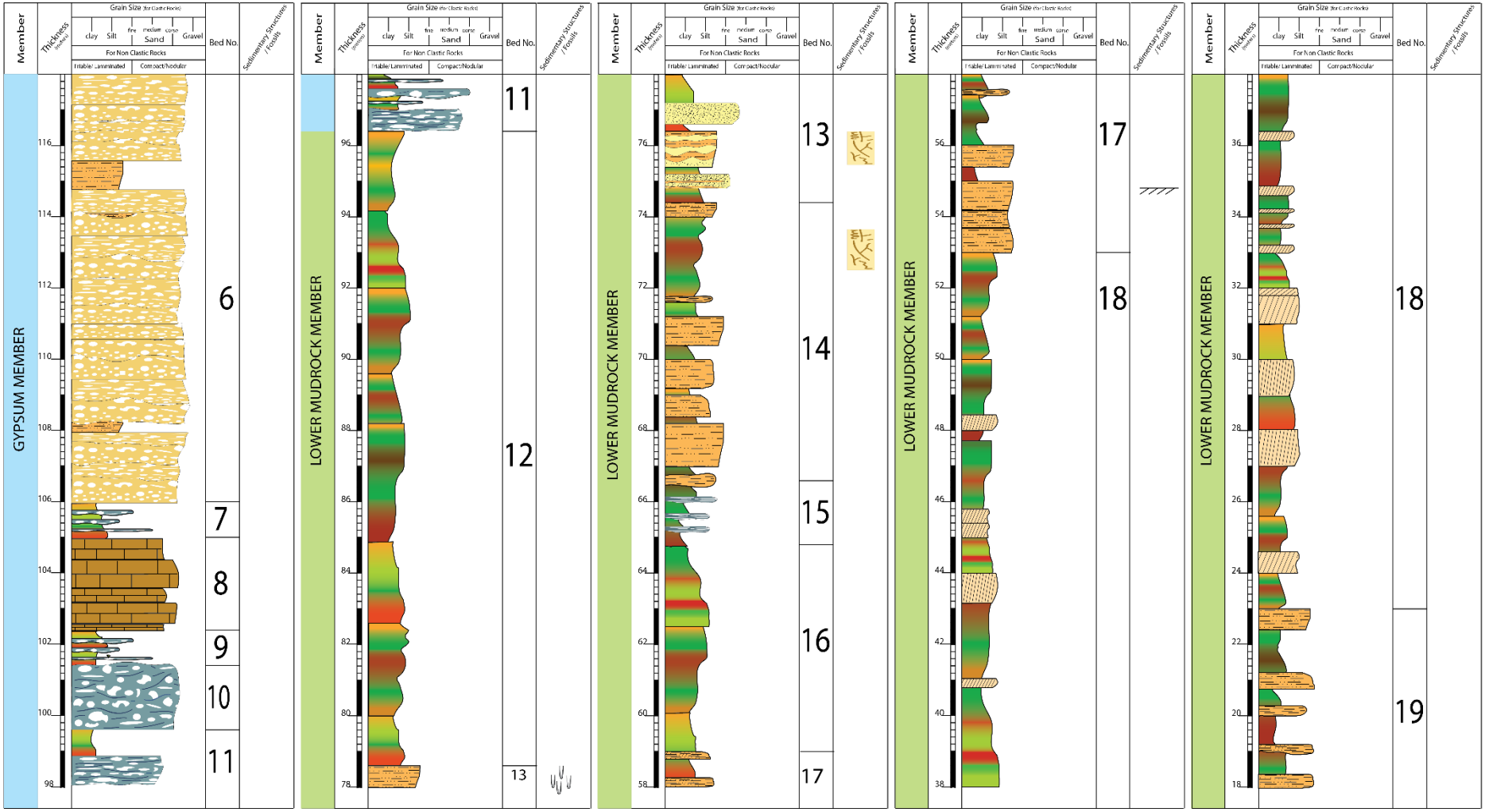

DEJEN SECTION	TOTAL SECTION : 398 meters	

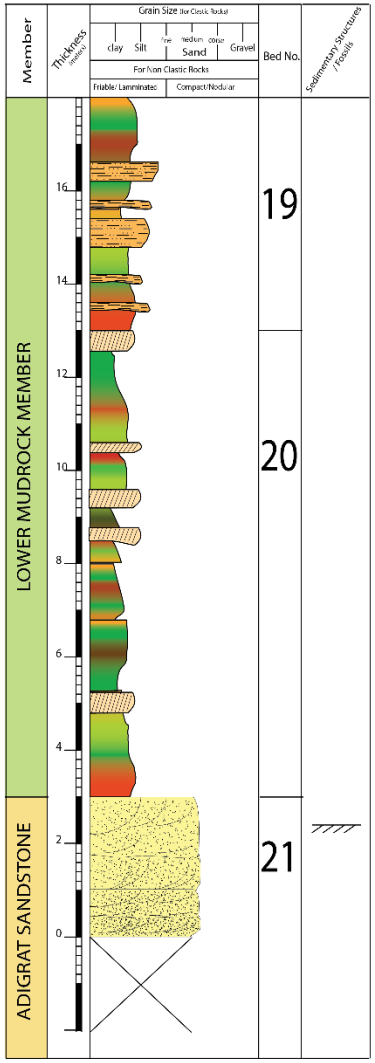

Lithostratigraphic Description of Dejen Section

Bed No.	Description
1	• **Inter Layered Marl, Limestone, Shale and Mudstone:** Marl light yellowish gray, friable, highly interbedded with limestone. Limestone, micritic, partly fossiliferous (mostly brachiopods and fragments of gastropods), bed thickness decreases towards the bottom near the contact with interlayered shales, Shale, variegated color with greenish gray and red being dominant colors. Partly calcareous, Lenticular beds of silt and marl also observed the contact between friable marl and shale beds seem to be irregular and partly discontinues. Silt and mudstone units are subordinate and are calcareous. The middle part of this unit is covered by recent colluvium so it is difficult to trace primary bedding.
2	• **Inter layered Shale, Siltstone and Dolostone:** Shale and Siltstone, Description Similar to bed 1, Dolostone, light yellowish to Khaki Color, compact, found forming uniform thin beds (0.2-0.6m) within calcareous silt and shale beds. Also found in the form of wavy bedding. Lack of exposure makes it difficult to identify and measure primary beds towards the bottom
3	• **Inter Layered Dolostone, Gypsum, Silty mudstone and Shale:** Dolostone, Description Similar to bed 2. Shale description similar to bed 1, silty mudstone, light gray to yellowish gray, thinly and uniformly bedded, partly calcareous, irregular laminations of clay stones also occur within some beds. Gypsum, light bluish gray to light gray, partly laminated (on top) and partly nodular (towards the bottom). It's also highly inter layered with thin Dolostone layers. Laminated gypsum tend to exist highly inter bedded with silty mudstone and shale. And near the contact mud clasts incorporated within gypsum beds can also be found. Thicker beds of gypsum tend to be dominated by nodular texture. Displacive post diagenetic gypsum crystals can also be found with in laminated gypsum beds near the bottom.
4	• **Clastic Gypsum and Dolostone:** Gypsum, clasts of gypsum matrixed by silty carbonate matrix, gypsum clasts are medium grained and unsorted. Dolostone, indurated, clasts of gypsum can be found near the contact with clastic gypsum. Both beds are often separated by secondary selenite gypsum laminations. Thin beds of shale and siltstone also separate the gypsum and dolomite beds especially towards the bottom.

Bed No.	Description
5	• **Interlayered Gypsum, Dolomite, Silty mudstone and Shale:** Gypsum, light bluish gray to light gray, shows irregular bedding, dominantly shows nodular texture. The size of nodules seem to vary with respect to bedding thickness and the degree of inter bedding of other lithologies (mainly silty mudstone and algal mats). Silty mudstone, description similar to bed 4. Shale, light gray to greenish gray, highly inter layered with nodular gypsum units, bedding thickness is highly irregular. Displacive gypsum crystals tend to be common towards the bottom. Dolomite, Description similar to bed no 2. Lack of proper exposure to log makes it difficult to properly measure thickness of each units especially in the middle part of the unit.
6	• **Calcareous Gypsum interbedded with clastic gypsum:** Light Yellowish to brownish gray, gypsum nodules within a clastic argillaceous and carbonaceous matrix, reworked gypsum clasts are also common along with insitu gypsum nodules. Also has cavities that are filled with *botryoidal* and '*daisy wheel'* type secondary gypsum crystals. Displacive gypsum crystals can also be found within the layers.
7	• **Interlayered Shale and Nodular Gypsum:** Shale, variegated color ranging from light greenish gray to reddish brown, partly calcareous, gypsiferous. Gypsum, light Bluish gray to light gray, nodular (medium to coarse nodules, laminated by algal mats and carbonate). Gypsum crests and secondary satin spar veins having an en-echelon like arrangement can be found within shale beds.
8	• **Limestone:** Yellowish gray to Khaki color, partly fossiliferous, shows uniform thick bedding at the top that gradually thins when going to bottom.
9	• **Interlayered Shale and Gypsum:** Description of this bed similar to bed 7
10	• **Gypsum:** light bluish gray, nodular but nodules show preferred orientation matrixed by thin algal laminae (almost like microbial gypsum texture), thinly and uniformly layered
11	• **Interlayered Shale and Gypsum:** Shale, Description similar to bed 7 with the addition of desert rose gypsum laminations. Gypsum, light gray to white, nodular (very coarse and alabastrine type).
12	• **Variegated Shale:** Shale Description similar to bed 7 with the exception that this shale unit is not calcareous.

Bed No.	Description
13	• **Variegated Shale interlayered wit silty sandstone:** Shale Description similar to bed 7 with the exception that this shale unit is not calcareous and heavily bioturbated along with thin irregular laminations of green claystone can be observed. Silty sandstone beds are either in the form of channel fill or forming thin lenticular bedding within shale units. Channel scouring and flute cast structures also observed.
14	• **Variegated Shale interlayered wit silt stone:** Shale Description similar to bed 13. Dominant at the top with thin layers (0.1m) of silt stone forming irregular beds. Siltstone, light brownish to yellowish gray, bed thickness increases towards the bottom
15	• **Shale:** Light greenish gray to brownish gray, gypsiferous, layers of dark green shales present at the top of this bed (indicative of increasing organic content). Rare thin beds (0.2m) of siltstone also intercalate with this bed.
16	• **Interlayered Variegated Shale and Mudstone**: dominantly reddish brown to red at the top that gradually becomes variegated towards the bottom. The bottom layers are monotones and massive with no trace of bedding but at the bottom laminations of irregular claystone can be observed
17	• **Interlayered Siltstone and Shale:** Description of Siltstone and Shale Similar to bed no 14 and 13. Siltstone is the dominant lithology and becomes sandier towards the bottom. Linguoid ripple marks and cross bedding also observed in this bed.
18	• **Interlayered Shale and mudstone:** Description of Shale Similar to bed 13 with the exception that this unit is neither calcareous nor gypsiferous. And dominantly show greenish gray color. Mudstone, light yellowish to brownish gray, calcareous show uniform thin bedding.
19	• **Interlayered Claystone, Shale and muddy Siltstone:** Claystone, partly variegated but dominantly greenish gray, thin beds of variegated shale also observed, calcareous muddy siltstone beds intercalate with shale and clay stone at the middle part of the bed.
20	• **Variegated Shale with occasional beds of mudstone:** Description of shale similar to bed 17. Mudstone beds having light greenish to brownish and reddish gray color intercalate with shale beds.
21	• **Sandstone:** light brownish to reddish gray, fine to medium grained, cross bedded (planar cross bedding). Also show consolidated massive cliff forming beds.

3. Jemma section

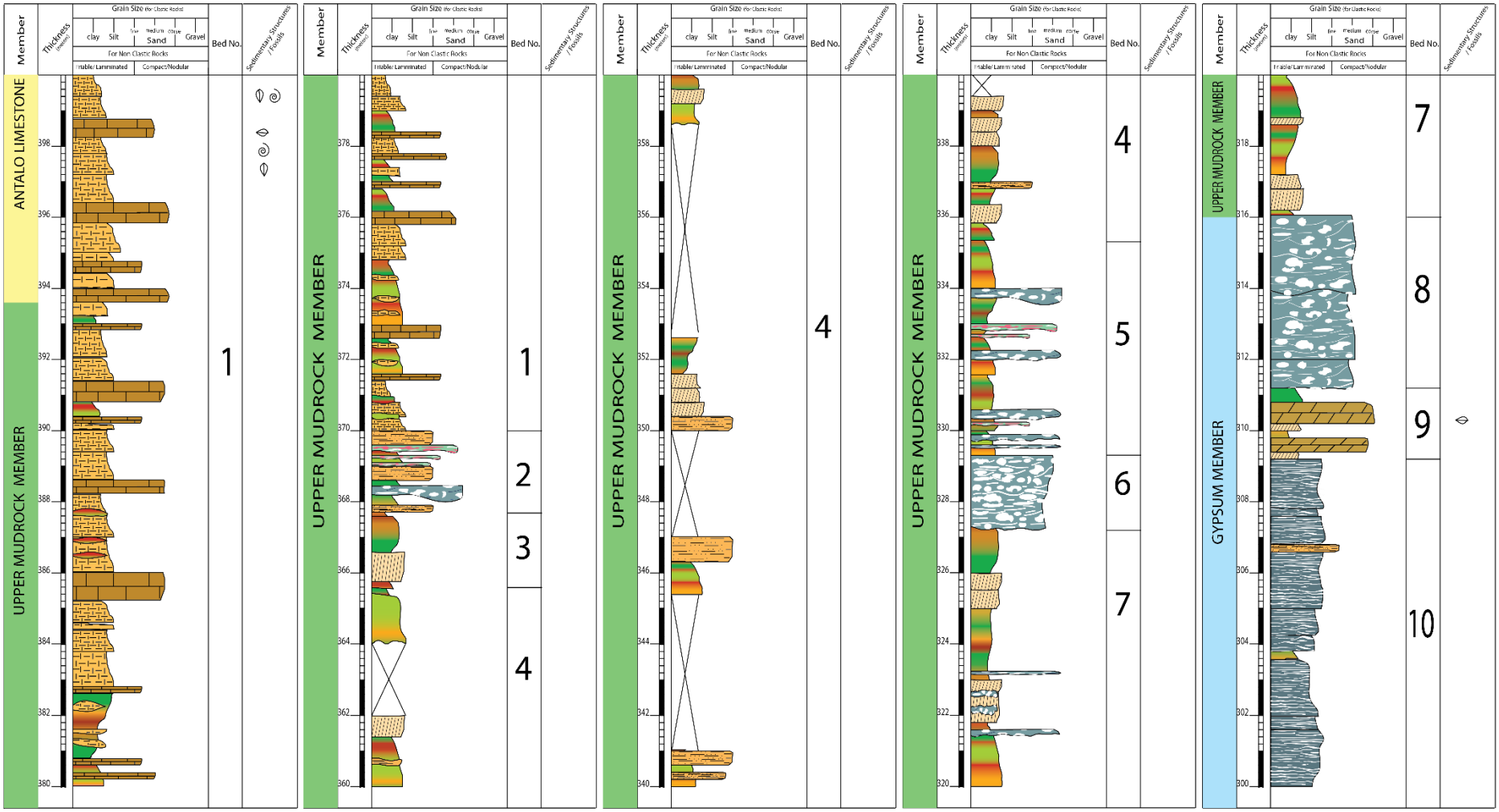

JEMMA SECTION	TOTAL SECTION : 400 meters	

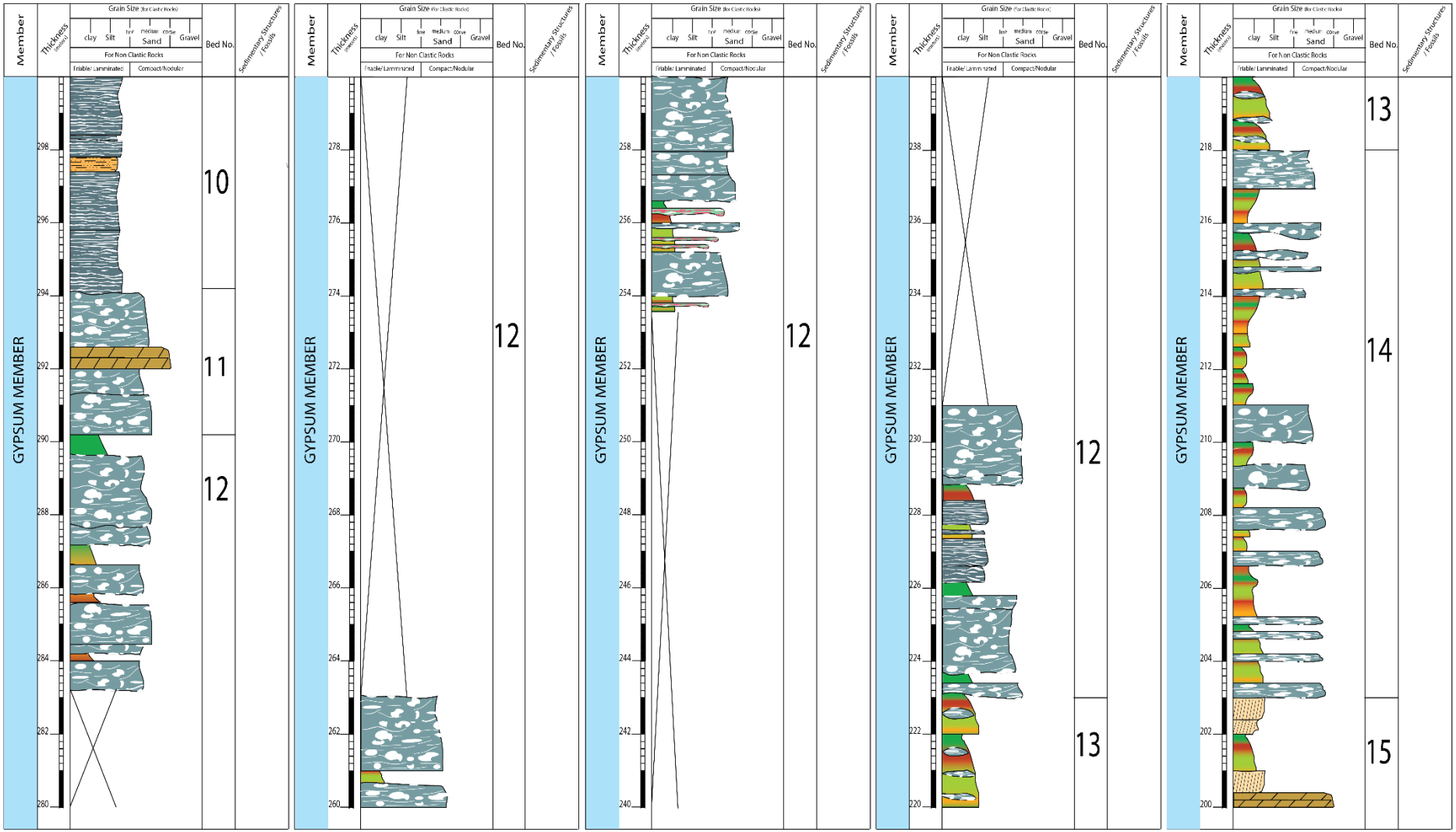

JEMMA SECTION	TOTAL SECTION : 400 meters	

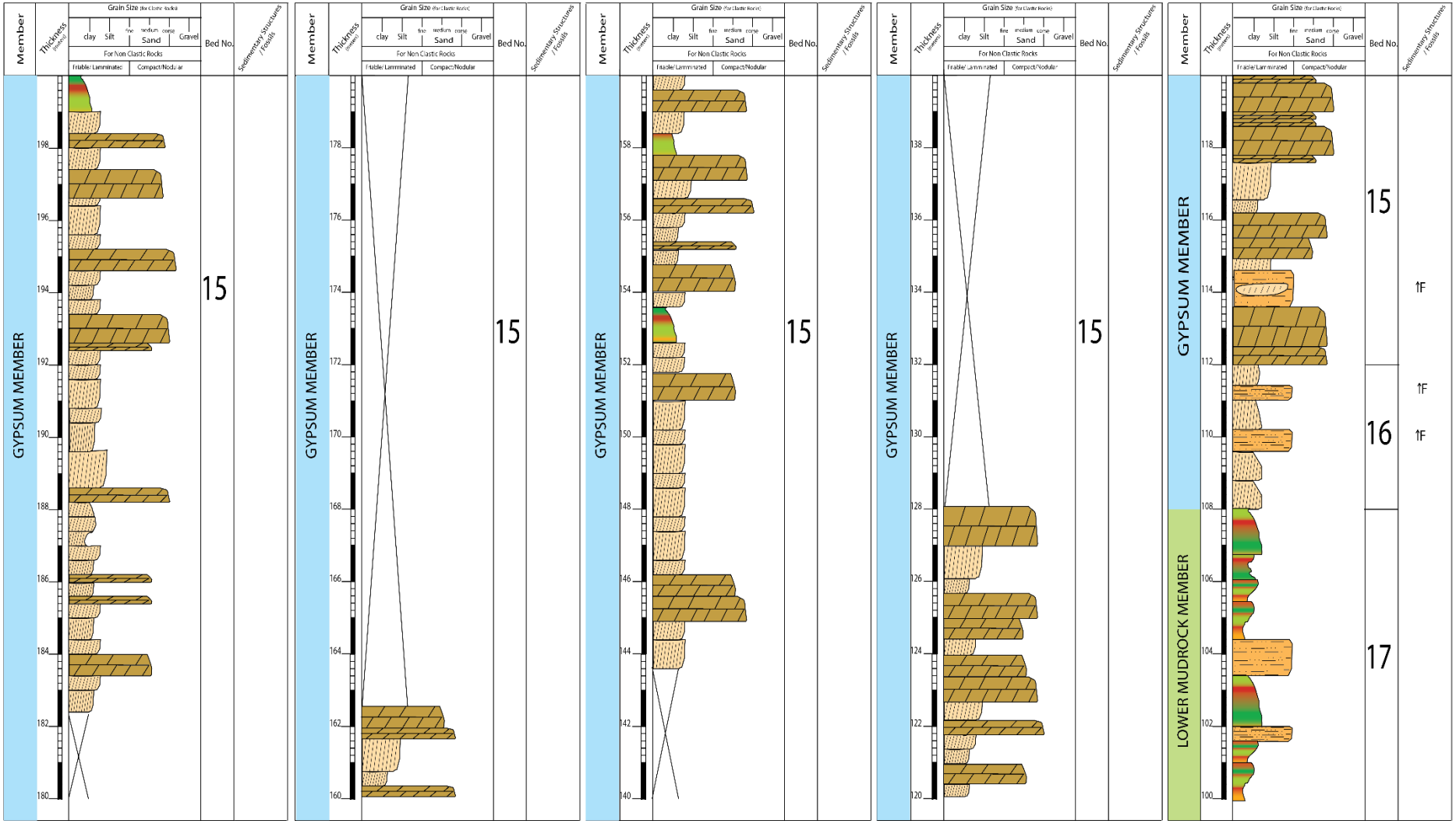

JEMMA SECTION	TOTAL SECTION : 400 meters	

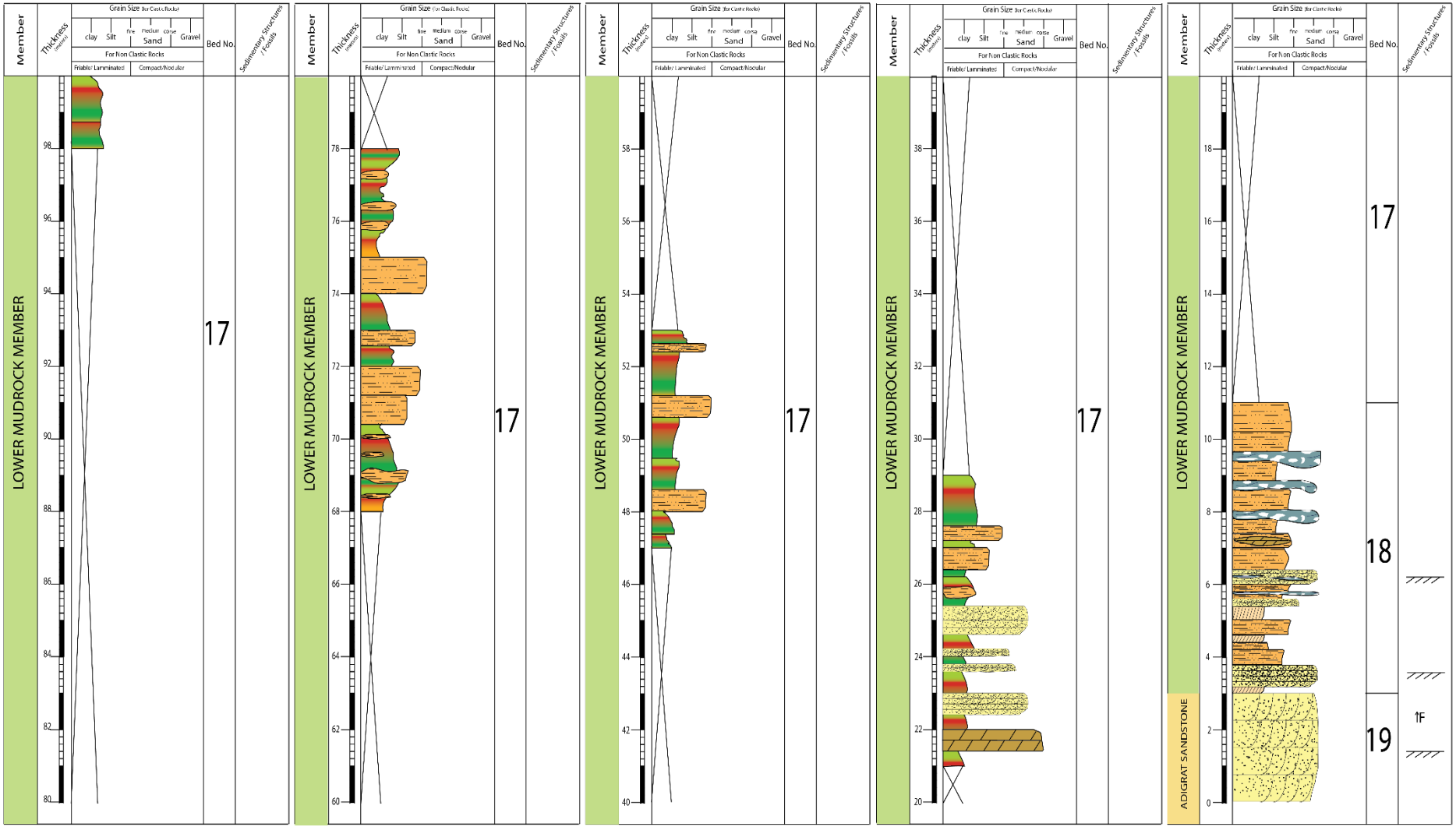

Lithostratigraphic Description of Jema Section

Bed No.	Description
1	• **Inter Layered Marl, Limestone, Shale and Mudstone:** Marl light yellowish gray, friable, highly interbedded with limestone. Limestone, have uniform beds, partly fossiliferous (mostly brachiopods and fragments of gastropods), bed thickness decreases towards the bottom, cross laminations observed. Shale, variegated color with greenish gray being dominant color. Lenticular beds of silt and marl also observed. Silt and mudstone units are subordinate and are calcareous.
2	• **Siltstone interlayered with desert rose gypsum and shale:** Siltstone, light yellowish gray to brownish gray, calcareous, gypsifurus. Desert rose gypsum, light pink to white (thickness 0.2-0.5m), highly intercalated with calcareous silt. Shale (0.2m), greenish gray, found intercalated with gypsum desert rose, also calcareous and gypsifurus, veins of satin spar cross cut all units in an erratic manner.
3	• **Variegated Shale:** light greenish gray, reddish to brownish gray, wavy laminations of claystone also observed semi-indurated mudrock that is partly gypsiferous
4	• **Interlayered Shale and mudstone along with minor siltstone:** Shale, description similar to bed 3, mud stone, friable to indurated, partly calcareous, light yellowish to greenish gray, siltstone shows similar characteristics as mud stone and often found forming lenses of beds in shale (average ~0.2m thickness)
5	• **Variegated Shale interlayered with Desert Rose Gypsum:** Description of Shale and desert rose gypsum similar to bed 2
6	• **Gypsum:** Light gray to bluish gray color nodular size of nodules seem to increase both vertically and laterally within this unit, gypsum crests and laminations of slit along with algal mats matrix large albastrine nodules (especially towards the bottom), secondary displacive gypsum crystals also observed
7	• **Interlayered Mud and shale:** Mudstone, khaki color, calcareous and gypsiferous, light greenish gray clay stones with irregular laminations and algal crests also observed. Shale, description similar to bed 2

Bed No.	Description
8	• **Gypsum:** Light gray to white, nodular, massive, algal mats and gypsum crests matrix gypsum nodules
9	• **Inter Layered Shale, Dolostone and Mudstone:** shale, description similar to bed 2, Dolostone, Khaki color, fragments of fossil observed, mudstone, light yellowish to khaki color, calcareous, fossiliferous (molds of brachiopods observed).
10	• **Gypsum, Interlayered with Shale and Siltstone:** Gypsum, Light gray to white, laterally thickens towards west, dominantly laminated and shows algal lamination towards the bottom and massive towards the top. Shale and siltstone description similar to bed 2 with the exception that some beds show wave formed ripples
11	• **Gypsum:** Light gray to bluish gray, uniformly bedded, Dolostone (0.4m) bed exists in the middle of this bed. Displacive gypsum crystals also occur within this bed.
12	• **Interlayered Gypsum and Shale:** Description of Gypsum similar to bed 11 with the exception that some beds (~3m thick) become laminated towards the bottom, whereas Description of Shale Similar to bed 2, the outcrop is highly affected by tectonics to the point that distinguishing primary beds becomes difficult especially towards the bottom
13	• **Shale:** Gypsiferous, light greenish to yellowish gray, calcareous, laminations of gypsum nodules exists at the top
14	• **Shale interlayered with desert rose and nodular gypsum:** Description of Shale and Desert rose similar to bed 2

Bed No.	Description
15	• **Interlayered Mudstone and Dolostone:** light Brownish to yellowish gray, calcareous dominant at the top of this unit, massive to thinly bedded, silty at the bottom, silty mudstone beds also show fining upwards sequence. Dolostone, light yellowish to khaki color, dominant towards the bottom of this sequence, massive to thinly bedded, both mudstone and Dolostone beds are highly affected by tectonics to the point that it becomes difficult to trace primary bedding along the road cut outcrop.
16	• **Silty Mudstone:** Description of this bed similar to bed 15 and bed 9
17	• **Interbedded Variegated Shale and Siltstone:** Shale and Siltstone, Description Similar to Bed 2 and bed 12, the outcrop of this bed becomes highly disturbed by tectonics and recent landslide when going from top to bottom; hence, it's difficult to trace primary horizontal bedding continuously. Siltstone and sandstone can also be found as channel fill and lenticular beds within shale at the bottom.
18	• **Sandy Siltstone and Gypsum:** Light yellowish to brownish gray, Calcareous, Gypsiferous, Sandy towards the bottom along with some lenticular sandstone beds, dolomitic beds (~0.2m) also accompany gypsum beds. Description of gypsum and dolomite beds similar to bed 11.
19	• **Sandstone:** light brownish gray to light gray, texturally mature, fine to medium gray, friable, cross bedding, hummocky and planar cross bedding also observed. Fining upwards bedding also present within cross bedded units.

4. Mugher Section

MUGHER SECTION	TOTAL SECTION : 172 meters	

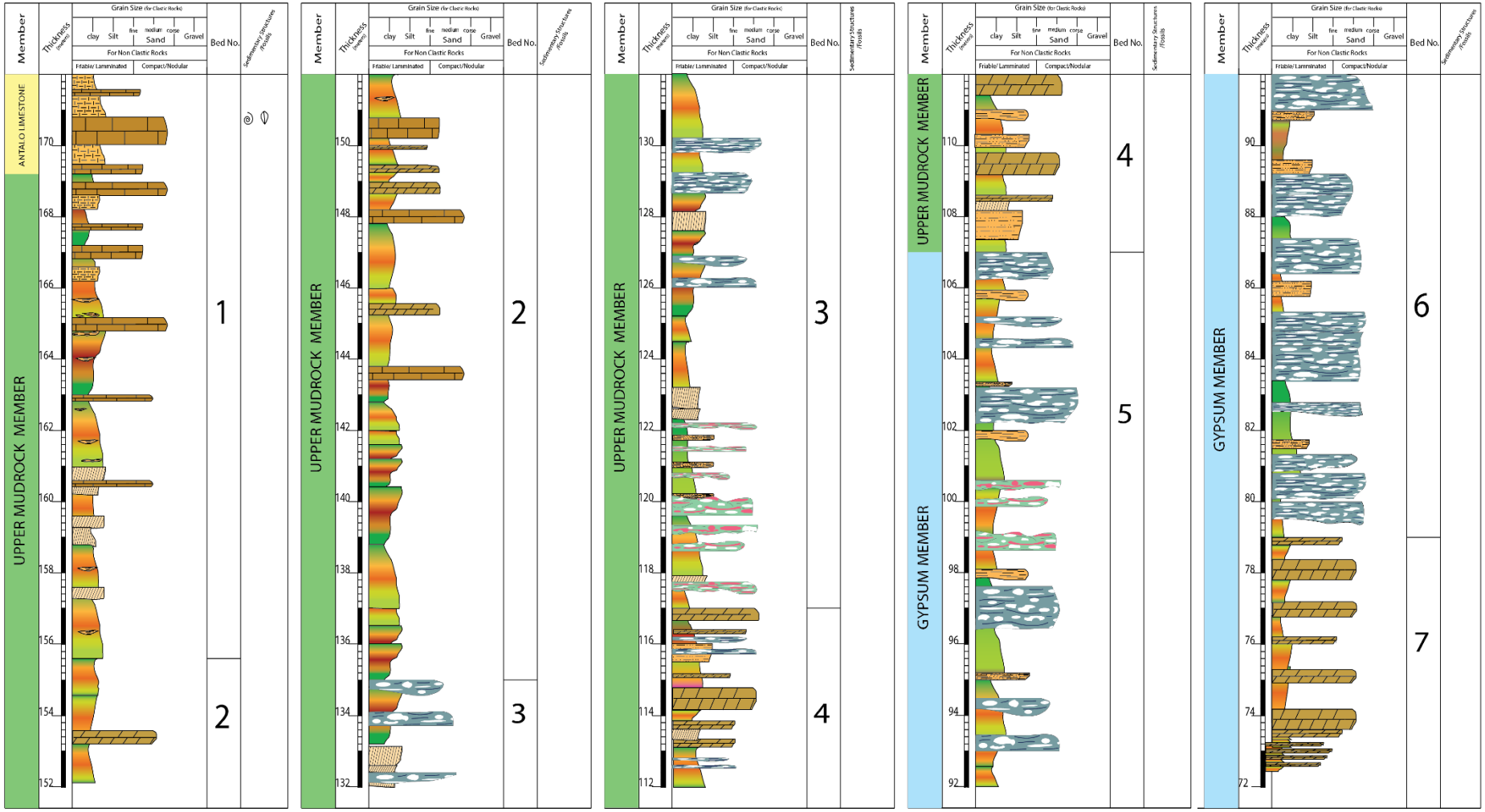

MUGHER SECTION	TOTAL SECTION : 172 meters	

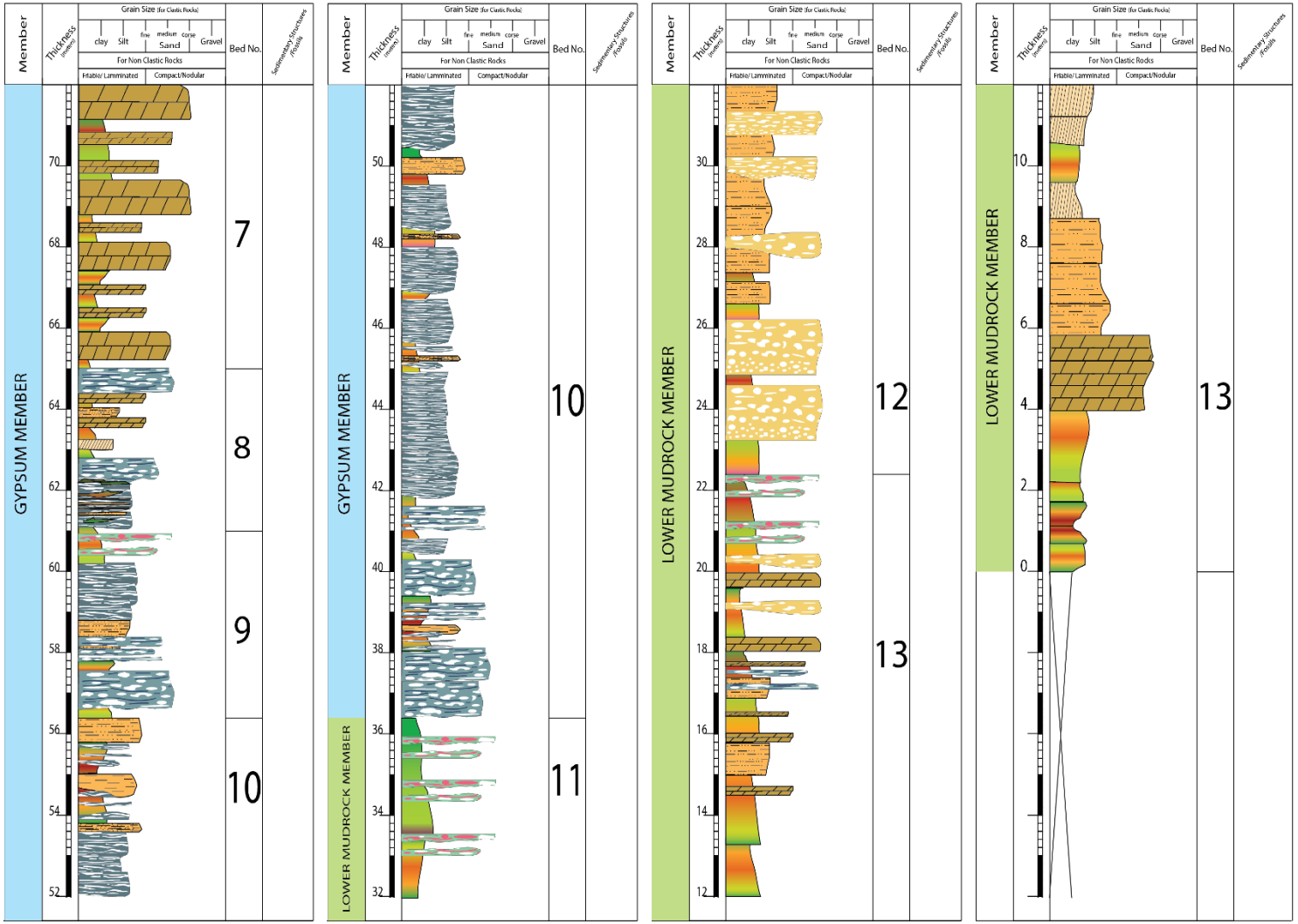

Lithostratigraphic Description of Mugher Section

Bed No.	Description
1	• **Marl inter bedded with Shale Limestone**: Limestone and marl light gray to yellowish gray, thin beds of partly fosiliferous limestone inter bedded with marl, shale showing light greenish gray color highly calcerious, subordinate mudstone also present
2	• **Variegated Shale and Dolomitic Limestone:** Shale, variegated color having reddish brown, shades of green and yellowish gray color, partly calcareous, very fissile, subordinate and undifferentiated mudstone beds also occur (mudstones also have fragmented fossils). Dolomitic limestone having thin uniform bedding (0.4-0.7meters), partly fossiliferous, fenestric.
3	• **Variegated Shale, Mudstone and Gypsum:** Both shale and mudstone show shades of green and gray along with reddish and brownish gray color. Clay stone beds tend to be more compact and occasionally contain lenticular beds of silt. beds of nodular gypsum (1-1.5m) interlayered with shale common towards the bottom of this unit. Individual nodules change both in color and size from small cobble sized and white to coarse boulder sized slightly pinkish gray color (almost like roseate gypsum) towards the bottom.
4	• **Inter Layard Shale, Mudstone Siltstone and Dolomitic Limestone:** Mudstone and siltstone show greenish to brownish gray color along with shale beds that are variegated and partly gypsiferous. Both Mudstone and Siltstone are calcareous. The top part of this unit shows intercalation with thin dolomitic limestone beds. Individual beds of limestone show thin uniform laminations along with fenestral fabric (birds eye fenestre??), beds are also show rare fossil fragments and are dissected by fractures filled with secondary satin spar veins.
5	• **Variegated Shale inter bedded with Gypsum:** description of this bed is similar to Bed 3 with the exception of absence of mudstone and the presence of subordinate lenticular beds of siltstone.
6	• **Inter bedded Gypsum and Muddy siltstone:** Description of this bed similar to bed 3 with the exception that gypsum becomes dominant and siltstone unit is muddy and calcarious

Bed No.	Description
7	• **Interlayered Dolostone, Shale and Mudstone:** Description of Shale, Mudstone similar to bed no 3 , Dolostone is thinly bedded and becomes dominant towards the bottom of this unit, it is also partly fosiliferous and vuggy very compact when compared with the over laying dolomitic beds. All units are partly affected by fractures filled with either secondary satin spar gypsum or calcite.
8	• **Gypsum Interlayered with Shale, Dolomite, Silt and Mudstone:** Gypsum light bluish gray to light gray, in terms of texture sharp contrast between nodular and chicken wire gypsum (possibly erosive) at the top and thinly laminated partly hetrolithic gypsum towards the bottom observed. Dolomite beds are subordinate and are only found at the top of this unit. Both shale and siltstone become dominant towards the bottom with description similar to bed no 3.
9	• **Interlayered Shale, Siltstone and Gypsum:** Shale and Siltstone description similar to bed 4. Thin gypsum beds with coarse nodular texture (partly roseate gypsum at the top) uniformly intercalate with shale and siltstone beds. Gypsum also seem to be affected by secondary displacive gypsum crystals with irregular orientation. Shale and Siltstone beds are also gypsiferous and intensely dissected by irregular networks of secondary fracture filling satin spar gypsum
10	• **Gypsum interbedded with Shale and Siltstone:** shale and silt stone bed description similar to bed no 9 but in this unit, both become subordinate. Gypsum shows purplish blue to light bluish gray color and becomes dominant in this unit. Primarily, gypsum shows laminated texture with microbial gypsum texture dominating. Towards the bottom, there are thick uniform and massive beds of gypsum with no internal structure with the exception of few scattered alabastrine nodules
11	• **Shale interlayered with Gypsum:** Shale beds become thicker and dominantly light greenish gray incolor, they are partly calcareous and gypsiferous with subordinate roseate gypsum nodules in some beds. An average 0.7-1m thick beds of laminated gypsum also exist at the top of this unit. Gypsum beds also show coarse displacive lenticular gypsum crystals with semi oriented to random fabrics
12	• **Inter bedded Gypsum and Muddy siltstone:** Gypsum is partly clastic with breccia of gypsum, limestone and calcareous siltstone matrixed by gypsum. Muddy siltstone with secondary alabastrine nodules filling voids and intensely affected by fracture filling gypsum. Its also calcareous and becomes sandy, especially towards the bottom.
13	• **Inter bedded Shale, Gypsum, Mudstone, siltstone and Dolomitic Limestone:** Description of Dolomitic limestone similar ot bed no 4, Mudstone, siltstone and shale description similar to bed no 4 and 12, Gypsum is subordinate in this unit and is rare towards the bottom, description similar to 9 and 12

Appendix B: Geochemical attributes of the analyzed samples

Gohatsion formation (this study)										Adigrat Sandstone		Basement Rocks			Standard References		
	Upper Murdock member			Gypsum Member				Lower Mudrock Member		BNB	MB[1]	Basement rocks of Wollega[2]					
Rock type	Shale		limestone	Gypsum				Shale		Sandstone		Felsic, Intermediate to mafic rocks					
Elements	GS-5-2	GS-9-1	GS-9-2	GS-3-1	GS-2-3	GS-2-4	DS-1-2	GS-3-4	GS-4-2	DS-1-4		G k-G	UGD	MIR	PAAS[3]	NASC[4]	UCC[5]
SiO_2	48.9	51.8	5.11	0.25	0.11	0.45	8.53	16.00	47.00	98.70	90.33	70.15	70.91	50.4	62.8	64.8	66
TiO_2	0.94	0.94	0.07	0.01	<0.01	0.01	0.14	0.14	0.82	0.06	0.51				1	0.7	0.6
Al_2O_3	16.0	16.2	1.30	0.04	0.02	0.11	2.56	3.15	12.40	0.41	5.13	14.43	14.65	17.32	18.9	16.9	16
Fe_2O_3	9.81	7.43	1.92	0.04	0.04	0.08	0.89	2.19	5.49	0.52	1.02				6.3	5.65	4.5
MgO	3.31	3.77	10.60	0.01	<0.01	0.02	0.45	15.85	6.49	0.03	0.16				2.2	2.86	2.3
CaO	2.34	0.93	37.70	33.40	32.60	32.50	27.20	23.20	5.36	0.08	0.53	2.20	1.66	9.83	1.3	3.63	3.5
Na_2O	0.31	0.30	0.03	<0.01	<0.01	<0.01	<0.01	0.12	0.11	0.01	0.11	4.40	4.30	3.04	1.2	1.14	3.8
K_2O	4.97	5.12	0.32	<0.01	<0.01	0.04	0.63	0.93	4.61	0.05	0.68	4.29	4.26	0.91	3.7	3.97	3.3
MnO	0.03	0.03	0.19	<0.01	<0.01	<0.01	<0.01	0.14	0.16	0.01	0.03				0.11	0.06	0.1

P_2O_5	0.14	0.24	0.07	<0.01	0.02	<0.01	0.03	0.18	<0.01	<0.01	0.06				0.16	0.13	0.2
LOI	12.20	12.75	42.30	20.60	21.20	21.10	22.70	36.40	16.50	0.33	1.44						
Cr_2O_3	0.01	0.01	<0.01	0.01	<0.01	<0.01	<0.01	<0.01	0.01	<0.01					110		
SrO	<0.01	0.01	0.01	0.13	0.13	0.14	0.02	0.01	0.03	<0.01							
BaO	0.04	0.02	<0.01	<0.01	<0.01	<0.01	0.01	<0.01	0.02	<0.01							
CaO*	0.04	0.01						0.66	0.12	0.0010							
CIA	61.9	69.4						6.83	45.43	68.10							
PIA	70.5	86.9						4.86	42.80	72.10							
ICV	1.36	1.14						13.51	1.86								
Sc	17	17	1	<1	<1	<1	3	4	15	<1		4.58	4.29	33.0	16	14.9	11
V	118	140	13	<5	<5	<5	23	29	76	22					150	130	60
Cr	80	80	10	10	<10	<10	20	20	60	10		10.80	5.21	73.0	110	125	35
Co	14	17	2	1	1	1	2	5	15	1		7.38	7.93	31.8	23	25.7	10
Ni	47	47	6	<1	<1	<1	2	10	35	2					55	58	20
Cu	14	68	6	1	1	2	11	9	54	3					50		25
Zn	90	92	94	2	2	2	14	16	28	4					85		71
As	<5	<5	<5	<5	<5	<5	<5	<5	<5	<5						28.4	1.5

Rb	123	157	10.3	0.3	0.2	1	21.8	24.6	142.5	1.6				160	125	112
Sr	77.7	100.5	123.5	1280	1215	1270	281	182	317	6.2				200	142	350
Y	41.7	34.2	9.3	<0.5	<0.5	<0.5	3.9	14	34.4	3.1				27	35	22
Zr	316	240	20	3	4	2	43	34	365	49				210	200	190
Nb	44.7	34.3	2.6	0.7	0.3	0.5	7.6	4.9	33.7	2				19	13	
Cs	4.03	5.16	0.41	0.01	0.02	0.04	0.99	0.88	4.96	0.06					5.16	3.7
Ba	350	208	43.2	3.8	3.2	6.6	51.2	30.2	181.5	13				15	636	550
La	50.9	44.4	10.8	1.3	1	1.3	7.6	18.2	31.6	10.1	28.80	34.45	15.7	650	31.1	30
Ce	99.7	91.3	22.7	0.5	<0.5	0.9	16.2	35.7	71.8	20.3				80	66.7	64
Pr	11.45	11.2	2.5	0.07	0.05	0.09	1.32	3.96	8.01	2.06						
Nd	44.9	45.4	10.5	0.3	0.2	0.4	4.6	16.7	30.6	7.7				32	27.4	26
Sm	9.02	8.77	1.71	<0.03	<0.03	0.05	0.69	3.15	6.17	1.28				5.6	5.59	4.5
Eu	1.41	1.63	0.39	<0.03	<0.03	<0.03	0.1	0.58	1.09	0.22				1.1	1.18	0.88
Gd	7.96	7.87	1.94	0.07	<0.05	0.06	0.55	2.76	5.8	1.08						3.8
Tb	1.33	1.15	0.26	0.01	0.01	0.01	0.11	0.39	0.97	0.15						0.64
Dy	7.86	6.62	1.43	0.06	<0.05	<0.05	0.67	2.26	6.15	0.63						
Ho	1.57	1.24	0.3	<0.01	<0.01	<0.01	0.15	0.48	1.33	0.12						

Er	4.29	3.68	0.85	<0.03	<0.03	<0.03	0.4	1.18	4.06	0.32						
Tm	0.64	0.49	0.1	<0.01	<0.01	<0.01	0.04	0.16	0.62	0.02						
Yb	3.8	2.79	0.7	0.03	<0.03	<0.03	0.47	0.99	4.25	0.22						
Lu	0.56	0.45	0.09	<0.01	<0.01	<0.01	0.06	0.12	0.69	0.04				0.43	0.46	0.32
Hf	8.7	6.1	0.6	0.2	0.2	<0.2	1.1	1	8.2	1.4				5	6.3	5.8
Ta	2.4	2	<0.1	<0.1	<0.1	<0.1	0.5	0.1	1.8	<0.1	14.96	7.07	1.24		1.12	2.2
Th	14.05	12.95	1.03	0.09	0.06	0.14	2.45	2.12	11.1	1.57				15	12.3	11
U	2.74	2.41	0.39	<0.05	<0.05	0.08	0.32	0.57	2.32	0.4				3.1	2.66	3
Li	50	50	10	<10	<10	<10	20	80	20	<10						
Ga	26.9	27.4	2	0.1	<0.1	0.2	4.9	4.6	20.2	0.9						
Mo	1	1	2	1	1	1	<1	1	1	<1						
Ag	<0.5	<0.5	<0.5	<0.5	<0.5	<0.5	<0.5	<0.5	<0.5	<0.5						
Cd	<0.5	<0.5	<0.5	<0.5	<0.5	<0.5	<0.5	<0.5	<0.5	<0.5						
Sn	4	3	<1	<1	<1	<1	1	1	3	<1						
W	2	2	1	1	<1	<1	1	1	2	<1						
Pb	7	9	7	2	<2	<2	2	3	6	3						20
Th/U	5.1	5.3				3.7	4.7	3.9						5	3.8	
Zr/Sc	18.6	14.1				8.5	24.3	49						13	17	

Secondary data sources:

1: Worash Getaneh (2002)

2: Tesfaye Kebede et al. (1999)

3: Nance and Taylor (1976); Cullers (1995); Nayakairu and Koeberl (2001); Ullah et al. (2015); Ejeh (2016)

4: Gormet et al. (1984); Nayakairu and Koeberl (2001); Ullah et al. (2015); Ejeh (2016)

5: Taylor and Mclennan (1995); Nayakairu and Koeberl (2001); Ullah et al. (2015); Ejeh (2016)